

Review

High-energy-density polymer dielectrics via compositional and structural tailoring for electrical energy storage

Rui Cheng,^{1,2} Yifei Wang,^{3,5,*} Rujia Men,^{1,2} Zhipeng Lei,^{1,2,*} Jiancheng Song,^{1,2} Yuanyuan Li,^{1,2} and Meiqing Guo⁴

SUMMARY

Dielectric capacitors with higher working voltage and power density are favorable candidates for renewable energy systems and pulsed power applications. A polymer with high breakdown strength, low dielectric loss, great scalability, and reliability is a preferred dielectric material for dielectric capacitors. However, their low dielectric constant limits the polymer to achieve satisfying energy density. Therefore, great efforts have been made to get high-energy-density polymer dielectrics. By compositional and structural tailoring, the synergistic integrations of the multiple components and optimized structural design effectively improved the energy storage properties. This review presents an overview of recent advancements in the field of high-energy-density polymer dielectrics via compositional and structural tailoring. The surface/interfacial engineering conducted on both microscale and macroscale for polymer dielectrics is the focus of this review. Challenges and the promising opportunities for the development of polymer dielectrics for capacitive energy storage applications are presented at the end of this review.

INTRODUCTION

With the shortage of fossil fuels and the increasing demand for energy supply, advanced and environmentally friendly energy storage technologies are highly desired. Compared with electrochemical devices, such as batteries and supercapacitors, electrostatic capacitors possess unique advantages of ultra-fast charge and discharge, ultrahigh power density, and long lifespan (Niu et al., 2015b). However, they are limited by low energy densities. Therefore, it is critical to explore high-energy-density dielectric materials.

For linear dielectrics, the energy density (U_e) equation is described as follows:

$$U_e = 0.5\epsilon_0\epsilon_r E_b^2 \quad (\text{Equation 1})$$

where ϵ_0 is the vacuum dielectric constant, ϵ_r is the relative dielectric constant and E_b is the breakdown strength. The dielectric constant (ϵ_r) and breakdown strength (E_b) are two key parameters to evaluate energy density. Polymer dielectrics with high breakdown strength, low dielectric loss, great scalability, and reliability are favorable candidates for high-energy-density capacitors (Cao et al., 2004; Qiao et al., 2013). But the dielectric constant of dielectric polymers is low, so a high electric field near the breakdown strength is required to achieve satisfying energy densities (i.e. $\geq 450\text{--}600$ MV/m) (Chen et al., 2019). For instance, as the best commercially available dielectric polymer, the biaxially oriented polypropylene (BOPP) can only deliver a low U_e (~ 5 J/cm³) near its E_b , limited by its low ϵ_r (usually < 3) (Chen et al., 2019). Compared with polymers, dielectric ceramics possess much higher ϵ_r . Therefore, a straightforward way is to fabricate composites by introducing ceramics into the polymers. The polymer composites comprising the high breakdown strength polymer matrix and the high dielectric constant ceramic fillers improve U_e via compositional tailoring.

Zero-dimensional (0D) ceramic nanoparticles were adopted as the high dielectric constant fillers for decades (Li et al., 2009; Kim et al., 2009; Mendes et al., 2011; Wang and Zhu, 2011; Zhou et al., 2011;

¹National & Provincial Joint Engineering Laboratory of Mining Intelligent Electrical Apparatus Technology, Taiyuan University of Technology, Taiyuan, Shanxi 030024, P.R. China

²College of Electrical and Power Engineering, Taiyuan University of Technology, No.79 West St Yingze, Taiyuan, Shanxi 030024, P.R. China

³Electrical Insulation Research Center, Institute of Materials Science, University of Connecticut, 97 N Eagleville Road, Storrs, CT 06269, USA

⁴College of Mechanical and Vehicle Engineering, Taiyuan University of Technology, Taiyuan, Shanxi 030024, P.R. China

⁵Lead contact

*Correspondence: y.wang@uconn.edu (Y.W.), leizhipeng@tyut.edu.cn (Z.L.)
<https://doi.org/10.1016/j.isci.2022.104837>



Yu et al., 2013b). However, through many experiments and theoretical studies, researchers found that high filler loading in nanocomposites is needed for high U_e , which increases the probability of filler agglomeration and phase separation from the polymer matrix. To achieve further enhanced ϵ_r with lower filler content, one-dimensional (1D) ceramic nanofibers with a high aspect ratio were developed to provide larger dipoles (Tang et al., 2012, 2014; Song et al., 2012; Tang and Sodano, 2013; Sodano et al., 2013). The well-aligned nanofibers that are perpendicular to the direction of the electric field can also improve the breakdown strength of polymer nanocomposites. Meantime, two-dimensional (2D) ceramic nanosheets with large bandgap (E_g), such as boron nitride, were introduced into nanocomposites to enhance their electrical insulation capability (Osada et al., 2006, 2011; He et al., 2009; Kim et al., 2014). Besides, the incorporation of ceramic fillers could cause air voids, inorganic-organic interfaces, and other defects, which increase the leakage current and decrease the E_b of nanocomposites. One effective way to address this issue is based on microscale surface engineering for the nanofillers (Pellerite et al., 2003; Spori et al., 2007; Schulmeyer et al., 2007; Paniagua et al., 2008; Iijima et al., 2009; Siddabattuni et al., 2011; Zhou and Yu, 2011; Choudhury, 2012; Schuman et al., 2012; Yu et al., 2013a; Rong et al., 2013; Niu et al., 2015a, 2015b, 2018). The surface modification for nanoparticles, via surfactant and covalent grafting, can facilitate their dispersion in the polymer matrix.

In addition to the composition adjustment, the rational design and elaborate control of the structure of inorganic fillers are also vital. For example, nanofillers with core-shell structure can reduce the energy loss and improve the discharged energy density of nanocomposites (Li et al., 2007, 2012; Ma et al., 2012; Yu et al., 2013c; Rahimabady et al., 2013; Gao et al., 2014; Zhang et al., 2014, 2019; Liu et al., 2015a, 2017a; Pan et al., 2016, 2017a; Wang et al., 2017c). In the recent decade, polymer dielectrics with optimized hierarchically layered structures have become an emerging approach to resolve the existing paradox between high dielectric constant and high breakdown strength in single-layered composite films, which resulted in substantial improvement in their capacitive energy storage performance (Wang et al., 2015a, 2017a, 2017b, 2018a, 2019a, 2020a; Chen et al., 2018a, 2019, 2020). Different from single-layered nanocomposites, layer-structured polymer composites enable to spatially regulate the distribution of the electric field, endowing them with high E_b even with high filler contents. The macroscale surfaces and interfaces in layered nanocomposites attract increasing attention, which triggers interfacial engineering by incorporating 2D materials with large E_g for achieving enhanced insulating capability (Azizi et al., 2017; Zhou et al., 2018; Zhu et al., 2019; Cheng et al., 2020; Wang et al., 2020b). This enables to interpose of high-aspect-ratio nanosheets as topological barriers to suppress the electrical conduction to improve the high-temperature capacitive properties.

This review addresses the recent advancements in the field of high-energy-density polymer dielectrics via compositional and structural tailoring for electrical energy storage. Correspondingly, section 2 presents the fundamental theory of dielectrics: polarization, breakdown, electrical conduction, and electrical energy storage. Section 3 illustrates the state-of-the-art polymer dielectrics for capacitive applications (i.e., ferroelectric polymers, linear polymers, and novel high-temperature polymers). Section 4 introduces polymer nanocomposites that incorporate nanofillers with different topologies, including nanoparticles (0D), nanofibers (1D), and nanosheets (2D). Then section 5 describes layer-structured all-organic polymer composites and ceramic/polymer composites. The surface/interfacial engineering conducted on both microscale and macroscale for polymer dielectrics is summarized in section 6. Finally, we present a summary and some future recommendations in section 7.

THEORY FOR DIELECTRICS

Polarization

Concept of polarization

Electric polarization refers to a phenomenon of inductive dipole moment in the dielectric under the action of an external electric field. After applying an external electric field, polarization charges appear at the dielectric surface that is vertical to the direction of the electric field, namely bound charges, which are opposite in polarity but equal in the magnitude to charges on the polar plate. The dipole moment is induced inside the dielectric, and the whole dielectric produces a macroscopic dipole moment not equal to zero. Owing to charges being bounded in atoms or molecules, the positive and negative charges in dielectric are relatively displaced at the microscopic scale when the dielectric is polarized.

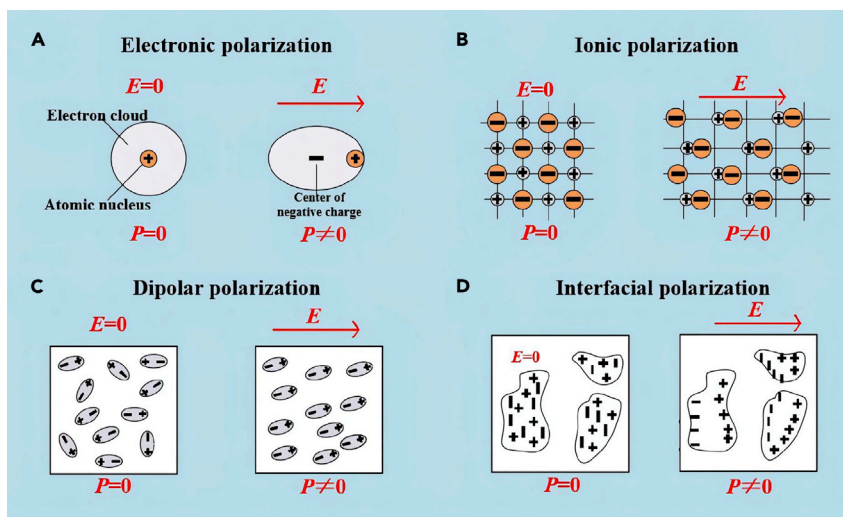


Figure 1. Polarization forms of dielectric in static electric fields

Adapted with permission (Li et al., 2021). Copyright [2022] Clearance Center, Inc. ("CCC").

A pair of electric dipoles consist of two heater charges with an equal charge quantity. The electric dipole moment μ is generated when the center of dipoles shifts under the action of the applied electric field, which can be represented as:

$$\mu = ql \quad (\text{Equation 2})$$

where q is the absolute value of the charge quantity of electric dipoles and l is the distance between positive and negative charge. The electric polarization, P , is the total dipole moments in a per unit volume of dielectric, which is represented as follows:

$$P = \frac{1}{V} \sum \mu \quad (\text{Equation 3})$$

Under the action of the applied electric field, the original chaotic dipole moment in the dielectric will be arranged along the direction of the applied electric field which is expressed as:

$$P = \chi \epsilon_0 E \quad (\text{Equation 4})$$

where χ is the polarizability, which reflects the polarization intensity and is an intrinsic characteristic of the dielectric. In a linear medium, P , is generally proportional to the electric field, E , in the same direction. According to Maxwell's electromagnetic equations, the electric displacement, D , can be described as:

$$D = \epsilon_0 \epsilon_r E \quad (\text{Equation 5})$$

Meanwhile, according to the definition of the potential shift, the relationship between D and P is:

$$D = \epsilon_0 E + P \quad (\text{Equation 6})$$

Polarization mechanism of dielectric

Dielectrics can be divided into nonpolar dielectrics and polar dielectrics, corresponding to the displacement polarization and the orientation polarization, respectively. Based on resonance and relaxation regimes, four typical electric polarization exist in dielectric materials, including electronic polarization, ionic polarization, dipolar (orientational) polarization, and interfacial (space charge) polarization. Electronic polarization and ionic polarization are displacement polarization. Dipolar polarization and interfacial polarization are orientation polarization. The macroscopic polarization phenomenon is a combination of several different polarization mechanisms. The response mechanism of four polarization types to the applied electric field in dielectrics is shown in Figure 1.

Electronic polarization

Electronic polarization refers to the deformation or translation of the originally symmetrical distribution of the electron clouds of atoms or molecules caused by the electric field. This is essentially the displacement

of the outer electron clouds for the inner positive atomic cores, which induces dipole moment along the direction of the electric field. Electron polarization exists in all dielectrics and is independent of temperature, but the polarization is lower than other polarization mechanisms.

Ionic polarization

Ionic polarization is caused by the relative displacement of ions in dielectric, which is widely found in ionic crystal materials. Under the action of the electric field, when the equilibrium state of the positive and negative ions in the dielectric is broken, the positive ions move along the electric field direction whereas the negative ions move in the opposite direction to form an induced dipole moment, resulting in ionic polarization. Like electron polarization, ionic polarization is independent of the temperature.

Dipole polarization

Dipole polarization occurs in materials containing molecules or particles with a permanent dipole moment. The electric field causes the reorientation of the dipoles toward the direction of the field. The molecular groups need a certain amount of energy to overcome the hindrance of adjacent molecules in this process, thus sensitive to the temperature. The higher the temperature, the stronger the electric dipole moment motion ability, resulting in a higher characteristic frequency.

Interfacial polarization

Interfacial polarization mainly occurs in materials with multiphase interfaces or inhomogeneous materials with defects, particles, and impurities. Under electric fields, the charges will move orientationally, but they cannot cross two sets of interfaces while accumulating at the phase interface of two materials or between two different regions of one material. Macroscopically, the dielectric constant increases rapidly. Therefore, interfacial polarization is the most obvious one among the four polarization mechanisms.

The time required for the establishment or disappearance of dielectric polarization is called the response time of polarization. The response time of electron polarization is about 10^{-14} – 10^{-16} s, and that of the ionic polarization is about 10^{-12} – 10^{-13} s. On the contrary, for orientation polarization, their response time is longer. The time required for the establishment of dipole polarization is about 10^{-8} – 10^{-2} s whereas that of interfacial polarization is longer, generally more than 10^{-1} s.

Dielectric breakdown

Dielectric breakdown is a form of dielectric failure in dielectric capacitors, mainly caused by the electrical conduction or mechanical structure failure of dielectric in a short time under the high electric fields, which eventually leads to the failure of the device. The insulation characteristics of dielectric materials can be maintained below a certain electric field strength. When the voltage applied to the dielectric exceeds a certain critical value, the dielectric insulation capability sharply decreases, and then breakdown occurs. The corresponding voltage is the breakdown voltage U_b and the corresponding field strength is E_b . Their relation is expressed as follows:

$$E_b = \frac{U_b}{d} \quad (\text{Equation 7})$$

where d is the thickness of the dielectric.

According to the mechanism of breakdown, the dielectric breakdown can be divided into three types: free volume breakdown, thermal breakdown, and electromechanical breakdown.

Free volume breakdown

Electrostatic breakdown refers to the accelerated movement of carriers in the dielectric under high electric fields. The energy or quantity of carriers will exceed certain critical values during collisions which will eventually lead to breakdown. The former is called intrinsic breakdown, while the latter is called electron avalanche breakdown.

Thermal breakdown

Under the applied electric field, the dielectric loss because of the electrical conduction and polarization produces heat. When the temperature exceeds a certain threshold, the thermal breakdown will occur. The thermal breakdown is mainly divided into two types: thermal instability and thermal runaway. The

former is that under high temperature, the physical structure of dielectric is changed thus causing the breakdown; and the latter is because of the continuous increase of the loss, which causes the temperature rise, resulting in runaway and final breakdown. The thermal equilibrium equation of dielectric is:

$$\rho C \frac{dT}{dt} - \lambda \nabla^2 T = \sigma E^2 \quad (\text{Equation 8})$$

where ρ and C are the density and heat capacity of the dielectric, and λ and σ are the thermal conductivity and electrical conductivity of the material, respectively. Obviously, in order to alleviate the thermal breakdown of the dielectric, it is necessary to improve the thermal conductivity and reduce the electrical conductivity of the material.

Electromechanical breakdown

The dielectric will undergo compression deformation under the applied electric fields so that the deformation becomes more and more significant by increasing the electric field intensity and the electromechanical breakdown will occur until the critical value is reached. According to the force balance of the dielectric before the breakdown, the theoretical strength of electrical breakdown, E_{em} , is as follows:

$$E_{em} = 0.606 \sqrt{\frac{Y}{\epsilon_0 \epsilon_r}} \quad (\text{Equation 9})$$

where Y is the Young's modulus of the dielectric. For polymer dielectrics, the increasing of temperature will not only bring about a significant increase in electrical conductivity, but also cause a decrease in Y , which is more susceptible to electrical breakdown. Therefore, in order to alleviate the electrical breakdown of the dielectric, it is necessary to raise Y of the dielectric.

Electrical conduction

The conduction current of dielectric materials is usually very small at a low electric field because of the lower conductivity on the order of 10^{-20} – 10^{-8} S/cm. When a relatively high electric field is applied to the dielectric film, the conduction current will be noticed and impacted by many different conductive mechanisms. At present, there are two types of conduction mechanisms in dielectric films, that is, electrode-limited conduction mechanism and bulk-limited conduction mechanism (Chiu, 2014).

Electrode-limited conduction mechanism

The electrode-limited conduction mechanism is related to electrical properties at the electrode-dielectric interface, in which the barrier height is the most important parameter. According to the charge injection conductive mechanism, the process of conduction can be divided into the crossing barrier and the tunneling barrier. The former includes Schottky (thermionic) emission and thermionic-field emission whereas the latter includes Fowler-Nordheim tunneling and direct tunneling. Schottky emission is a conduction mechanism that if the electrons in the metal can obtain enough energy provided by the thermal activation, they will overcome the potential barrier at the metal-dielectric interface to go to the dielectric, which is highly dependent on the temperature. The tunneling current is nearly temperature independent. Both Fowler-Nordheim tunneling and direct tunneling belong to the field emission mechanism. Fowler-Nordheim tunneling may occur if the applied electric field is high enough. The electron wave function may penetrate through the potential barrier into the conduction band of the dielectric. If the dielectric film thickness is thin enough, direct tunneling will also happen at a low electric field.

Bulk-limited conduction mechanism

The bulk-limited conduction mechanism is determined by the electrical properties of the dielectric itself, in which the trap energy level in dielectric films is the most important parameter. The bulk-limited conduction mechanisms include (1) Poole-Frenkel (P-F) emission, (2) hopping conduction, (3) ohmic conduction, (4) space-charge-limited conduction, (5) ionic conduction, and (6) grain-boundary-limited conduction. P-F emission, called the internal Schottky emission, is owing to the thermal activation under an electric field and the thermal excitation of electrons may emit from traps into the conduction band of the dielectric, and thus the conduction mechanism is often observed at high temperature and high electric field. The trapped electrons "hopping" from one trap site to another is called hopping conduction, which corresponds to the tunnel effect. In the dielectric film, the movement of mobile electrons in the conduction band and holes

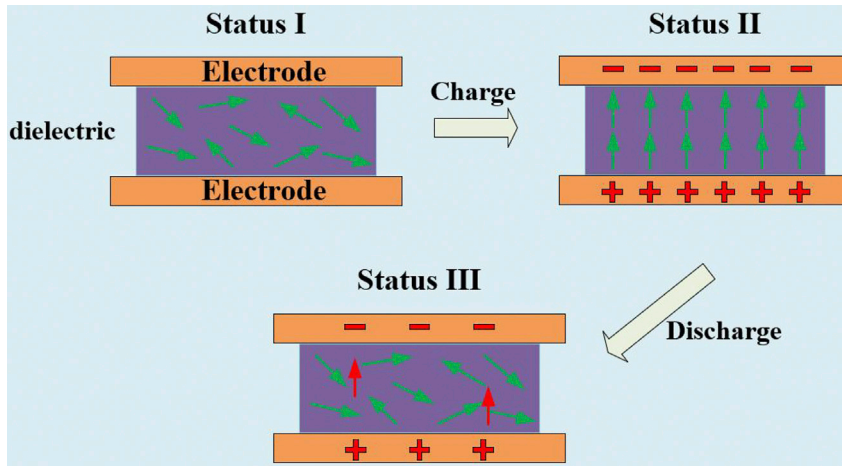


Figure 2. Schematic diagram of the charge and discharge process of the dielectric capacitor
(Green arrow represents the electric dipole moments. Status III: Red arrow represents some of the electric dipole moments still arranged in orientation after removing the electric field.)

in the valence band attributes to Ohmic conduction. For ionic conduction, ions jump over a potential barrier from one defect site to another under an applied electric field. Space-Charge-Limited Conduction is caused by the spatial charge accumulation at the electrode when the external electric field exceeds a certain threshold.

Electrical energy storage

The energy storage process of dielectric material is the process of dielectric polarization and depolarization when the external electric field is applied and withdrawn. The energy storage process of dielectric capacitors mainly includes three states, as shown in Figure 2. I: When there is no applied electric field, the dipole moment inside the dielectric is arranged in disorder and there is no net polarization. II: As the external electric field E is applied, the dipole moment inside the dielectric is arranged gradually to reach the maximum polarization intensity, and the macroscopic polarization charge is induced on the electrode surface to complete the process of energy storage. III: After removing the electric field because of the combined action of depolarization field and thermal motion produced by the internal dipole moment, the oriented dipole moment will return to the original random state, and the macroscopic polarization charge on the electrode will be reduced. At this time, the external release of electrical energy is completed. During charging (from I to II), the external circuit stores energy in capacitors is as follows:

$$U = \int_0^{D_{\max}} EdD \quad (\text{Equation 10})$$

During discharging (from II to III), the energy released from capacitors is as follows:

$$U_e = \int_{D_{\max}}^0 EdD \quad (\text{Equation 11})$$

where U is the charged energy density and U_e is the discharged energy density, namely the energy density. Because of the inevitable leakage loss and bound charge motion of all dielectrics during polarization, the energy consumption makes energy loss in the charge and discharge process. The U_e and the energy loss can be characterized by the electric displacement-electric field (D-E) loop, as shown in Figure 3. Capacitor charge-discharge efficiency (η) is usually used to describe the energy efficiency as follows:

$$\eta = \frac{U_e}{U} \times 100\% \quad (\text{Equation 12})$$

Hence, to obtain higher U_e , higher ϵ_r (enhancing D), higher E_b , and higher η (decreasing energy loss) are required.

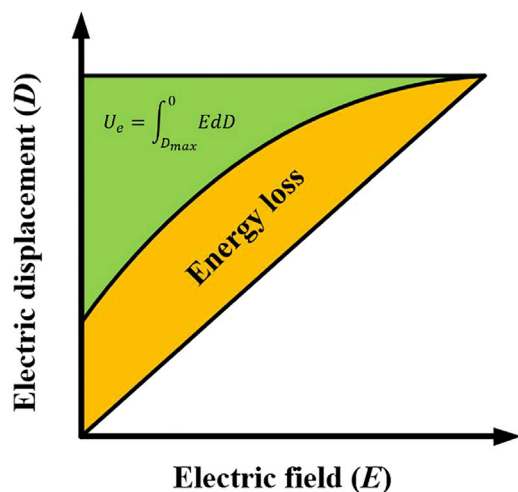


Figure 3. Schematic D-E loop of a dielectric material

POLYMER DIELECTRICS

Dielectric polymers are a class of organic compounds with high molecular mass composed of one or more monomers. Based on the polymer polarity and its dielectric properties at high electric fields, the polymer dielectric can be divided into four categories: ferroelectric, relaxor ferroelectric, antiferroelectric, and linear dielectric materials, which can be distinguished by the D-E loop tested by the ferroelectric analyzer, as shown in Figure 4. In this chapter, we mainly detail describe the chemical composition and structure of some ferroelectric polymers and their copolymers, linear polymers, and high-temperature dielectric polymers, with a summary of their key dielectric properties. To provide the readers with a more intuitive comparison, the key dielectric properties of the polymers are summarized in Table 1.

Ferroelectric polymer

Under the Curie temperature (T_c), ferroelectric polymers have spontaneous polarization, and the polarization direction can be redirected under the action of an electric field. However, when the temperature is higher than T_c , the ferroelectric phase changes to the paraelectric phase, and the spontaneous polarization disappears. Poly(vinylidene fluoride) (PVDF) and its copolymers are ferroelectric polymers that have been widely concerned and studied.

PVDF

PVDF is the polymer of vinylidene fluoride (VDF) and consists of $-\text{CH}_2-\text{CF}_2-$ repeating units with the chemical formula $(\text{CH}_2-\text{CF}_2)_n$ (Prateek et al., 2016). PVDF has the excellent UV resistance, the good thermal and chemical stability, and can be dissolved or swelled by a few chemicals. Compared with other dielectric polymers, PVDF has an exceptionally high ϵ_r and high E_b (~ 500 MV/m). Because of the high electronegativity and small size of fluorine atoms, PVDF has high dipole moment and packing density for C-F bonds to get superior ϵ_r (Li et al., 2014). PVDF is a semicrystalline polymer with multiple crystalline phases, namely,

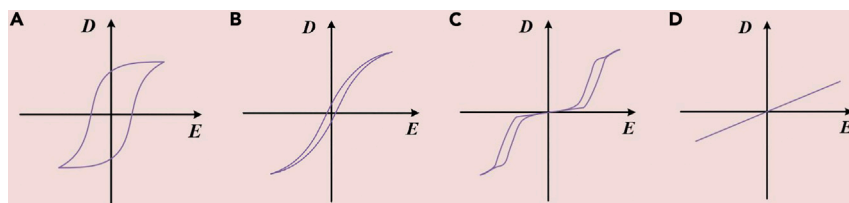


Figure 4. Schematic hysteresis loops

(A) normal ferroelectric.

(B) relaxor ferroelectric.

(C) antiferroelectric.

(D) linear dielectric materials. Adapted with permission (Yang et al., 2013). Copyright [2022] Elsevier.

Table 1. Dielectric properties of polymers

Polymer	Dielectric constant (1kHz)	loss tangent (1kHz)	Glass transition temperature (°C)	Dielectric breakdown strength (MV/m)	Energy density (J/cm ³)	Ref
BOPP	~2.25@20°C	~0.0001@20°C	< 0	496@120°C	1.28 @110MV/m 120°C and 10 Hz	(Zhou et al., 2018; Li et al., 2021)
PC	~2.25@25°C	~0.0001@25°C	~150-160	528@150°C	1.29@400MV/m 150°C and 10 Hz	(Zhou et al., 2018; Rabuffi and Picci, 2002; Li et al., 2021)
PPS	~3-3.1@25°C	~0.0003@25°C	~90	550@150°C	0.22 @400MV/m 150°C and 10 Hz	(Zhou et al., 2018; Rabuffi and Picci, 2002; Li et al., 2021)
PET	~3@25°C	~0.0002@25°C	~70-80	570@150°C	0.93 @400MV/m 150°C and 10 Hz	(Zhou et al., 2018; Rabuffi and Picci, 2002; Li et al., 2021)
PEN	~2.9-3@25°C	~0.0015@25°C	~125	550@150°C	1.41 @400MV/m 150°C and 10 Hz	(Zhou et al., 2018; Rabuffi and Picci, 2002; Li et al., 2021)
Kapton (PI)	~3.3-3.4@25°C	~0.0001@25°C	~360	314@150°C	0.82 @250MV/m 150°C and 10 Hz	(Li et al., 2015b; Ai et al., 2020; Li et al., 2021)
Ultem (PEI)	~3.2@25°C	~0.0001@25°C	~217	439@150°C	1.6 @400MV/m 150°C and 10 Hz	(Li et al., 2021; Li et al., 2015b; Li et al., 2019)
PEEU	~4.7@25°C	~0.0015@25°C	> 250	400@150°C	2.9 @400MV/m 150°C and 10 Hz	(Zhang et al., 2020a)
PEKK	~3.6@25°C	~0.003@25°C	155	468@70°C	2.37 @450MV/m 140°C and 10 Hz	(Pan et al., 2009)
PPEK	~3.5@25°C	~0.0063@25°C	~250	470@25°C	2.1 @450MV/m 190°C and 10 Hz	(Pan et al., 2010)
PEEK	~3.2@25°C	~0.0015@25°C	~150	290@150°C	0.5 @250MV/m 150°C and 10 Hz	(Ho and Jow, 2009; Li et al., 2021; Li et al., 2015b)
PVDF	10@25°C	0.04@25°C	-40	150-500 @25°C	14@500 MV/m 25°C and 10 Hz	(Li et al., 2010)
P(VDF-TrFE)	12@25°C	0.018@25°C	-	~160@25°C	1.13@130 MV/m 25°C and 10 Hz	(Hu et al., 2013)
P(VDF-HFP)	15@25°C	0.05@25°C	-90	~750@25°C	25 @700 MV/m 25°C and 10 Hz	(Zhou et al., 2009)
P(VDF-TrFE-CFE)	55@25°C	0.05@25°C	-	~400@25°C	10@400 MV/m 25°C and 10 Hz	(Chu et al., 2006b; Chen et al., 2007)
PMMA	~3@25°C	0.0418@25°C	107	240@25°C	1.5 @330 MV/m 25°C and 10 Hz	(Gross et al., 2007; Xie et al., 2013)

PVDF: poly(vinylidene fluoride); P(VDF-TrFE): poly(vinylidene fluoride-trifluoroethylene); P(VDF-HFP): poly(vinylidene fluoride-hexafluoropropylene); P(VDF-TrFE-CFE): poly(vinylidene fluoride-trifluoroethylene-chlorofluoroethylene); BOPP: biaxially-oriented polypropylene; PC: polycarbonate; PPS: polyphenylene sulfide; PET: poly(ethylene terephthalate); PEN: poly(ethylene naphthalate); PI: polyimide; PEI: polyetherimide; PEEU: poly(arylene ether urea); PEKK: poly(ether ketone ketone); PPEK: poly(phthalazinone ether ketone); PEEK: poly(ether ether ketone); PMMA: poly(methyl methacrylate); PPS: polyphenylene sulfide.

α -, β -, γ -, δ -, and ε -phases, based on different chain conformations (Martins et al., 2014). The majorly used polymers with conformations of TGTG' for α and δ , TTT for β , and T₃GT₃G' for γ phases, as shown in Figure 5.

The α -phase crystal patterns are usually obtained by PVDF melt under atmospheric pressure cooling conditions. In the α -phase, two chains with the *trans*-gauche conformation are packed in opposite directions. Therefore, the electric dipole moments formed by the electronegative H atom and the electronegative F

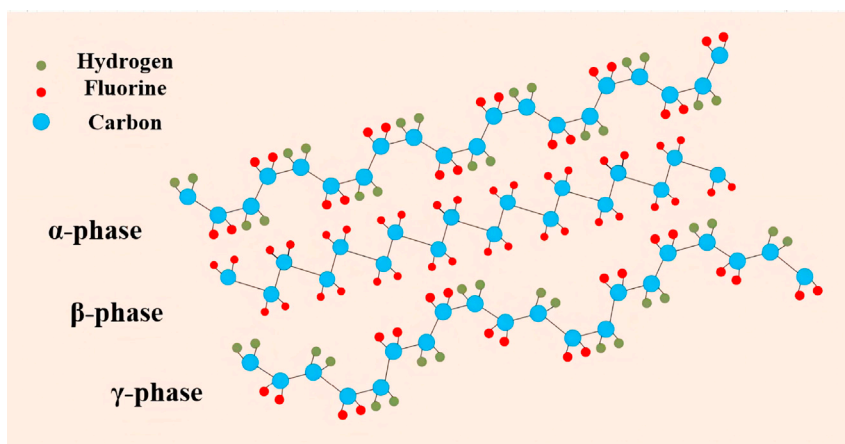


Figure 5. Schematic representation of the chain conformation for the α , β , and γ phases of PVDF. Adapted with permission (Ai et al., 2020). Copyright [2022] Elsevier.

atom are equal in magnitude and opposite in direction, which cancels each other out and causes a zero of macroscopic electric dipole moment and none external polarity.

The β -phase crystal can be obtained under melt stretching conditions. In the β -phase, there are two parallel and homo-aligned molecular chains, in which the electric dipole moment formed by the electronegative H atom and the electronegative F atom are in the same direction, thereby producing a high net polarization. The β -phase crystal is the stronger spontaneous polarization structure of all the crystals. The maximum polarization intensity of each cell is about 0.19Cm^{-2} . Thus, β -phase PVDF has good ferroelectric and piezoelectric properties. But the residual polarization of the β -phase crystal is also the highest, and the energy loss is great during the response of the external electric field. A facile process of pressing-and-folding is proposed to produce β -PVDF (β -phase content: $\sim 98\%$), which achieved an ultrahigh energy density (35J/cm^3) with a high efficiency (74%) in a pressed-and-folded PVDF (670–700 kg/mol), which is higher than that of other reported polymer-based dielectric capacitors (Meng et al., 2019).

When PVDF begins to crystallize from the initial state of melting, it mainly forms α -phase nonpolar crystals whereas the polar β -phase crystals are not easy to form directly. The α -phase crystals are generally converted into β -phase crystals by controlled annealing and low-temperature mechanical stretching. The β -phase film shows comparable efficiency and evidently higher energy density than the α -phase film at high fields (Yuan et al., 2020). Moreover, the α -phase crystals can be annealed at the high temperature to obtain a γ -phase crystal with polar crystallization, and the polarization treatment at high voltage makes up the ϵ -phase crystal with polar crystallizations (Xu, 2001). Among different types of PVDF, α -phase is nonpolar as the dipole moments cancel out each other whereas δ -, γ -, and β -phases exhibit high polarizability because of the presence of net dipole moments and hence have high dielectric constants as compared to α -phase. Compared with α -phase, the γ -phase with high maximum polarization with relatively low remnant polarization is the optimal configuration for dielectric energy storage.

P(VDF-TrFE)

To satisfy the increasing demands of high dielectric performance, different copolymers of PVDF, such as poly(vinylidene fluoride-trifluoroethylene) (P(VDF-TrFE)), have been developed for improving the PVDF properties (Martins et al., 2014). P(VDF-TrFE) is one of the most studied copolymers, as its electrical properties can be tailored by using high-energy irradiation or the addition of different monomer units (Yang et al., 2013). When VDF is copolymerized with trifluoroethylene (TrFE) or tetrafluoroethylene (TFE), the lateral dimensions of the unit cell are enlarged by the inclusion of bulky TrFE and TFE comonomers because of isomorphism. Intriguingly, the enlarged lateral dimensions of the unit cell weaken the intermolecular interactions among P(VDF-TrFE) chains and thermodynamically destabilize the ferroelectric phase with all-trans zigzag chain conformation. As a result, the ferroelectric-to-paraelectric T_c decreases from just below the melting temperature (T_m) for β -PVDF to temperatures significantly below the T_m depending on the TrFE content. Moreover, P(VDF-TrFE) (75/25 mol %) has relatively higher remnant polarization of about

7.5 $\mu\text{C}/\text{cm}^2$ than that of PVDF, which results in lower energy density (1.13 J/cm^3 at 1300 kV/cm) that may even reduce to zero, when the electric field becomes zero (Wang et al., 2010; Hu et al., 2013; Chu et al., 2006a). The dielectric constant of P(VDF-TrFE) has a higher value of about 18, compared with that of PVDF (6–12), with loss tangent of less than 0.1 at 1 kHz (Xu, 2001).

P(VDF-HFP)

The hexafluoropropylene (HFP) is introduced into the PVDF matrix to fabricate poly(vinylidene fluoride-hexafluoropropylene) (P(VDF-HFP)). P(VDF-HFP) with different content of HFP is obtained with a variety of attractive properties. The flexible PVDF with low HFP contents are thermoplastic as well as semicrystalline in nature. But the PVDF with higher HFP contents is amorphous and elastomeric. Besides, the remnant polarization decreases with increasing HFP content, which is similar to P(VDF-TrFE). When 5% of HFP is introduced into PVDF, the remnant polarization of P(VDF-HFP) is a maximum of 8 $\mu\text{C}/\text{cm}^2$ at 80 MV/m (Yang et al., 2013; Zhang et al., 1998; Jayasuriya et al., 2001). The polymer P(VDF-HFP) has a comparatively lower crystallinity than that of PVDF because of the presence of bulky CF_3 groups. P(VDF-HFP) films can achieve a higher energy density of 25 J/cm^3 at 700 MV/m (Zhou et al., 2009).

P(VDF-TrFE-CFE)

The PVDF terpolymers are based on P(VDF-TrFE) copolymer, such as poly-(vinylidene fluoride-trifluoroethylene-chlorotrifluoroethylene) (P(VDF-TrFE-CFE)) (Bharti et al., 1998). P(VDF-TrFE-CFE) has a comparatively higher interchain distance in comparison to P(VDF-TrFE) because of the addition of the bulky group, chlorofluoroethylene (CFE) so that the terpolymer shows relaxor ferroelectric behavior (Chen et al., 2013; Jeong et al., 2004; Jayasuriya et al., 2001). It is found that regions of low and high CFE contents have different effects on the terpolymer. Low CFE content shows all-trans conformation, whereas high content is associated with mixed chain conformation. With the increase of the CFE content from 0 to 9 mol % for the VDF/TrFE mole ratio between 64/36 to 75/25, the polymer shows relaxor ferroelectric behavior (Klein et al., 2005).

Linear polymer

BOPP

Features of linear dielectric such as high intrinsic E_b , low loss, and large E_g , are favorable for high-temperature applications. The main bottleneck of linear dielectric is their low ϵ_r , which needs to be increased without sacrificing E_b for achieving a high energy density (Fan et al., 2018).

BOPP is a state-of-the-art polymer dielectric material, mainly applied in high voltage and high frequency. BOPP has a high E_b of 730 MV/m and a low dielectric loss ($\tan\delta = 0.0003$). But, the maximum U_e of BOPP is about 5 J/cm^3 at ambient temperature and breakdown, because of its low ϵ_r ($\epsilon_r = 2.25$). Under high temperatures, the electrical conductivity of BOPP will sharply increase so its maximum operating temperature is on more than 105°C. For example, the DC volume electrical resistivity of BOPP measured at the electric field of 200 MV/m and 120°C is about $2.53 \times 10^{11} \Omega\text{m}$ (Zhou et al., 2018). Meanwhile, the U_e and η also significantly decrease under high temperatures. For example, U_e is about 2.43 J/cm^3 at ambient temperature, which decreases to 2 J/cm^3 at 100°C and 1.28 J/cm^3 at 120°C. η decreases from 99.3% to 80.5 and 52.1%, respectively (Zhou et al., 2018).

For many pulsed power systems and power electronics (Zhang et al., 2012), BOPP film capacitors are critical components to control and convert direct current from batteries into alternating current. At present, cooling systems are introduced into BOPP film capacitors of inverters in hybrid electric vehicles (HEVs) to solve the difference of BOPP's properties between ambient temperature and the maximum operating temperature. Usually, the environmental temperature is required to decrease from 140°C to 70°C (Li et al., 2015b). However, it is adverse for HEVs that the auxiliary cooling system brings extra weight and volume and make the design of power systems more complex, as well as the performance reduction of HEVs and the rise of manufacturing costs (Li et al., 2018).

PMMA

In the last decades, Poly(methyl methacrylate) (PMMA) is one of the most widely studied polymers, because of the favorable combination of chemical and physical properties and outstanding mechanical properties (Gross et al., 2007). PMMA has good thermal stability, optical clarity, and excellent weather and chemical resistance. Specific electrical properties of PMMA make it an appealing starting material

for the development of dielectric films. In addition, PMMA is widely used in high voltage applications because of its high resistance and non-tracking characteristics. Its dielectric constant is 3.7 and dielectric loss is 0.0418 at 1 kHz and 25°C whereas the dielectric constant is 2.6 at 1 MHz (Xie et al., 2013). Therefore, ϵ_r of PMMA is unstable and dependent on the temperature, which has been proved by dielectric constant measurements at the frequency from 400 Hz to 100 kHz and the temperature from 35°C to 80°C (Mittal et al., 2001). Meantime, the thickness of PMMA film also affects its electrical properties and the thickness dependence of the dynamics in thin films of isotactic PMMA was investigated (Ngaia, 2003; Rawlins et al., 1996). The breakdown strength of PMMA films with a thicknesses ($\sim 3 \mu\text{m}$) is about 240 MV/m (Paniagua et al., 2014). At ambient temperature, the electric displacement of PMMA is about $0.101 \mu\text{C}/\text{cm}^2$ at 10 Hz (Xie et al., 2013). In addition, U_e of PMMA films reaches $1.5 \text{ J}/\text{cm}^3$ at 330 MV/m (Prateek et al., 2016).

High-temperature polymers

The U_e of ferroelectric polymer matrix composites can reach more than $20 \text{ J}/\text{cm}^2$, but it should be noted that these excellent energy storage properties are mainly obtained at ambient temperature. The high-temperature environment can accelerate the aging of polymer materials, seriously affects the breakdown performance of polymer dielectric materials, and further impairs their energy storage performance and service life. In most practical application scenarios, such as new energy vehicles, power equipment, electronic systems, and so on, because the heat generated by the system operation cannot be dissipated in time, polymer-based dielectric materials must be operated above ambient temperature. Therefore, their temperature stability is crucial for system performance, safety, and service life. It is of great academic value and engineering significance to systematically study the effect of temperature on energy storage properties and to develop polymer-based dielectric materials with high-temperature resistance.

Currently, high-temperature polymer-based dielectrics are mainly focused on the search, design, and synthesis of high-temperature resistant polymer matrix with high glass transition temperature (T_g). It is found that the strong intermolecular and intramolecular interactions initiated within the polymer chemical structure by hydrogen bonds, conjugated polymer chains, aromatic/heterocyclic molecular frameworks, and high-strength chemical bonds (carbon-fluorine bonds, etc.) have a significant effect on enhancing the thermal stability of the polymer at high temperatures. Therefore, polymer materials with above chemical structures, such as polyimide (PI), polycarbonate (PC), polyphenylene sulfide (PPS), poly(ether ether ketone) (PEEK), and poly(ether ketone ketone) (PEKK), are resistant to higher temperatures and shows higher T_g .

PI and PEI

PI is a kind of polymer with a main chain containing imide structure, usually constructed by the polycondensation of dihydride and diamine monomers. PI has excellent heat resistance, chemical resistance, and good mechanical strength, which are mainly derived from PI's unique molecular chain structure. The imide structure in the backbone combined with the aromatic heterocyclic structure has a thermal decomposition temperature of up to 500°C. In addition, PI has not only a higher ϵ_r than that of polypropylene (PP) for engineering applications but also excellent insulation properties such as low loss factor, high E_b , and high volume resistivity. More importantly, because of PI's good thermal stability and excellent dielectric properties, it has great potential for high-temperature film capacitors.

Poly (ether imides) (PEIs), a modified version of PI, are amorphous dielectric polymers with improved processability at the expense of compromised thermal stability compared to PIs. The improved processability and reduced thermal stability are because of the presence of flexible ether linkages incorporated into the backbone of PEIs through the nucleophilic aromatic substitution of leaving groups from phthalic anhydride by bisphenol A.

PC and PPS

PC is a dielectric polymer synthesized from carbonic acids and dihydric alcohols and is mostly in the amorphous phase. The T_g of PC is around 150–160°C so the rating temperature of PCs is limited to approximately 150°C. The dielectric constant is about 3 with high stability over temperature (Li et al., 2021). For example, the temperature coefficient of the capacitance is only 2% at 125°C, and a low dielectric loss is about 0.1% at 1 kHz from 25°C to 125°C. In addition, PC exhibits an U_e of $1.29 \text{ J}/\text{cm}^3$ and a η of 47% at 400 MV/m (Prateek et al., 2016).

PPS consists of aromatic rings linked with sulfides and has been regarded as an ideal replacement for PC in high-temperature capacitor applications, because they have very similar dielectric properties, including a low dissipation factor and decent dielectric stability with temperature. The breakdown strength of PPS is 500 MV/m at elevated temperatures. At 150°C, PPS remained unchanged whereas the decrease ratio of breakdown strength relative to ambient temperature for PEI is about 16% and about 13% for PEEK (Ho and Jow, 2009). Notably, although the T_g ($\sim 120^\circ\text{C}$) of PPS is lower than other high-temperature polymer dielectrics, it can be used up to temperatures higher than T_g for film capacitor applications because of its high crystallinity of 60–65% and a high T_m of 285°C (Ho and Jow, 2009; Li et al., 2021). The low E-field conductivity of PPS is 6.90×10^{-14} S/m at 165°C and 1.72×10^{-11} S/m at 200°C (Ho and Jow, 2009).

PEEK and PPEK

PEEK is one of the most important members of the poly ketone family. PEEK is considered a high-temperature thermoplastic polymer and is known for its insulation performance against electrical coronas, where mineral fillers are usually added. Neat PEEK films are classified into amorphous and crystalline phases. A thermal stability study showed that amorphous PEEK has a lower T_g and is subjected to high shrinkage in comparison with crystalline PEEK when approaching its T_g (140°C) (Pan et al., 2010). PEEK are synthesized via a reaction between diphenylether and a mixture of benzene dicarboxylic acid halides. Poly(phthalazinone ether ketone) (PPEK) displays excellent stability in dielectric properties in the broad frequency and temperature range. Little change in the breakdown field (>440 MV/m) and discharge time has been observed in PPEK with an increase of temperature up to 150°C (Pan et al., 2010). Kepstan provided by Arkema is a commercialized PEEK copolymer with a T_g of 162°C. This PEEK can discharge an U_e of ~ 0.6 J/cm³ with an efficiency of 90% under an electric field of 200 MV/m and at 160°C (Tan et al., 2014). This performance is among the best in all high-temperature polymer dielectrics under comparable conditions.

Novel high-temperature polymers

Although high-temperature polymer dielectrics have high T_g to resist higher temperatures, the polymers are unable to efficiently impede electrical conduction under elevated temperatures and high electric fields (Ho and Greenbaum, 2018; Li et al., 2018). In the last decade, researchers have discovered and manufactured some novel high-temperature capacitive materials based on crosslinked polymers, flexible polymers with large E_g , and dipolar glass polymers. They exhibit superior electric discharging performance to the current dielectric polymers at high temperatures.

Crosslinked polymers

Crosslinking is an effective way to reduce conduction loss and increase the energy storage performance of dielectrics at high temperatures. The molecular trapping centers created by the crosslinked structures can effectively limit charge transport and reduce conduction loss at elevated temperatures and high applied electric fields. Li et al. (2020a, 2020b) introduced a new class of all-polymer-based high-temperature dielectric materials prepared from crosslinking of melt-processable fluoropolymers. The crosslinked polymers exhibit excellent capacitive stability over 50,000 charge-discharge cycles at 150°C and discharge a stable power density over a wide temperature range. The implementation of melt-extrudable polymers would enable scalable processing that is compatible with the current fabrication techniques used for polymer dielectrics, which is in sharp contrast to the dielectric polymer composites with inorganic fillers. Furthermore, the structure tunability and designability of polymers and crosslinking chemistry will allow the further development of novel high-temperature energy materials for compact, lightweight, and robust energy storage systems.

Flexible polymers with large bandgaps

The dominant role of E_g was found in determining the electrical conduction and intrinsic breakdown strength of the polymer dielectrics (Chen et al., 2015a, 2018b; Sun et al., 2012). However, conventional high-performance polymer dielectrics generally have conjugated aromatic backbones, leading to limited E_g and hence high conduction loss and poor energy densities, especially at elevated temperatures. Wu et al. (2020) introduce an all-organic polymer, polyoxafluoronor-bornene (POFNB), with saturated fused bicyclic structure in the backbone, rather than the aromatic structures, to break the aforementioned design constraint. In POFNB, the nonplanar structure avoiding π - π stacking and nonconjugated polymer backbones could restrict charge mobility between and along polymer chains concurrently. With this strategy,

large E_g (4.9 eV) and high T_g (186°C) are achieved, making POFNB an outlier compared to common high-temperature polymers. The flexible polymers with large E_g offer intrinsically stable and temperature invariant high electric field dielectric characteristics, especially at elevated temperatures because of their large E_g and high T_g .

Dipolar glass polymers

The isolated molecular dipoles of dipolar glass polymer exhibit weak dipole-dipole interactions because of the limited amount of free volumes in glassy polymers (Binder, 1986). Most dipolar glass polymers contain highly polar groups such as nitrile (dipole moment of 3.9 D) (Bendler et al., 2013), and sulfone (dipole moment of 4.5 D) groups (Wei et al., 2015). These dipolar glass polymers have high dielectric constants in the range of 4–15. But, the T_g of dipolar glass polymers is relatively low and cannot meet the requirement of 150°C for operation. The post-polymer functionalization is a novel effective method to attain high T_g dipolar glass polymers. Zhang et al. (2018d) synthesized a new class of high-temperature dipolar polymer, sulfonylated poly (2,6-dimethyl-1,4-phenylene oxide) (SO₂-PPO), showing enhanced dielectric performance. Because of efficient rotation of highly polar methylsulfonyl side groups below T_g (~220°C), enhanced dipolar polarization and thus high dielectric constant was obtained for these SO₂-PPOs. Consequently, the discharged energy density reached as high as 22 J/cm³. Moreover, SO₂-PPO₂₅ also exhibited a low dielectric loss with a dissipation factor of 0.003 and a high discharge efficiency at 800 MV/m of 92%. These dipolar glass polymers are promising for high temperature, high energy density, and low loss electric energy storage applications.

POLYMER NANOCOMPOSITES WITH CERAMIC NANOFILLERS

In order to achieve high U_e , dielectric materials must have high E_b and high ϵ_r , but it is difficult for a single dielectric material to satisfy two performances at the same time (Wang and Zhu, 2011; Chen et al., 2015b). At present, constructing polymer nanocomposites with ceramic nanofillers is an effective way to obtain high U_e . The composite material inherits the advantages of each component material so that nanocomposites acquire the complementary performance of each component (Zhou et al., 2011; Tang and Sodano, 2013; Luo et al., 2014, 2020; Tang et al., 2014; Fu et al., 2015; Zhang et al., 2015; Cai et al., 2017, 2018). The method is to fill ceramic particles with high ϵ_r into high E_b polymer matrix to form ceramic/polymer composites with high energy storage density. The ceramic materials filled in composites can be divided into nanoparticles (0D), nanofibers (1D), and nanosheets (2D) according to their spatial dimensions. The corresponding composite structure types are 0–3 composites, 1–3 composites, and 2–3 composites, in which the polymer matrix is a three-dimensional structure.

Nanoparticle (0D)

0D ceramic particles are generally spherical. The earliest way to prepare 0–3 ceramic/polymer composites is to fill ceramic particles directly into the polymer matrix. Ceramic particles with high dielectric constant, such as TiO₂ (TO), ferroelectric dielectric ceramic BaTiO₃ (BT), and so on, are considered as excellent nanofillers. Yu et al. (2013b) prepared homogeneous nanocomposites comprising surface-modified BT nanoparticles and PVDF polymer matrix, as shown in Figure 6A. As the volume fraction of BT increases, the dielectric constant of nanocomposites increases and then decreases, as shown in Figure 6B. However, it can be seen that the ceramic/polymer nanocomposites with high ϵ_r are obtained only under the condition of high volume fraction filling, which causes the decrease of electrical breakdown strength. The significant enhancement of the energy storage performance in the nanocomposites was achieved at a BT content of 10 vol % (i.e. the calculated energy density was enhanced to 6.8 J/cm³), as shown in Figure 6C. This could be explained by the agglomeration of nanoparticles and the increased air voids when the content of ceramic fillers is high, which results in nonuniform electric field in the polymer matrix (Kim et al., 2009). Hao et al. (2017) prepared P(VDF-HFP)-based nanocomposites by introducing BT nanocrystals into the polymer matrix to realize both the high ϵ_r and E_b . They had reported that smaller-sized nanocrystals could benefit to the alleviation of interfacial electric field strength between fillers and polymer matrix. The nanocomposite films with BT nanocrystal a volume fraction less than 40% presented high discharged energy density and a maximum discharged energy density value of 9.7 J/cm³ was obtained for the nanocomposite film with a volume fraction of 30%, as shown in Figure 6D. When the nanocrystal loading is further increased, although the higher electric displacement is obtained, the discharged energy density drops sharply because of the high leakage current and the low E_b .

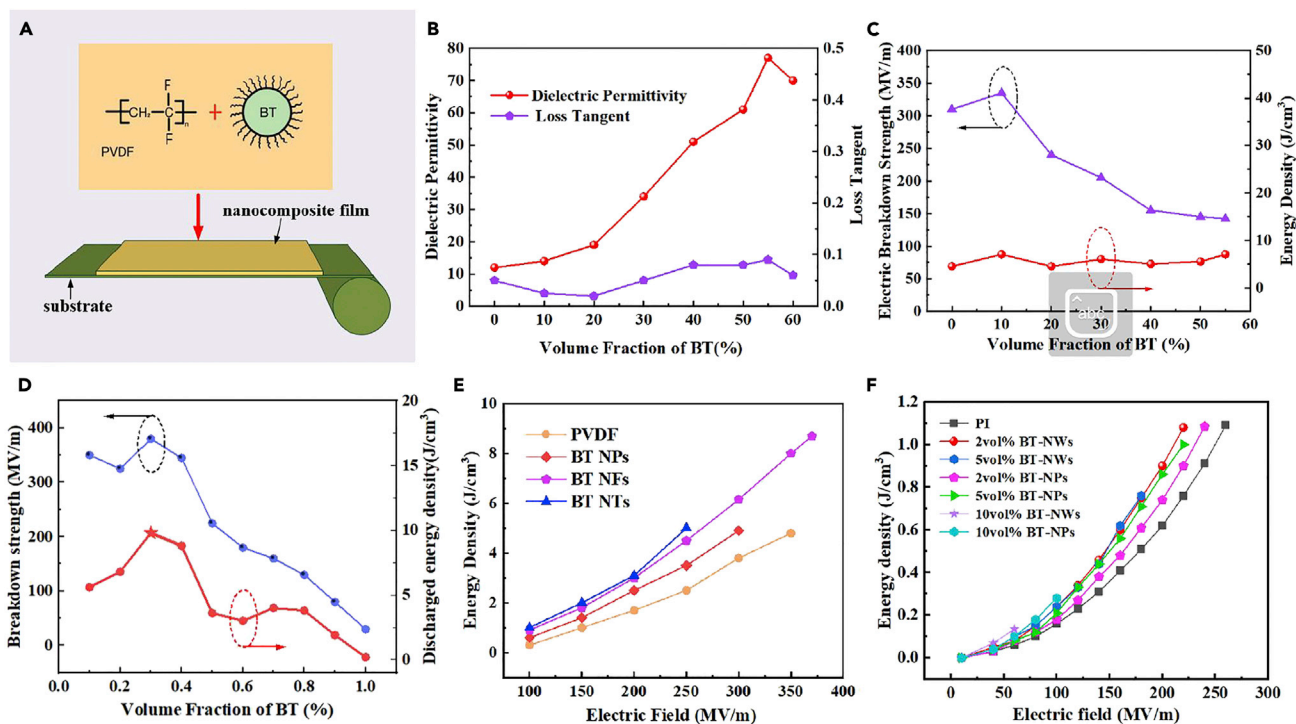


Figure 6. Polymer nanocomposites with 0D ceramic nanofillers

(A) The schematic of the fabrication of BT/PVDF nanocomposite films using a solution casting processing. Adapted with permission (Yu et al., 2013a).

Copyright [2022] John Wiley and Sons.

(B) The dielectric constant and loss tangent, and (C) the electric breakdown strength and energy density of nanocomposites with the treated BT as a function of the volume fraction of BT, measured at 1 kHz. Adapted with permission (Yu et al., 2013b). Copyright [2022] John Wiley and Sons.

(D) Breakdown strength and maximum discharged energy density variation related to the BT volume fraction. Adapted with permission (Hao et al., 2017). Copyright [2022] Elsevier.

(E) Energy density of pure PVDF and nanocomposites filled with 4 vol % BT NTs, BT NFs and BT NPs. Adapted with permission (Pan et al., 2017d). Copyright [2022] American Chemical Society.

(F) Energy density of pure PI and BT/PI nanocomposites filled with the same content BT-NPs and BT-NWs (2 vol %, 5 vol %, and 10 vol %). Adapted with permission (Wang et al., 2015b). Copyright [2022] Elsevier.

Generally, the ceramic/polymer nanocomposites for energy storage applications are divided into three categories according to the volume ratio of filled ceramic particles: high fill volume ratio polymer-based nanocomposites with volume ratio greater than 50 vol %, medium fill volume ratio polymer-based nanocomposites with volume ratio of 10–50 vol % and low fill volume ratio polymer-based nanocomposites with volume ratio less than 10 vol %. Among them, the medium-filled volume ratio of polymer-based nanocomposites can balance the relative dielectric constant and E_b of polymer-based nanocomposites while increasing the relative dielectric constant and avoiding the sharp decrease of E_b . Although the low fill volume ratio polymer-based nanocomposites are mainly used in the field of high voltage insulation because E_b does not decrease too much with the low fill concentration. Compared with these two categories, although ϵ_r is increased, E_b of the high fill volume ratio of polymer-based nanocomposites is extremely decreased. Thus, polymer nanocomposites with high energy storage density cannot be realized by increasing the filling ratio of nanoparticles in practical applications.

In addition to the filling ratio of nanoparticles, the size of ceramic particles filled into the polymer matrix will also affect the energy storage density of composites. PVDF/BT composites with different sizes and contents of BT particles were prepared by solution casting (Mendes et al., 2011). To determine the appropriate particle size of ceramic particles, the high-energy-density nanocomposite films were prepared by introducing the final size ferroelectric nanocrystals into the polymer matrix for the first time. The researchers found that BT nanocrystalline fillers with good dispersion and an average particle size of 6.9 nm are advantageous to improve dielectric properties and enhance the energy storage density (Hao et al., 2017). However, it should be noticed that smaller particles lead to larger interaction areas between the ceramic filler

and the polymer matrix whereas ceramic particles tend to aggregate with each other to reduce surface energy, which leads to the decrease of ϵ_r and the increase of E_b .

For ceramic/polymer composites, the dielectric constant of the polymer matrix is also of great importance for nanocomposites. The nanocomposites with high U_e need to rationally select a combination of polymer matrix and nanoparticles with balanced dielectric properties. Li et al. (2009) introduced TO nanoparticles into P(VDF-TrFE-CTFE) and P(VDF-CTFE) to fabricate nanocomposites, separately. The P(VDF-TrFE-CTFE)-based nanocomposite containing 10 vol % TO nanoparticles exhibits a much higher U_e than the nanocomposite based on the P(VDF-CTFE) matrix. This is because P(VDF-TrFE-CTFE) and TO fillers possess comparable dielectric constants of 42 and 47 at ambient temperature and 1 kHz, respectively. Similarly, the energy density of P(VDF-TrFE-CTFE) nanocomposites has a strong dependence on the TO concentration. The nanocomposite loading with 10 vol % TO nanoparticles shows a maximal U_e of 6.9 J/cm³. But, a further increase in the TO concentration leads to decreased U_e .

Nanofibers (1D)

The incorporation of 0D nanoparticles into composites can improve ϵ_r at the expense of E_b , which in turn limits the energy density of the capacitor. Thus, the integration and geometry of nanofillers should be optimized along with the filler to reach the highest possible U_e of nanocomposites (Sodano et al., 2013). Compared with 0D nanoparticles, 1D materials (e.g., nanowires, nanofibers, nanorods, and nanotubes) could provide the highest polarizability and E_b (Pan et al., 2017c). One possible reason is that the 1D material with a large aspect ratio could be more significantly improved in terms of the dielectric constant of nanocomposites. Besides, the 1D material has a smaller specific surface, which can help to reduce the surface energy and thus prevent the agglomeration of nanofillers in the polymer matrix (Song et al., 2012). For instance, different BT nanostructures (e.g., nanoparticles, nanofibers, nanotubes) were synthesized and used to prepare polymer composite films in the PVDF matrix (Pan et al., 2017c). Obviously, the energy density of nanocomposites filled with BT nanotubes/nanofibers (BT-NTs/BT-NFs) is higher than BT nanoparticles (BT-NPs), as shown in Figure 6E. Besides, BT nanowires/PI (BT-NWs/PI) and BaTiO₃ nanoparticles/PI (BT-NPs/PI) composites with different volume fractions of ceramic fillers were successfully prepared. Compared with BT-NPs/PI composites, the energy density of composites filled by BT-NWs was higher at the same concentration (Wang et al., 2015b), as shown in Figure 6F.

The various types of 1D nanofillers have different inherent characteristics and there will be discussed four main nanofillers, including linear, ferroelectric, paraelectric, and relaxor-ferroelectric nanofillers. Because of the high polarization responses and high D_{\max} , 1D ferroelectric nanofillers are one of the most widely used nanofillers inside polymer nanocomposites. Wang et al. (2015a) selected a series of surface-modified nanowires with different inherent characteristics to fabricate the P(VDF-HFP)-based nanocomposites. Four nanowires, including non-ferroelectric Na₂Ti₃O₇ nanowires (NTO NWs) and TiO₂ nanowires (TO NWs), ferroelectric BT NW, and paraelectric SrTiO₃ nanowires (ST NWs), were synthesized respectively and then functionalized by dopamine. As a result, compared with ST NWs, TO NWs, and NTO NWs, the P(VDF-HFP)-based nanocomposites with DA-modified BT NWs reveal the best potential in the dielectric constant and discharged energy density. However, the charge-discharge efficiency of nanocomposites with 1D ferroelectric nanofillers is limited by their high remnant polarization and thus does not meet the application demand.

Except for high remnant polarization, another drawback of 1D ferroelectric nanoparticles is the wide D-E loop, which leads to large energy loss. Therefore, 1D relaxor-ferroelectrics nanofillers with intrinsically thinner D-E loop, such as were incorporated to reduce the energy loss and improve the charge-discharge efficiency of nanocomposites (Liu et al., 2016; Chi et al., 2017, 2018; Zhang et al., 2018a; Pan et al., 2017b). Nevertheless, because of the low E_b , the energy density of nanocomposites with 1D relaxor-ferroelectric nanofillers ranged between 6 and 9 J/cm³, which is still lower than that of 1D ferroelectric nanofillers.

The advantages of 1D paraelectric nanofillers are the lower remnant polarization and higher maximum polarization, which can compensate for the shortcomings of 1D ferroelectric nanofillers. The lower remnant polarization and larger maximum polarization can translate into maximum discharge energy density and charge-discharge efficiency (Wang et al., 2015c), as shown in Figure 7A. For example, the fabricated P(VDF-CTFE)-based nanocomposites containing a 3 vol % of paraelectric ST NWs exhibit an enhanced U_e of 8.8 J/cm³ at 338.1 MVm, which exceeds some reported at the same electric field. By direct comparison

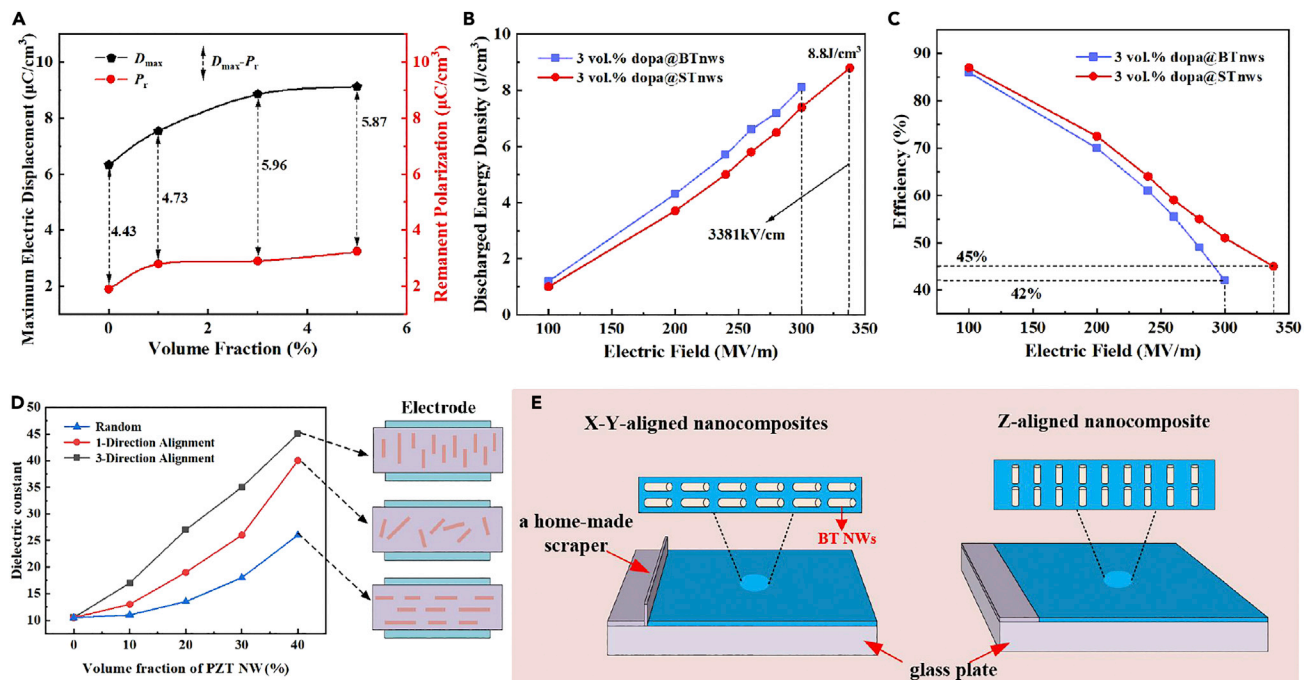


Figure 7. Polymer nanocomposites with 1D ceramic nanofillers

(A) The ($D_{max}-P_r$) values of the P(VDF-CTFE)-based nanocomposites with different amounts of STnws versus the maximum electric field. Adapted with permission (Zhang et al., 2018b). Copyright [2022] Elsevier.

(B) The discharged energy density and (C) efficiency of the nanocomposites with 3 vol % STnw and BTnw. Adapted with permission (Zhang et al., 2018d). Copyright [2022] Elsevier.

(D) Comparison of measured dielectric constant (at 1 kHz) of nanocomposites under different orientations (Random, 1-Direction Alignment, and 3-Direction Alignment) as a function of PZT NW volume fraction. Adapted with permission (Tang et al., 2012). Copyright [2022] John Wiley and Sons.

(E) Schematic illustration of X-Y-aligned nanocomposite and Z-aligned nanocomposite. Adapted with permission (Xie et al., 2017). Copyright [2022] Clearance Center, Inc. ("CCC").

with ferroelectric BaTiO₃ nanowires fillers, the result shown paraelectric ST NWs can simultaneously improve the breakdown strength, the maximum discharged energy density, and make a higher efficiency (Zhang et al., 2018b), as shown in Figures 7B and 7C.

The 1D linear nanofillers (like 1D TO) could enhance D_{max} at the high electric field because of the large area enclosed between D-E loops and the vertical D-axis. Meantime, a small dielectric difference between the linear fillers and polymers (like TO and PVDF) contributes to achieving higher E_b and U_e in the final nanocomposites. For example, the dielectric breakdown strength of 2.5 vol % TO NWs/P(VDF-HFP) nanocomposites reached 520 MV/m because of the great compatibility between polymer and filler (Wang et al., 2017a, 2017b). In practical experiments and applications, the orientation of 1D nanofillers inside a polymer is of great importance, because the alignment affects the dielectric, ferroelectric and energy storage performances of nanocomposites (Zhang et al., 2018c; Andrews et al., 2010; Tang et al., 2012). In early research, Tang et al. (2012) prepared nanocomposites with the aligned PbZrTiO₃ nanowires (PZT NWs) and samples with randomly dispersed PZT NWs to investigate the effect of the filler orientation on the energy storage properties of nanocomposites. Under three different orientations (random, 1-direction alignment and 3-direction alignment), the dielectric constant of the nanocomposites with various volume fractions of PZT NWs, is shown in Figure 7D. The results demonstrated that the dielectric constant of 3-direction aligned PZT NW samples are much larger than that of random and 1-direction aligned PZT NW samples at the same volume fraction.

In further research, Xie et al. (2017) tuned the alignment of BT NWs in the P(VDF-CTFE) matrix. The nanocomposite with nanowires aligned in the direction of the applying electric field (z axis) is noted as Z-aligned nanocomposite whereas X-Y-aligned nanocomposite refers to nanowires aligned perpendicular to the applying electric field, as shown in Figure 7E. Compared with the pure P(VDF-CTFE), the energy density

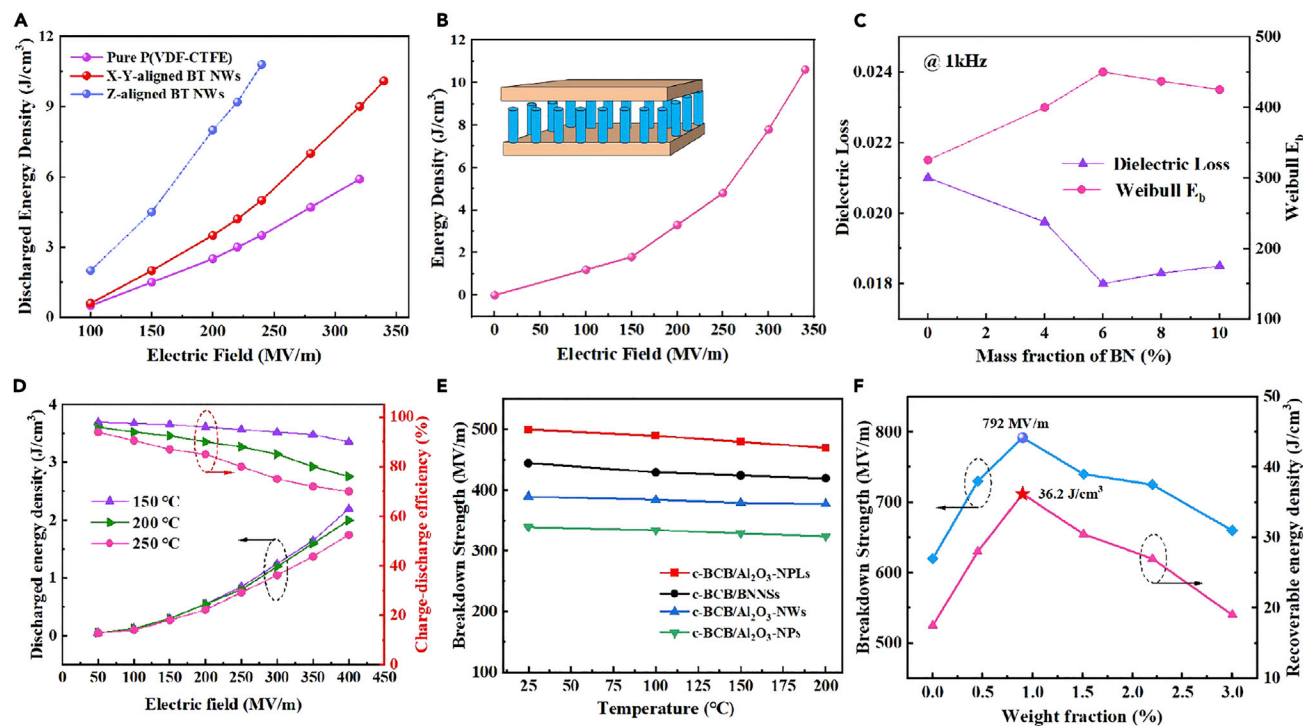


Figure 8. Polymer nanocomposites with 2D ceramic nanofillers

(A) The discharged energy density of pure P(VDF-CTFE), X-Y-aligned BT NWs, and Z-aligned BT NWs nanocomposites. Adapted with permission (Yao et al., 2016). Copyright [2022] American Chemical Society.

(B) The energy density of TNA/PVDF nanocomposites with 18% height ratio fillers. Adapted with permission (Yao et al., 2016). Copyright [2022] American Chemical Society.

(C) Dielectric loss and breakdown strength of RCH/BN composites measured at 1kHz as a function of BN content. with different content of BN. Adapted with permission (Wang et al., 2020c). Copyright [2022] Elsevier.

(D) The discharged energy density and charge-discharge efficiency of c-BCB/BNNS nanocomposite measured at 150°C, 200°C, and 250°C. Adapted with permission (Li et al., 2015b). Copyright [2022] Springer Nature.

(E) Temperature-dependent breakdown strength of the nanocomposites filled with BNNSs, Al₂O₃-NPs, Al₂O₃-NWs and Al₂O₃-NPLs. Adapted with permission (Li et al., 2019). Copyright [2022] John Wiley and Sons.

(F) CNO nanosheet weight fraction dependence of the breakdown strength and the corresponding maximum recoverable energy density. Adapted with permission (Bao et al., 2020). Copyright [2022] John Wiley and Sons.

of X-Y-aligned nanocomposite increased (10.1 J/cm³ at 340 MV/m). Meantime, Z-aligned nanocomposite could exhibit an enhanced U_e of 10.8 J/cm³ and discharge efficiency of 61.4% at a lower electric field of 240 MV/m, as shown in Figure 8A. Obviously, the energy storage properties of Z-aligned nanocomposites are superior to X-Y-aligned nanocomposites. In addition, the significantly enhanced energy density in nanocomposite capacitors combining the TiO₂ nanorod array (TNA) with PVDF has been achieved (Yao et al., 2016). The maximum U_e of TNA/PVDF nanocomposites with 18% height ratio fillers is 10.62 J/cm³ under a breakdown strength of 340 MV/m, as shown in Figure 8B. More importantly, the way does not need any modification of the surface or some other complicated treating process.

Nanosheets (2D)

With the continuous improvement of the manufacturing process, the application of 2D nanosheets is becoming more and more extensive. 2D nanosheets have higher breakdown strength and lower dielectric loss than the other two ceramic nanofillers (Li et al., 2019; Ji et al., 2019; Feng et al., 2017; He et al., 2009; Wang et al., 2019b, 2019c). Usually, to compensate for the decrease in E_b caused by introducing the nanoparticles with high ϵ_r , 2D nanosheets, such as 2D montmorillonite (MMT) and hexagonal boron nitride nanosheets (BNNS), are employed for their capability of improving E_b of polymer matrix.

Boron nitride nanosheets

Hexagonal boron nitride (BN), a layered structure similar to graphite, is a wide E_g (ca. 6eV) insulator with an E_b of 800 MV/m (Wu et al., 2018a; Zhang et al., 2020a). Therefore, the introduction of BNNS is beneficial to improve the E_b markedly, and the excellent insulating and mechanical properties can also decrease the energy loss (Wang et al., 2020a; Li et al., 2015a). Wang et al. (2020a) fabricated flexible film based on regenerated chitin and BNNSs. Taking 1 kHz as an example, the dielectric loss decreased from 0.021 of the neat regenerated chitin (RCH) film to only 0.018 of the composites filled with 6 wt % BN (RCH-BN6), and the maximum value of breakdown strength is 451 MV/m in RCH/BN composite film with 6 wt % BN loading, as shown in Figure 8C. Besides, Li et al. (2015a) utilized ferroelectric P(VDF-TrFE-CFE) terpolymers incorporated with ultra-thin BNNSs to prepare P(VDF-TrFE-CFE)/BNNS nanocomposites. It is found that U_e and η of P(VDF-TrFE-CFE)/BNNS nanocomposites remarkably improved in comparison to the pristine terpolymer.

The working temperatures of polymer dielectrics usually are always low because of the dramatically increased electrical conduction at elevated temperatures. However, researchers found that the dielectric properties of polymer nanocomposites filled with BNNSs are stable over a broad temperature and frequency range, which is attributed to its excellent thermal properties. The ultrahigh thermal conductivity of BNNS makes polymer nanocomposites achieve satisfying energy storage properties at different elevated temperatures by adjusting the matrixes (Xu et al., 2019; Hu et al., 2021; Li et al., 2015b; Liu et al., 2017a). For example, by thermally crosslinked divinyltetramethyldisiloxane-bis(benzocyclobutene) (BCB), Li et al. (2015b) made the crosslinked c-BCB/BNNS nanocomposite which is of both high discharged energy density and ultrahigh charge-discharge efficiency at 150°C, 200°C, and 250°C, as shown in Figure 8D. In addition, Xu et al. (2019) prepared the nanocomposites by anchoring poly(aryl ether sulfone) (DPAES) on the surface of functionalized BNNSs (BN-BCB), which obtain a giant discharged energy density (2.7 J/cm³) and high charge-discharge efficiency (>90%) at 150°C and 400 MV/m.

2D oxide ceramic materials

2D oxide ceramic fillers also reveal obvious advantages in improving the energy storage properties of polymer nanocomposites, including electroneutral nanoplates and nanosheets, and negatively charged nanosheets. Electroneutral nanoplates (like BT nanoplates (BT-NPLs) and Al₂O₃ nanoplates (Al₂O₃-NPLs)) as fillers effectively improve the breakdown strength by alleviating the concentration of local electric fields under high external electric fields and elevated temperatures (Shen et al., 2016; Li et al., 2019; Wen et al., 2019). Li et al. (2019) fabricated c-BCB-based nanocomposites filled with BNNSs and various types Al₂O₃ nanoparticles of Al₂O₃ nanofillers (Al₂O₃ nanoparticles (Al₂O₃-NPs), Al₂O₃ nanowires (Al₂O₃-NWs), Al₂O₃-NPLs), among which c-BCB/Al₂O₃-NPLs nanocomposites with the same filling content have the highest E_b of 482 MV/m at 200°C, as shown in Figure 8E. At present, compared with single metal oxides easily prepared by a hydrothermal reaction (Zhu et al., 2018; Li et al., 2019), the preparation of multiplex metal oxides usually needs a one-step or two-step molten salt method (Wang et al., 2018a, 2019a; Fu et al., 2020; Pan et al., 2019).

Similarly, the introduction of negatively charged nanosheets is an effective way to improve E_b , resulting in enhanced energy density and lower energy loss. More importantly, most of those flexible polymer nanocomposites with high energy density are obtained by only adding a small loading of negatively charged 2D nanosheets along with concurrent improvements of breakdown strength. For example, the significantly enhanced E_b of 792 MV/m and the record-high recoverable energy density of 36.2 J/cm³ are reported in PVDF-based nanocomposite capacitors with negatively charged C_{a2}Nb₃O₁₀ (CNO) nanosheets (Bao et al., 2020), as shown in Figure 8F. According to the phase-field simulations, the local electric field contributes to the enhanced breakdown strength which is produced by the negatively charged CNO nanosheets sandwiched with the positively charged PEI. Because it suppresses the secondary impact-ionized electrons and blocks the breakdown path in nanocomposites, thus preventing a complete breakdown of nanocomposites.

2D multiphase materials

Although the incorporation of single 2D nanofillers enhances the energy density to a certain degree, the nanocomposites are still unsuitable for energy storage because of high energy loss of high ϵ_r fillers or low polarization of highly insulating fillers. To further enhance the energy density and meet the need for energy storage applications, multiphase 2D nanofillers are introduced into the polymer matrix in

single-layered polymer nanocomposites (Liu et al., 2020; Wang et al., 2018b; Ke et al., 2019; Zhu et al., 2020; Feng et al., 2019; Deng et al., 2019; He et al., 2018; Luo et al., 2018; Li et al., 2019; Song et al., 2020) or different 2D materials are filled separately into multilayer-structured nanocomposites (Guo et al., 2020; Chi et al., 2019; Wu et al., 2018a; Liu et al., 2017b; Shen et al., 2015).

In single-layered polymer nanocomposites, the 2D multiphase systems with both conductive 2D fillers and relatively insulating fillers enable to achieve both high ϵ_r and low loss tangent (Ke et al., 2019; Zhu et al., 2020). Ke et al. (2019) prepared the thermoplastic polyurethane (TPU) composites by filling hybrids of carbon nanostructures (CNS, also known as branched carbon nanotubes) and graphene nanoplatelets (GNP). The results demonstrated improved dielectric properties (i.e. dielectric constant of 10 with a low loss tangent of 0.008). Moreover, introducing ultra-small Ag nanoparticles had effectively decreased the dielectric loss and conductivity of TPU/GNS/Ag composites, which resulted in the improvement of energy storage characteristics of the composite (Zhu et al., 2020). In comparison to binary BT/polymer composites, the 2D multiphase systems with 2D MXene nanosheets significantly improved the dielectric constant, which ascribes to remarkably increased interface types and enhanced interface polarization (Feng et al., 2019). Similarly, by adding a low concentration of 2D titanium carbide (Ti_3C_2) MXene nanosheets into the alpha-SiC/PVDF nanocomposites, the SiC/MXene/PVDF nanocomposites showed an improved high ϵ_r , because of the multiple interfaces instead of a single interface (Deng et al., 2019).

The insulating 2D fillers in multiphase systems mainly include BNNS (Luo et al., 2018; Li et al., 2019), and MMT (Wang et al., 2018b; Song et al., 2020). Li et al. (2019) prepared PEI-based nanocomposites consisting of two inorganic fillers with complementary functionalities, including BNNSs with high dielectric strength and BT NPs with large electric polarization. Enhancements of both E_b and ϵ_r have been achieved in the resulting ternary polymer nanocomposites, which lead to outstanding electrical storage and discharging performance in comparison with pristine PEI and other engineering polymer films and excellent cyclability at elevated temperatures. In addition, the PVDF/IL/MMT nanocomposite exhibited improved energy storage performance compared with the nanocomposites containing ionic liquid (IL) or nano-montmorillonite (Na+ MMT) independently (Song et al., 2020).

However, conductive 2D fillers and relatively insulating filler could be filled into a multilayer-structured nanocomposite at the same time, which are introduced into different layers. Guo et al. (2020) designed a novel micro-sandwich-structured PI-based nanocomposites by rationally arranging highly aligned conductive reduced graphene oxide (rGO) and insulating BNNS layers in an alternating manner. The alternating stacking of rGO and BNNS synergistically exploits the large difference in their electrical conductivities to yield a high dielectric constant with a moderate breakdown strength. Consequently, the micro-sandwich nanocomposite prevails over the PI film with a simultaneously high dielectric constant of ≈ 579 , a high energy density (43-fold higher than PI) and an excellent thermal conductivity (11-fold higher than PI) at a low hybrid filler content of only 2.5 vol %.

LAYER-STRUCTURED POLYMER COMPOSITES

The layer-structure design has been reported as an effective method to solve the above paradox between high E_b and enhanced ϵ_r of the ceramic/polymer nanocomposites. Recently, a series of topologically sandwich-structured polymer composites are emerging as a promising route to provide concurrent enhancements in U_e and η . The layer-structured polymer composite with superior energy storage properties is a combination of compositional and structural tailoring by synergic integrations of the multiple components in the layered structures and deliberately adjusting the interfaces and the relative ratios of the constituent layers (Wang et al., 2019a). Two major layer-structured polymer composites will be introduced here, which are layered all-organic polymer composites and layered ceramic/polymer composites.

Layered ceramic/polymer composites

The multilayered hierarchical structures enable to well adjust the distribution of the electric field by rearranging the organization of the constituents in multi-component composite materials, resulting in optimized overall performance (Wang et al., 2019b). In the single-layer ceramic/polymer nanocomposites, the highly heterogeneous field distribution would cause a significant reduction of the breakdown strength to limit the enhancement of U_e . However, the interface between the matrix and fillers would overlap together, especially when fillers with high loadings aggregate in the matrix, leading to nonuniform field

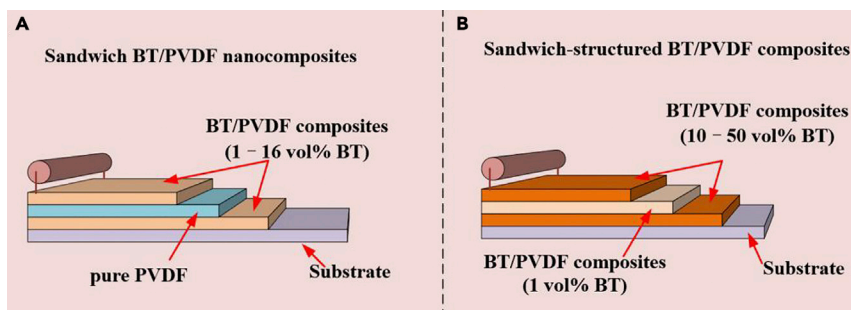


Figure 9. Schematic illustration of the sandwich-structured BT/PVDF composites

(A) Sandwich BT/PVDF nanocomposites. Adapted with permission (Wang et al., 2017d). Copyright [2022] Clearance Center, Inc. ("CCC").

(B) Sandwich-structured BT/PVDF composites. Adapted with permission (Wang et al., 2015a). Copyright [2022] John Wiley and Sons.

distribution, which provides conductive paths for charge carriers. The layer-structured ceramic/polymer nanocomposites could spatially regulate the distribution of the electric field even at high filler contents. In the early studies, Wang et al. (2017a) designed and prepared sandwich-structured ceramic/polymer nanocomposites by stacking the layer with high ϵ_r and the layer with high E_b . The pure PVDF was adopted as the middle layer to offer high E_b , whereas two outer layers were BT/PVDF composite layers with high permittivity, as shown in Figure 9A. By tailoring BT contents in the outer layers varies from 1 to 16%, it is found that the best energy storage performance has been achieved at the outer layer with 3 vol % BT, showing a breakdown strength of 410 MV/m, an energy density of 16.2 J/cm³ and discharge efficiency of 70%, which are much higher than those of pure PVDF. This is because more applied voltage concentrates on the middle layer, resulting in a weak electric field region formed in the outer layer to hinder the growth of electrical trees during the breakdown process, and decrease the conductivity of PVDF in the outer layer simultaneously. In addition, Wang et al. (2015a) designed the middle layer with a small amount of BT nanoparticles to prepare the sandwich-structured nanocomposites, which is a stacking of three layers of convenient 0–3 composites, as shown in Figure 9B. In the growth process of electrical trees during the breakdown, the introduction of electron traps increased the path tortuosity to improve the energy density and breakdown strength.

Although the sandwich-structured composites have obtained enhanced energy storage properties, the charge carrier injection and associated electrical conduction still limit their energy storage capability, especially under high electric fields. The energy density and discharge efficiency of sandwich-structured polymer composites are rarely higher than 20 J/cm³ and 70%, respectively. Thus, structural optimization needs to be further studied. Different from most traditional sandwiched structures, Wang et al. (2018b) designed a sandwich-structured nanocomposite with a high ϵ_r polarization layer as the middle layer and the high E_b insulation layer as the outer layers, as shown in Figure 10A. The outer layers were adopted with small BT nanoparticles placed near the electrodes to prevent the charges injection whereas the middle layer with high BT nanoparticles offers high ϵ_r . As a result, compared with most sandwich-structured nanocomposites, the reverse sandwich structure with the optimized compositions and configurations obtained an ultrahigh energy density of 26.4 J/cm³ at E_b of 526 MV/m along with a much-enhanced η of 72%, as shown in Figure 10E.

The gradient-layered polymer nanocomposite is a new class of hierarchically structured multi-component materials, whose design strategy applies to a variety of advanced composites with integrated contradictory characteristics for outstanding comprehensive performance. The gradient-layered ceramic/polymer composites would form the gradient electric fields at the interfaces between the adjacent layers by gradually increasing the contents of ceramic fillers from the upper to bottom layers. The interfacial barrier effect attributed to the gradient electric field distribution hampers the growth of electrical trees and thus leads to the improvement of the breakdown strength. Wang et al. (2017b) prepared the gradient-layer BT/PVDF nanocomposites, in which the BT contents of the bottom layer, middle layer, and upper layer were high (10–30 vol %), medium (5–20 vol %), and low (1 vol %) respectively, as shown in Figure 10B. As

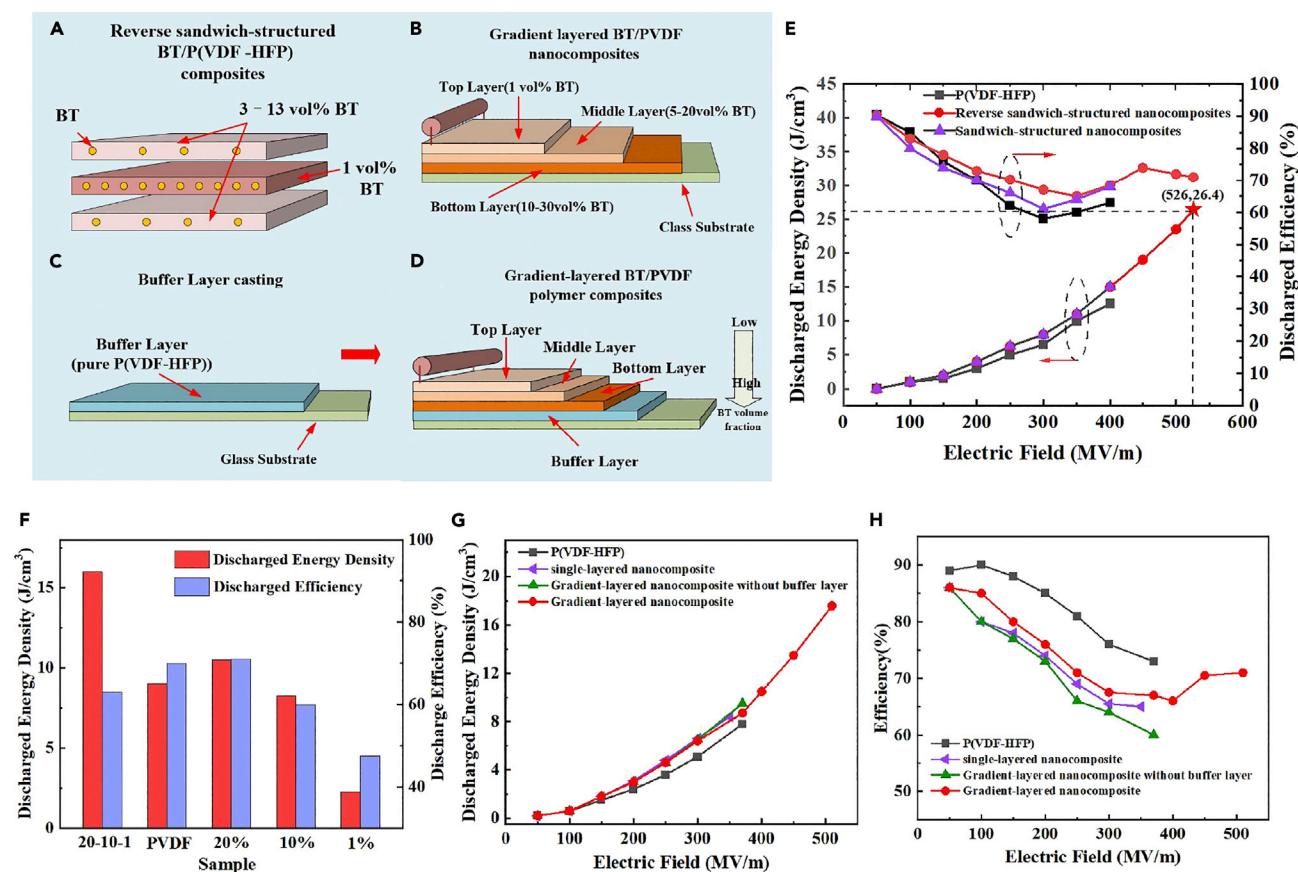


Figure 10. Layered ceramic/polymer composites

Schematic illustration of (A) the reverse sandwich-structured BT/P(VDF-HFP) composites, (B) the gradient-layer BT/PVDF nanocomposites, (C) the P(VDF-HFP) pure buffer layer and (D) the gradient-layered polymer composites with a buffer layer. Adapted with permission (Wang et al., 2020c). Copyright [2022] Elsevier.

(E) Discharged energy density and discharged efficiency of pure P(VDF-HFP), sandwich-structured BT/P(VDF-HFP) composites, and reverse sandwich-structured BT/P(VDF-HFP) composites. Adapted with permission (Wang et al., 2018c). Copyright [2022] Elsevier.

(F) Discharged energy density and discharged efficiency of "20-10-1", pure PVDF, and single layer BT/PVDF nanocomposites with BT contents of 1 vol %, 10 vol %, and 20 vol %, near their breakdown strength respectively. Adapted with permission (Wang et al., 2017e). Copyright [2022] Clearance Center, Inc. ("CCC").

(G) The discharged energy density and (H) efficiency of pure P(VDF-HFP), single-layered nanocomposites, gradient-layered nanocomposites, and gradient-layered nanocomposites with a buffer layer. Adapted with permission (Wang et al., 2020c). Copyright [2022] Elsevier.

as a result, the optimization of the composite compositions achieved an ultrahigh discharged energy density of 16.5 J/cm^3 at E_b of 390 MV/m, when the BT contents were 1, 10, and 20 vol % respectively, as shown in Figure 10F. However, the breakdown strength of the gradient layered nanocomposites was limited below 400 MV/m, which is attributed to the fillers, namely spherical ceramic nanoparticles. Thus, to realize the full potential, Wang et al. (2020a) selected P(VDF-HFP) as the matrix and BT NWs as filler instead of BT NPs to prepare gradient-layered polymer composites. Meanwhile, a buffer layer with pure polymer was introduced into the gradient-layered structure to reduce the charge injection from the electrodes, as shown in Figures 10C and 10D. Therefore, the gradient-layered nanocomposite with a buffer layer obtained a further enhancement in the breakdown strength to 510 MV/m, which is $\sim 34\%$ higher greater than the sample without the buffer layer. And the highest energy density is 17.6 J/cm^3 at 510 MV/m accompanied by a charge-discharge efficiency of 71.2%, as shown in Figures 10G and 10H.

Layered all-organic polymer composites

Greatly improved energy densities have been achieved in layered ceramic/polymer composites, but suppressed η ($<80\%$) and elevated loss (>0.1 @ 1 kHz) cannot meet the requirements of practical applications.

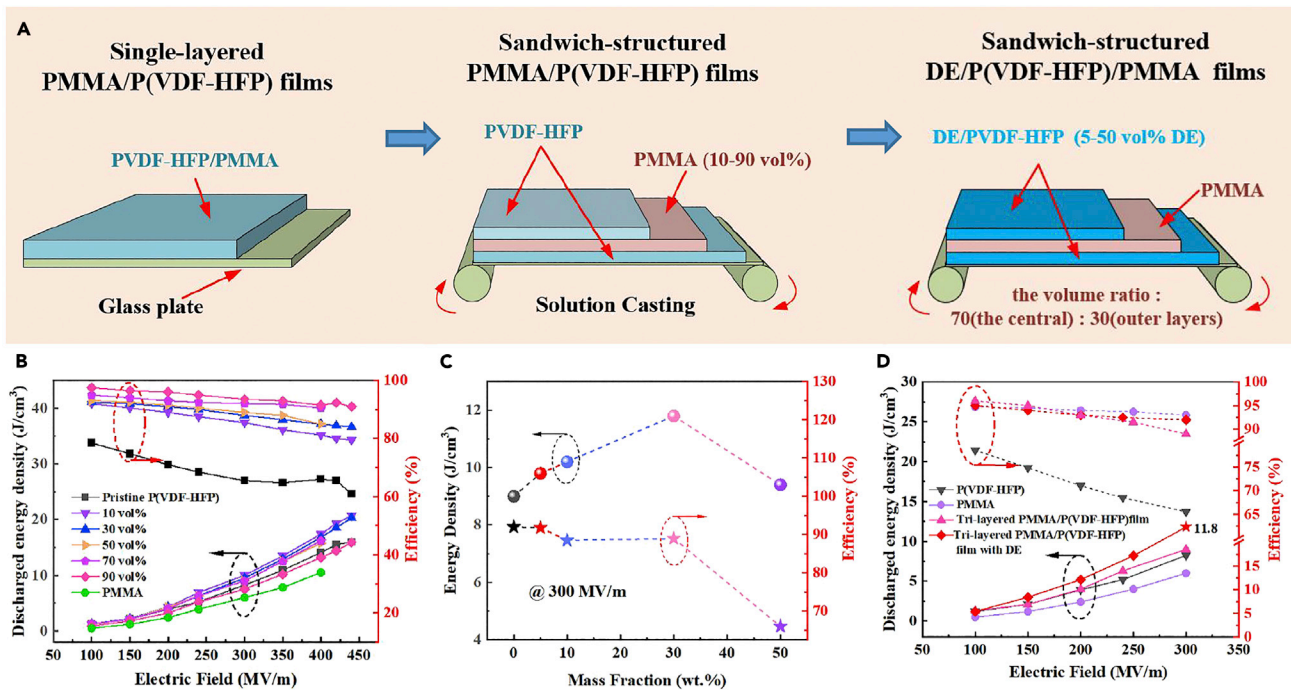


Figure 11. Layered all-organic polymer composites

(A) Schematic illustration of single-layered PMMA/P(VDF-HFP) films, sandwich-structured PMMA/P(VDF-HFP) films, and DE/PMMA/P(VDF-HFP) films. Adapted with permission (Chen et al., 2018a). Copyright [2022] Elsevier.

(B) Discharged energy density and efficiency of pristine P(VDF-HFP) and the tri-layered all-polymer films with different PMMA volume fractions as a function of the applied field. Adapted with permission (Chen et al., 2018b). Copyright [2022] Elsevier.

(C) Discharged energy density and efficiency of sandwich-structured DE/PMMA/P(VDF-HFP) films measured at 300 MV/m. Adapted with permission (Chen et al., 2019). Copyright [2022] Clearance Center, Inc. ("CCC").

(D) discharged energy density and efficiency of pristine P(VDF-HFP) and PMMA, tri-layered PMMA/P(VDF-HFP) films and DE/PMMA/P(VDF-HFP) films. Adapted with permission (Chen et al., 2019). Copyright [2022] Clearance Center, Inc. ("CCC").

Therefore, more attention should be paid to the concurrent improvement of U_e and η rather than solely U_e (Sun et al., 2020). Paraelectric polymers, such as PEI (Sun et al., 2020), PP (Dang et al., 2007), and PMMA (Luo et al., 2017a; Kang et al., 2009), have extremely low dielectric loss and high discharge efficiencies, so that are incorporated into ferroelectric PVDF or its copolymers to suppress the ferroelectricity and then reduce the conduction loss and improve η of polymer dielectric materials. The single-layered P(VDF-HFP)/PMMA blend films with 42.6 vol % PMMA could achieve an efficiency of 85.8% at the electric field of 475 MV/m (Luo et al., 2017b). However, high loadings of PMMA in polymer blends substantially deteriorate ϵ_r in turn and limit the further enhancement of U_e . Instead of the single layer films, PMMA was introduced into the middle of the topological structure as the insulating layer, which effectively hinders the electron propagation and impedes the breakdown across the film thickness (Fournier and Lamarre, 1992). In addition, excellent cycling and mechanical reliability have been demonstrated in the tri-layered all-polymer films. Chen et al. (2018b) prepared the multilayered PMMA/P(VDF-HFP) polymer films via a simple solution-casting process, as shown in Figure 11A, resulting in a much improved discharged efficiency of 84% and higher U_e of 20.3 J/cm³ at 440 MV/m with 30 vol % PMMA, which reduce the conduction loss in comparison with the single-layer blend film with an U_e of 17.5 J/cm³ and a charge-discharge efficiency of 72% measured at 440 MV/m, as shown in Figure 11B.

Although the tri-layered PMMA/P(VDF-HFP) polymer films achieve large enhancement in the charge-discharge efficiency (>80%) and the energy density (>20 J/cm³) at high electric fields, there is room for improving the energy density of multilayered PMMA/P(VDF-HFP) polymer films at low electric fields. For example, the tri-layered film with 70 vol % PMMA obtained an ultrahigh charge-discharged efficiency of 92% at 300 MV/m, but U_e is only 9.1 J/cm³. The dielectric elastomers (DE) can undergo large elastic deformation with increasing the electric field, and thus are a class of field responsive electroactive polymers

(Yu et al., 2014; Pelrine et al., 2000). The organic DE was blended in ferroelectric P(VDF-HFP) matrix as the outer layers of the sandwich-structured PMMA/P(VDF-HFP) polymer film to provide high maximum displacement (Chen et al., 2019), resulting in a high U_e of 11.8 J/cm³ at 300 MV/m whereas the tri-layered films maintain the high energy storage efficiency of 89%, which is attributed to the volume ratio of the central to outer layers (70:30), as shown in Figures 11C and 11D. This work provides a promising paradigm for the design of flexible dielectric materials operating efficiently at relatively low electric fields.

Recently, asymmetric trilayer all-polymer dielectric composites were reported, which is a unique trilayer paraelectric-moderate-ferroelectric (PMF) structure (Sun et al., 2021a, 2021b). For example, paraelectric PMMA offers a high E_b and high η , and ferroelectric P(VDF-HFP) improves the polarization intensity and U_e . Particularly, the Moderate layer, which is a PMMA/P(VDF-HFP) blend composite, can partially undertake the applied voltage of the PMF structure and then homogenize the electric field. This structure shows tremendous potential for application in advanced dielectric energy-storage devices.

MICRO-/MACRO-SURFACE AND INTERFACE ENGINEERING FOR POLYMER DIELECTRICS

Micro-surface engineering

The nanofillers with a high volume fraction tend to have high surface energy in the ceramic/polymer nanocomposites, which usually leads to agglomeration and phase separation from the polymer matrix, and results in a decreased breakdown strength of the nanocomposites. Nevertheless, to achieve high energy storage density, it is necessary to increase the volume fraction for nanocomposites filled with 0D nanofillers. The 1D nanofillers with the small specific surface area reduce the surface energy instead of 0D nanofillers to prevent themselves from agglomerating in the polymer matrix and then contribute ordered traps, and scattering centers to restrict charge shifting (Song et al., 2012; Xie et al., 2016). Unfortunately, the nanocomposites with high loading 1D nanofillers still result in agglomeration of fillers, air voids, inorganic-organic interfaces, and other defects, which will increase the leakage current and decrease E_b of the nanocomposites (Lin et al., 2016; Almadhoun et al., 2012). At present, micro-surface engineering is focusing on alleviating the negative influences of the inorganic filler aggregation on the nanocomposites.

Surface modification

The surface modification for nanofillers is a useful method to facilitate their dispersion in the polymer matrix (Niu et al., 2015b). From many experimental and theoretical studies, researchers found that the elaborate modification of nanofillers can facilitate the subsequent performance improvement of the polymer nanocomposites (Xie et al., 2016; Pan et al., 2017a; Wang et al., 2017a, 2017b; Liu et al., 2015b, 2016). Modification means the introduction of organic coatings onto the surface of inorganic fillers, which can be carried out by utilizing physical and chemical interactions between the filler and the modifier. Normally modifier consists of two major components. One is a functional group, such as $-\text{OH}$, $-\text{NH}_2$, $-\text{NR}_3^{2+}$, $-\text{COOH}$, $-\text{COO}^-$, $-\text{SO}_3\text{H}^-$, $-\text{SO}_3^{2-}$, and $-\text{PO}_4^{3-}$, which helps the anchoring of the modifiers to the particle's surface through hydroxyl and electrostatic bonds. The other is a solvable macromolecular chain, such as polyolefin, polyester, poly different, and polyether, which is appropriate to be dispersed in different media (Chen et al., 2018a). Except for the above modifiers, a series of modifiers were used to improve the dispersion of metal oxide nanoparticles in polymers (Choudhury, 2012; Schuman et al., 2012; Zhou and Yu, 2011; Rong et al., 2013), such as silanes (Iijima et al., 2009), carboxylic acids (Yu et al., 2013a), and phosphonic acid (Siddabattuni et al., 2011). Silane coupling agents were used to modify the surface of BT particles in different solvents, which improved the dielectric properties of BT/epoxy composites (Iijima et al., 2009). The phosphonic acids were usually used to surface modifications on various oxides including ITO (Paniagua et al., 2008), TO (Spori et al., 2007), ZrO_2 (Gao et al., 1996), Al_2O_3 (Pellerite et al., 2003), and BT (Schulmeyer et al., 2007).

Among the various modifiers, it is relatively less about the research on carboxylic acids as modifiers for ceramic nanoparticles due to the small coverage level of them binding to the surface of metal oxides (Niu et al., 2015a). The high adsorption level of modifiers in nanocomposites will lead to significantly lower dielectric constant or high leakage current and dielectric loss. Therefore, Niu et al. (2018) used three carboxylic acids to treat the surface of BT NPs including 2,3,4,5-tetrafluorobenzoic acid (F4C), tetrafluorophthalic acid (F4C2) and phthalic acid (C2) and tried to change the coverage level of carboxylic acids on the surface of metal oxides by adjusting the number of carboxyl groups in the modifier molecule. They found that a higher coverage level on the surface of BT nanoparticles can make the dielectric constant of the nanocomposites increase, but meantime E_b will be reduced. The amount of modifier on the surface of the nanoparticle should be as small as possible while ensuring good dispersion of the nanoparticles and

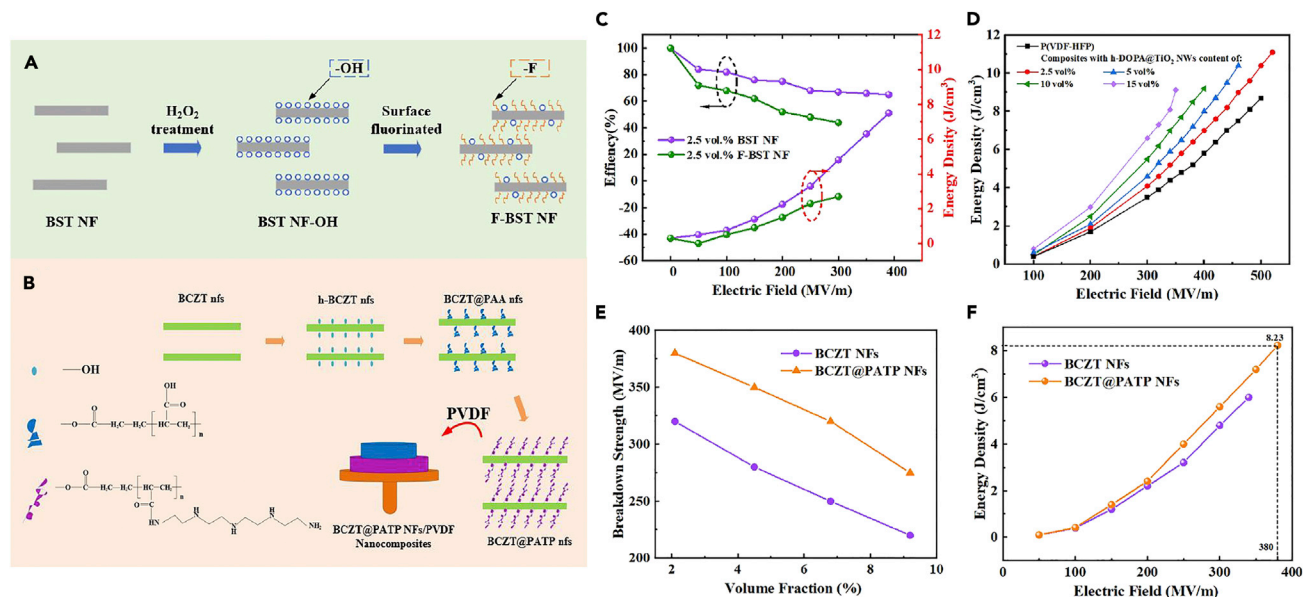


Figure 12. Surface modification and covalent grafting in micro-surface engineering

(A) Schematic diagrams of the fabrication of F-BST NFs and the nanocomposites processes. Adapted with permission (Liu et al., 2015a). Copyright [2022] Clearance Center, Inc. ("CCC").

(B) Schematic diagrams of the fabrication of BCZT@PATP NFs and the nanocomposites processes. Adapted with permission (Pan et al., 2017d). Copyright [2022] American Chemical Society.

(C) Energy density and energy efficiency under various applied electric fields for 2.5 vol % BST NF/PVDF and 2.5 vol % F-BST NF/PVDF nanocomposites. Adapted with permission (Liu et al., 2015b). Copyright [2022] Clearance Center, Inc. ("CCC").

(D) Energy densities of h-DOPA@TiO₂ NWs/P(VDF-HFP) nanocomposites with different volume fractions under varied applied fields. Adapted with permission (Wang et al., 2017a). Copyright [2022] Springer Nature.

(E) The breakdown strength of the BCZT@PATP NFs/PVDF and BCZT NFs/PVDF nanocomposites with different volume fractions and (F) the energy density of 2.1 vol % BCZT@PATP NFs/PVDF and BCZT NFs/PVDF nanocomposites. Adapted with permission (Pan et al., 2017a). Surface coating in micro-surface engineering Copyright [2022] American Chemical Society.

improved compatibility with the matrix. In addition, through the studies of the performance of the nanocomposites filled with BT nanoparticles modified by carboxylic acids, they found that the structure of modifiers including type, number, and position of functional groups in molecules have different effects on the performance of the nanocomposites (Niu et al., 2015b).

Another example is the functionalization of the Ba_{0.6}Sr_{0.4}TiO₃ nanofibers (BST NFs) by hydroxylation using H₂O₂ treatment and subsequent fluorination. The surface-modified BST NFs were filled into the PVDF polymer matrix to prepare the nanocomposites (Liu et al., 2015b), as shown in Figure 12A. The nanocomposites with surface-fluorinated BST NFs (F-BST NFs) exhibit better dielectric performance than that with untreated BST NFs. Meanwhile, the composites with 2.5 wt % F-BST NF achieved U_e of 7.5 J/cm³ at 390 MV/m, as shown in Figure 12C. Similarly, Liu et al. (2016) fabricate the nanocomposite films based on surface-modified Ba(Zr_{0.3}Ti_{0.7})O₃ nanofibers (BZT NFs) and PVDF. As a result, the energy storage density of 6.3 J/cm³ was obtained at 380 MV/m with 2.5 vol % surface-modified BZT NF. At a relatively low electric field, significant enhancement in energy density was also achieved because of the synergistic effect of both surface modifications by dopamine and large aspect ratio nanowires. For example, the nanocomposite films with 3 vol % surface-modified BaTiO₃ nanowires exhibited a high energy density of 8.4 J/cm³ at 280 MV/m (Xie et al., 2016).

Inspired by adhesive proteins in mussels, Wang et al. (2017a, 2017b) employed fluoro-polydopamine(f-DOPA) to reinforce the compatibility of TiO₂ NWs in the fluoropolymer matrix. As a result, the energy storage performances of nanocomposites exceed most previously reported nano-TiO₂ based nanocomposites at both low and high electric fields. The nanocomposites with 2.5 vol % f-DOPA@TiO₂ NWs possessed an ultrahigh discharged energy density of 11.13 J/cm³ at 520 MV/m, and a gratifying high U_e of 9.12 J/cm³ was also obtained with nanofiller loading as high as 15 vol % at 360 MV/m, as shown in Figure 12D.

Covalent grafting

Except for using surfactants, covalent grafting of the nanoparticles to polymer chains also can enhance the dispersion of nanoparticles in the polymer matrix. The covalent is “grafting to” the polymer chain or “grafting from” the organic monomer on the filler surface, which is also an approach for modulating the polymer-filler interface route to enhance the dielectric energy density in ceramic-polymer nanocomposites. Because the way not only can alleviate filler aggregation but also retard the movement of charge carriers on the surface between the polymer matrix and fillers. Pan et al. (2017b) proposed a novel approach to fabricate nanocomposite films employed PVDF blends as the polymer matrix and high-aspect-ratio BCZT@PATP NFs as fillers by grafting the polypropylene acyl tetraethylene pentamine (PATP) into 1D $0.5(\text{Ba}_{0.7}\text{Ca}_{0.3})\text{TiO}_3-0.5\text{Ba}(\text{Zr}_{0.2}\text{Ti}_{0.8})\text{O}_3$ nanofibers (BCZT NFs), as shown in Figure 12B. The nanocomposite films loading with BCZT@PATP NFs could more effectively improve the dielectric performance compared with the BCZT NFs, as shown in Figure 12E. The energy density was improved to 8.23 J/cm^3 by small loading fillers at the electric field of 380 MV/m, as shown in Figure 12F. In another work, ST NWs were grafted onto the surface of BT NPs functionalized with polyphenol- Sr^{2+} shells on the surface via a hydrothermal process. As a result, BT-ST-P(VDF-HFP) composites also exhibited superior dielectric properties compared with both pure P(VDF-HFP) and BT-P(VDF-HFP) composites (Yu et al., 2015).

Surface coating

High energy density polymer nanocomposites with high loading of nanofillers give rise to more interfacial imperfections, such as holes or voids (Zhang et al., 2014). Although modifying the interface between the fillers and the polymer matrix has made some improvements, the large contrast in the dielectric constant and conductivity at the interface between the polymer matrix and fillers results in nonuniform electric field and thus the energy loss of nanocomposites (Gao et al., 2014; Li et al., 2007; Rahimabady et al., 2013). Energy loss of nanocomposites could be attributed to the hysteresis loss of the PVDF matrix, interfacial polarization, and leakage current. Because of the significant difference in dielectric constant and conductivity between ceramic fillers and PVDF matrix, space charges are blocked at the interfaces between the two media under a high electric field, which leads to an increase in dielectric loss and a decrease in breakdown strength (Liu et al., 2015a). To overcome this issue, an effective way is a core-shell structure designed based on interfacial engineering to introduce a shell layer with a moderating dielectric constant on the surface of the nanofiller, which not only focuses solely on the interface between filler and polymer matrix but also pays attention to the interface inside the dielectric fillers. The interface between polymers and ceramics plays an important role in determining the dielectric properties of nanocomposites (Rahimabady et al., 2013). For the core-shell structured nanocomposites, there are two main forms: one is encapsulating a low dielectric constant ceramic nanolayer (a shell) on top of a high ϵ_r 1D ceramic nanofillers (a core), on the contrary, the other is that the high ϵ_r ceramic nanolayer serves as the shell, which is on top of a low dielectric constant 1D ceramic nanofillers. At present, the latter case has rarely been examined owing to polymer-nanofiller ϵ_r mismatch and distortions accompanied by low E_b in the low ϵ_r -core@ high ϵ_r shell structures (Zhang et al., 2019).

In the former case, when ceramic nanofillers with high ϵ_r , as a core, for the shell layer, the ceramic nanolayers with moderate ϵ_r , such as TO, Al_2O_3 , and SiO_2 (SO), are preferred as a buffer layer, which alleviates the electric field concentration in the polymer matrix to achieve the substantial improvement of energy storage capability for polymer nanocomposites. To reduce the energy loss of the nanocomposites under high applied electric fields, Yu et al. (2013c) prepared homogeneous ceramics-polymer nanocomposites comprising core-shell structured BT/SO nanoparticles (BT@SO NPs) and a PVDF polymer matrix. They found that the nanocomposites with BT@SO NPs exhibited much lower DC leakage current compared to those of BT nanoparticles, as shown in Figure 13A, and the nanocomposite of 2 vol % BT@SO NPs exhibited 46% reduced energy loss compared to that of BT NPs accompanied with an U_e of 6.28 J/cm^3 under an applied electric field of 340 MV/m, as shown in Figures 13C and 13D. Those are attributed to the SO coating layers on the surface of BT NPs, which reduces the Maxwell-Wagner-Sillars interfacial polarization and space charge polarization. Besides, Liu et al. (2015a) also prepared core-shell structured BT@SO nanofibers (BT@SO NFs) by coating SO layers into the surface of 1D BT NFs, as shown in Figure 13B. According to the results, similarly, coating SO layers can block the movement of charge carriers through the nanocomposites by playing a shielding role on the charge-rich interlayer, which results in weak MWS interfacial polarization, reduces the energy loss and improves the energy discharged density of the nanocomposites. The energy discharged density in the nanocomposite with 2.5 vol % BT@SO NFs is 6.28 J/cm^3 at 3.3 MV/cm.

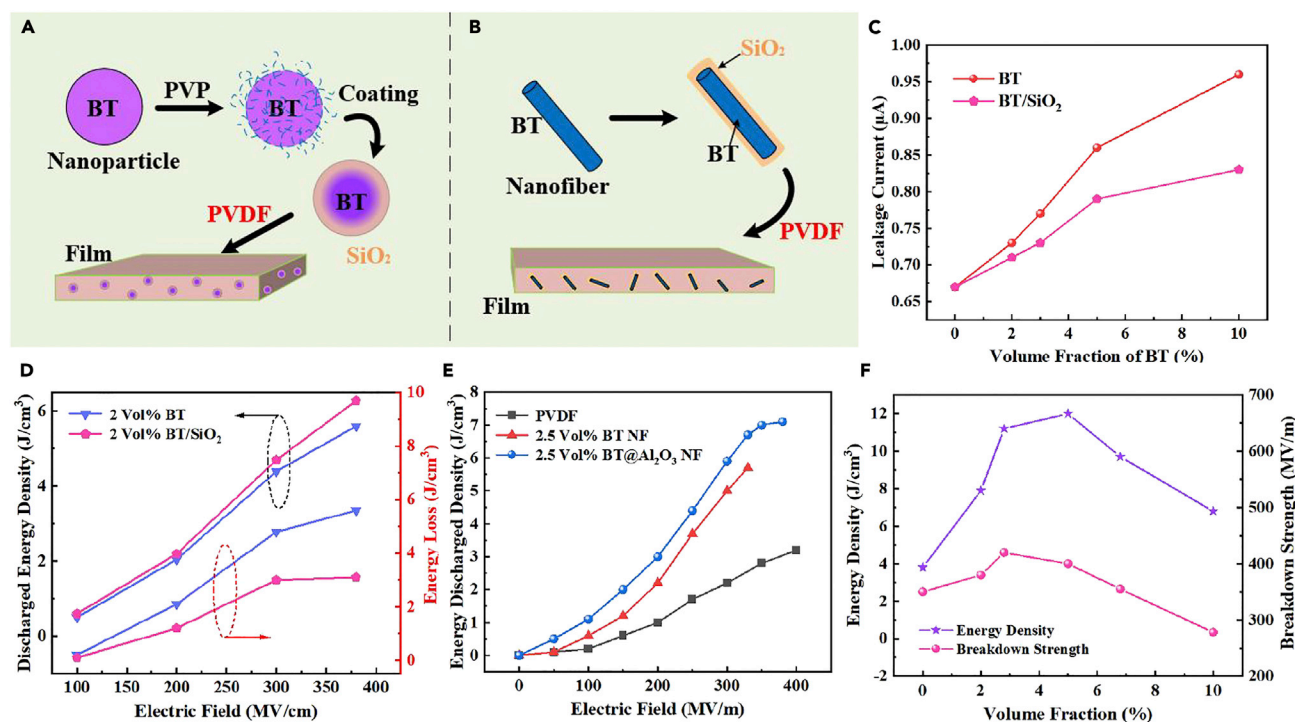


Figure 13. Surface coating in micro-surface engineering

(A) Schematic illustration of the synthesis of core-shell structured BT/SiO₂ nanoparticles and the fabrication of polymer-based nanocomposites. Adapted with permission (Yu et al., 2013a). Copyright [2022] AIP Publishing.

(B) Schematic illustration of the synthesis of core-shell structured BT/SiO₂ nanofillers and the fabrication of polymer-based nanocomposites. Adapted with permission (Wang et al., 2017b). Copyright [2022] Clearance Center, Inc. ("CCC").

(C) The dc leakage current of the nanocomposites as a function of the volume fraction of ceramic fillers. Adapted with permission (Yu et al., 2013b). Copyright [2022] AIP Publishing.

(D) The energy discharged and energy loss of the nanocomposite of BT/SiO₂ nanoparticles and that of BT nanoparticles with a concentration of 2 vol %, as a function of the applied electric field. Adapted with permission (Yu et al., 2013c). Copyright [2022] AIP Publishing.

(E) The energy discharged density for BT@Al₂O₃ NF/PVDF and BT NF/PVDF nanocomposites with a concentration of 2.5 vol %, as functions of the applied electric field. Adapted with permission (Liu et al., 2017a). Copyright [2022] Elsevier.

(F) The dielectric breakdown strength and energy density of BT@Al₂O₃ NFs/PVDF nanocomposites with different volumes. Adapted with permission (Pan et al., 2016). Copyright [2022] Clearance Center, Inc. ("CCC").

In addition to SO, the Al₂O₃ with moderate ϵ_r were incorporated as a shell layer on the surface of the BT nanofibers to form a moderate interfacial area, which led to the gradient of the dielectric constant between the filler and polymer matrix. Liu et al. (2017b) prepared 1D core-shell structured BT@Al₂O₃ nanofibers (BT@Al₂O₃ NFs), which were homogeneously distributed in the PVDF polymer matrix to form the nanocomposite films. As a result, the maximum discharged energy density of 7.1 J/cm³ was achieved in the nanocomposite with 2.5 vol % BT@Al₂O₃ NFs at 3800 kV/cm with an efficiency of above 65.1%, as shown in Figure 13E. In another study, Pan et al. (2016) also prepared nanocomposite films with BT@Al₂O₃ NFs, which exhibited an excellent discharged energy density of 12.18 J/cm³ under a field of 400 MV/m when the loading of BT@Al₂O₃ NFs was 5 vol %, as shown in Figure 13F.

TO with a moderate ϵ_r was also introduced into the surface of BT nanofillers to form the hierarchical interfaces in polymer nanocomposites. Compared with SO and Al₂O₃, the nanocomposites with BT@Al₂O₃ NFs could obtain better dielectric performance. Zhang et al. (2016) prepared TO nanofibers embedded with BT nanoparticles via electrospinning and then fused them with PVDF into polymer nanocomposite films, as shown in Figures 14A and 14B. The nanocomposites with a low loading of 3 vol % core-shell structured BT@TO nanofibers (BT@TO NFs) achieved a giant U_e of ~31.2 J/cm³ and raised E_b up to 797.7 kV/mm, which is evidence that one can manipulate the topological structure of interfaces for enhancing interfacial polarization, as shown in Figure 14C. This is by far the highest energy density ever achieved in polymer nanocomposites dielectrics, as shown in Figure 14D. Along this line, in other research (Song et al., 2012;

twelve times greater than BOPP ($\approx 1.2 \text{ J/cm}^3$ at 640 MV/m). Moreover, the nanocomposite exhibited a superior power density of 4.7 MW/cm^3 and an ultra-fast discharge speed of $0.37 \mu\text{s}$.

Macro-interface engineering

The polymer-based dielectrics must withstand ever-increasing and enormous operating electric fields, but a clear negative correlation between U_b and E_b of surface states in polymer dielectrics has been demonstrated experimentally (Wang et al., 2021). The surface state dramatically reduces the charge injection barrier height lead to high electrical conduction. Therefore, the ideal Schottky barrier is hardly achieved and cannot sufficiently impede the charge injection. At present, macro-interface engineering is a useful strategy to enhance the breakdown strength by nanocoating on polymer films to eliminate surface states, resulting in reviving the injection barrier and promoting lateral dissipation of injected charges (Zhang et al., 2021).

Introducing highly insulating nanostructures

The addition of 2D nanosheets with wide E_g such as BNNS and alumina nanoplates into the polymer matrix is an effective method to improve the capacitive properties at high electric fields and elevated temperatures. In the polymer matrix, these high-aspect-ratio nanosheets function as topological barriers, which increase the propagation path length of charge carriers and prevent the progress of electrical treeing. Thus, introducing highly insulating nanostructures suppresses the electrical conduction and improves E_b .

BNNSs are a 2D nanomaterial with a wide E_g ($\approx 6 \text{ eV}$), which have proved to be an intriguing dopant in dielectric polymer nanocomposites to enhance E_b and η . Because they have high intrinsic breakdown voltage, great thermal conductivity, mechanical strength as well as large electrical resistance, which can serve as efficient scattering centers for charge carriers. Zhu et al. (2019) fabricated a novel high energy density polymer composite with a nanosized interlayer of BNNSs through a simple layer-by-layer solution-coating process, as shown in Figure 15A. The BNNSs were directly assembled as a compact and successive interlayer located in the middle of PVDF films, which were aligned along the in-plane direction. Thus, the amount of BNNSs in the sandwich-structured composite film is substantially lower than that in the conventional polymer nanocomposites containing BNNSs. The experimental results reveal that introducing the nanosized insulating interlayer impedes charge conduction and blocks the propagation of electrical treeing, giving rise to suppressing the leakage and hence achieving a high breakdown strength and a superior energy density. For instance, the composite film with 0.16 vol % BNNSs possesses a superior discharged energy density of 14.3 J/cm^3 and an excellent breakdown strength of 612 MV/m. Especially, the discharged energy density and efficiency of the composite film with 0.16 vol % BNNSs (BPB3) is superior to that of a conventional PVDF-based nanocomposite with uniformly dispersed BNNSs of the same loading content, as shown in Figures 15B and 15C. Because BNNS in conventional nanocomposites cannot form a continuous topological barrier, resulting in the fact that the electrical tree propagates freely across the nanocomposite films. Therefore, the compact and successive BNNS interlayer can more effectively inhibit the development of electric damage, leading to a higher breakdown strength.

In the sandwich-structured nanocomposite films, interposing the 2D nanosheets between adjacent layers based on macro-interface engineering is also able to suppress the energy loss at high electric fields and elevated temperatures. The nanoscale MMT nanosheets were introduced into layered polymer nanocomposites to form 2D interfaces, giving rise to structural optimization (Wang et al., 2020b). The MMT interfaces could impede the charge penetration through the whole film, which were because of providing paths to relationally regulate the charges transport along the in-plane direction while suppressing the through-plane conduction. For example, the energy loss can be suppressed by 45% with ceramic content increased to 40 wt % at 250 MV/m and 150°C , which thereby provokes a significant enhancement of 52% for charge-discharge efficiency, as shown in Figures 15D and 15E.

Coating wide-bandgap insulating materials with refined manufacturing technology

In order to enable the high-temperature capacitive energy applications of a wide range of engineering polymers, coating wide-bandgap insulating materials onto the surface of engineering polymers is another effective strategy. At present, chemical vapor deposition (CVD) and physical vapor deposition (PVD) are commonly existing thin-film-deposition technology for the synthesis of 2D materials to deposit the wide-bandgap 2D materials onto both sides of polymers.

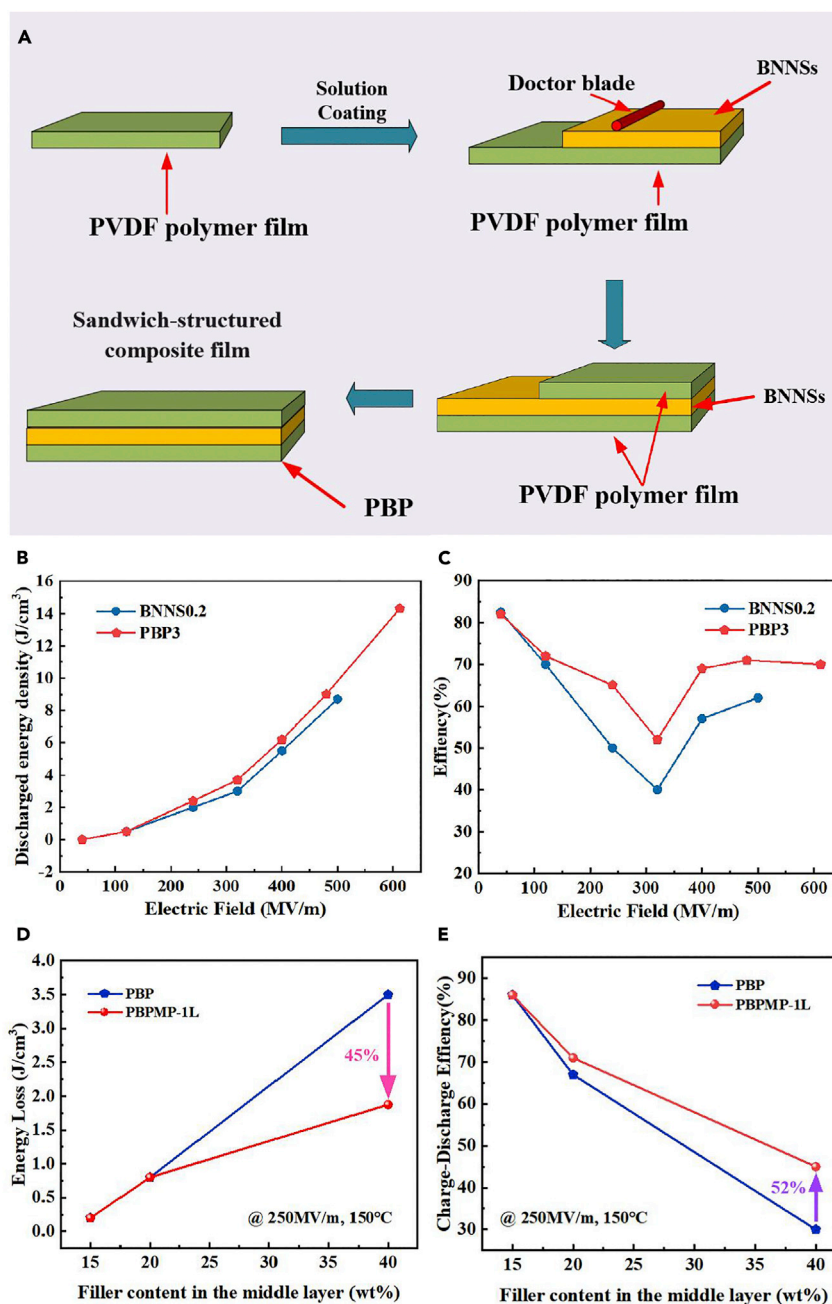


Figure 15. Macro-interface engineering

(A) Schematic illustrations of the fabrication process of sandwich-structured films (P stands for the PVDF layer, and B denotes the BNNs layer). Adapted with permission (Zhu et al., 2019). Copyright [2022] John Wiley and Sons.

(B) The discharged energy density and (C) charge-discharge efficiency as a function of the electric field of PBP3 and BNNs 0.2 (the conventional nanocomposites with the same loading content BNNs). Adapted with permission (Zhu et al., 2019). Copyright [2022] John Wiley and Sons.

(D) Energy losses and (E) charge-discharge efficiency of PBP (the layered nanocomposites without MMT interfaces) and PBPMP-1L (the layered nanocomposites with nano-scale 2D MMT interfaces (1-time spraying)) with the BT content varied from 15 wt % to 40 wt % in the middle layer at 150°C. Adapted with permission (Wang et al., 2020a). Copyright [2022] Elsevier.

CVD is a reproducible and scalable method for the synthesis of 2D materials, such as graphene, BN, and transition metal dichalcogenides (Song et al., 2010). h-BN films were prepared from the CVD and transferred onto PEI films to form sandwich-structured h-BN/PEI/h-BN films. Impressively, the h-BN-coated PEI films were capable of operating efficiently and delivering high energy densities even at a temperature close to the T_g of polymers (Azizi et al., 2017). Thus, the scalability and processability of the method are expected to enable the continuous production of 2D nanomaterial-functionalized polymers at large scales for advanced electronics and energy devices. PVD, a straightforward thin-film-deposition technology, was used to deposit various inorganic materials by just altering the target materials (Cheng et al., 2020). The films deposited by this method exhibited different mechanical and electrical properties from CVD deposited ones (Ye et al., 1998). Cheng et al. (2020) deposited h-BN of optimal thickness onto both sides of PI films by using magnetron sputtering, a common PVD approach. The experimental results showed that the dense and compact coating layer of h-BN could effectively suppress the charge injection at the electrode/dielectric interfaces by improving the barrier height. Therefore, the sandwiched film exhibited a discharge energy density of 0.493 J/cm^3 with charge-discharge efficiency of 91.3% under an electric field of 200 MV/m at 150°C .

In addition, plasma-enhanced chemical vapor deposition (PECVD) is also a general and scalable approach to surface-modified polymer dielectric films, which is faster than other existing film coating technologies, such as CVD and PVD. Because PECVD capitalizes on highly reactive chemical species in ionized and excited states as well as free radicals in the discharge region (Merche et al., 2012). Although PVD usually requires vacuum, high-quality deposition of PECVD can be achieved at atmospheric pressure as a consequence of stable and uniform discharge plasma by placing a dielectric layer between the electrodes to increase the mean free path of plasma species and avoid arc discharge (Kogelschatz, 2003). Zhou et al. (2018) deposited wide-bandgap SiO_2 onto the dielectric polymer films under ambient temperature and atmospheric pressure by using the specially designed roll-to-roll PECVD, which is a general and environmentally benign method for high-throughput preparation of high-performance polymer dielectrics operating at elevated temperatures. Similarly, the introduced SiO_2 layer impedes the charge injection from electrodes by increasing the potential barrier at the electrode/dielectric interface and hence improves high-temperature capacitive performance. The roll-to-roll ambient-temperature PECVD approach overcomes one of the key challenges of the field of dielectric materials and is also readily adaptable to large-scale production of a variety of surface-functionalized polymer thin films for flexible energy and electronic applications.

SUMMARY AND OUTLOOK

High-energy-density polymer dielectrics via compositional and structural tailoring for electrical energy storage are discussed in this review. To provide readers with a more intuitive comparison, the energy storage properties of the main polymer nanocomposites discussed in this review were summarized in Table 2.

The dielectric materials play a significant role in dielectric capacitors, thus, to get high-energy-density polymer dielectrics, researchers have made great efforts. The high dielectric constant ceramic fillers are introduced into the high breakdown strength polymer matrix to comprise the ceramic/polymer nanocomposites with high energy storage density. With regards to ceramic filler, ferroelectric ceramics with high ϵ_r , such as BT and SrTiO_3 are typical choices, but the high ϵ_r would be accompanied by lower E_b values, which seriously limits the ultimate U_e . Linear dielectric nanoparticles with moderate ϵ_r and high E_b , such as TiO_2 , Al_2O_3 , ZrO_2 and SiO_2 , have been used to improve the E_b . They are usually incorporated onto the surface of the nanofiller to suppress the energy loss, thereby increasing the E_b value of the nanocomposite films. In addition, the BNS is also beneficial to improving the E_b markedly, and the excellent insulating and mechanical properties can decrease the energy loss. At present, the ultrahigh specific surface area of BNS has been proved to more effectively improve the energy density compared with other nanofillers.

According to their spatial dimensions, different kinds of ceramic materials including nanoparticles (0D), nanofibers (1D), and nanosheets (2D) are filled into various polymers. However, the nanocomposites containing high loadings will give rise to agglomeration and phase separation from the polymer matrix resulting in a decreased breakdown strength. Besides, air voids, inorganic-organic interfaces, and other defects will also increase the leakage current and decrease the electric breakdown strength of the nanocomposites. Micro-surface engineering is focusing on minimizing the negative influences of the inorganic fillers on the nanocomposites. The surface modification for nanoparticles, such as surfactant and covalent grafting, is a useful method to facilitate their dispersion in the polymer matrix. The nanocomposites with

Table 2. Energy storage properties of polymer nanocomposites

Polymer Nanocomposites	Structure	Polymer matrix	Fillers	Dielectric breakdown strength (MV/m)	Maximum discharged energy density (J/cm ³)	Charge–discharge efficiency (%)	Ref
P(VDF-HFP)/BT composites	Single layer	P(VDF-HFP)	m-BT NPs	164@25°C	3.2@25°C and 1kHz	–	(Kim et al., 2009)
P(VDF-TrFE-CTFE)/TiO ₂ composites	Single layer	P(VDF-TrFE-CTFE)	m-TiO ₂ NPs	220@25°C	7.5@25°C and 1kHz	–	(Li et al., 2009)
PVDF/PZT composites	Single layer	PVDF	PZT NWs	–	1.28@25°C and 100Hz	–	(Tang et al., 2012)
BSBT/P(VDF-TrFE) composites	Single layer	P(VDF-TrFE)	BSBT	155@25°C	4.72@25°C and 10Hz	–	(Hu et al., 2013)
P(VDF-HFP)/BT@TiO ₂ nano composites	Core-shell structure	P(VDF-HFP)	BT@TO	340@25°C	12.2@25°C and 1kHz	–	(Rahimabady et al., 2013)
BST NWs/PVDF composites	Single layer	PVDF	BST NWs	450@25°C	14.86@25°C and 1kHz	–	(Tang and Sodan, 2013)
m-TiO ₂ NWs/PVDF composites	Single layer	PVDF	m-TiO ₂ NWs	450@25°C	12.4@25°C and 100Hz	–	(Sodano et al., 2013)
PVDF/BT@SiO ₂ nanocomposites	Core-shell structure	PVDF	BT@SiO ₂	340@25°C	6.28@25°C and 1kHz	–	(Yu et al., 2013c)
PVDF/BT nanocomposites	Single layer	PVDF	m-BT NPs	285@25°C	5.1@25°C and 10Hz	–	(Yu et al., 2013a)
PVDF/BT nanocomposites	Single layer	PVDF	m-BT NPs	340@25°C	6.28@25°C and 10Hz	–	(Yu et al., 2013b)
PVDF/BT nanocomposites	Single layer	PVDF	m-BT NPs	260@25°C	9.01@25°C and 10Hz	–	(Gao et al., 2014)
PVDF/BT/AR71 nanocomposites	Single layer	PVDF	AR71/BT NPs	400@25°C	8.8@25°C and 10Hz	–	(Yu et al., 2014)
The crosslinked c-BCB/BNNS nanocomposite	Single layer	c-BCB	BNNSs	400@25°C	2.2@25°C	90@25°C	(Li et al., 2015b)
P(VDF-TrFE-CTFE)/BNNS composites	Single layer	P(VDF-TrFE-CTFE)	BNNSs	650@25°C	20.3@25°C and 10Hz	78@25°C	(Li et al., 2015a)
F-BST NF/PVDF nanocomposites	Single layer	PVDF	F-BST NF	390@25°C	7.5@25°C and 100Hz	64@25°C	(Liu et al., 2015b)
PVDF/BT nanocomposites	Single layer	PVDF	m-BT NPs	400@25°C	9.4@25°C	61@25°C	(Niu et al., 2015a)
PVDF/BT nanocomposites	Sandwich-structure	PVDF	BT NPs	450@25°C	12.4@25°C	–	(Wang et al., 2015b)
BT-ST/P(VDF-HFP) composites	Single layer	P(VDF-HFP)	BT-ST	200@25°C	5@25°C and 100Hz	–	(Yu et al., 2015)

(Continued on next page)

Table 2. Continued

Polymer Nanocomposites	Structure	Polymer matrix	Fillers	Dielectric breakdown strength (MV/m)	Maximum discharged energy density (J/cm ³)	Charge-discharge efficiency (%)	Ref
PVDF/TO @ BT NFs nanocomposites	Core-shell structure	PVDF	TO @ BT NFs	646@25°C	20@25°C and 10Hz	75@25°C	(Zhang et al., 2015)
PVDF/TO @ BT NFs nanocomposites	Single layer	PVDF	TO @ BT NFs	360@25°C	10.94@25°C and 10Hz	–	(Lin et al., 2016)
PVDF/ <i>m</i> -BZT NF nanocomposites	Single layer	PVDF	<i>m</i> -BZT NF	380@25°C	6.3@25°C and 100Hz	64@25°C	(Liu et al., 2016)
PVDF/BT@Al ₂ O ₃ NFs nanocomposites	Core-shell structure	PVDF	BT@Al ₂ O ₃ NFs	400@25°C	12.8@25°C and 10Hz	65@25°C	(Pan et al., 2016)
PVDF/ZrO ₂ NSs nanocomposites	Single layer	PVDF	ZrO ₂ NSs	519@25°C	11.3@25°C and 100Hz	67.4@25°C	(Shen et al., 2016)
P(VDF-CTFE)/BT NWs nanocomposites	Single layer	P(VDF-CTFE)	BT NWs	280@25°C	8.4@25°C and 100Hz	–	(Xie et al., 2016)
TNA/PVDF nanocomposites	Single layer	PVDF	TNA	340@200°C	10.62@200°C and 1kHz	–	(Yao et al., 2016)
TO @ BT NFs/P(VDF-HFP) nanocomposites	Core-shell structure	P(VDF-HFP)	TO @ BT NFs	797.7@25°C	31.2@25°C and 10Hz	–	(Zhang et al., 2016)
BZT-BCT NFs/PVDF nanocomposites	Single layer	PVDF	BZT-BCT NFs	310@25°C	7.86@25°C and 100Hz	58@25°C	(Chi et al., 2017)
GNs-HAP-PBO nanocomposites	Single layer	PBO	GNs-HAP	132.5@25°C	6@25°C and 100Hz	–	(Feng et al., 2017)
BT/P(VDF-HFP) nanocomposite	Single layer	P(VDF-HFP)	BT NPs	330@25°C	9.7@25°C and 100Hz	–	(Hao et al., 2017)
PMMA/BNNS nanocomposites	Single layer	PMMA	BNNS	400@25°C	3.55@25°C and 10Hz	84@25°C	(Liu et al., 2017b)
PVDF/BT@Al ₂ O ₃ NFs nanocomposites	Core-shell structure	PVDF	BT@Al ₂ O ₃ NFs	380@25°C	7.1@25°C and 100Hz	65.1@25°C	(Liu et al., 2017c)
P(VDF-HFP)/PMMA flexible composite	Single layer	P(VDF-HFP)	PMMA	475@25°C	11.2@25°C and 10Hz	85.8@25°C	(Luo et al., 2017a)
BT-DA NTs/PVDF nanocomposites	Single layer	PVDF	BT-DA NTs	330@25°C	7.03@25°C and 10Hz	–	(Pan et al., 2017a)
BCZT@PATP NFs/PVDF composites	Single layer	PVDF	BCZT@PATP NFs	380@25°C	8.23@25°C and 10Hz	58@25°C	(Pan et al., 2017b)
PVDF/BT@Al ₂ O ₃ NFs nanocomposites	Core-shell structure	PVDF	BT@Al ₂ O ₃ NFs	450@25°C	12.37@25°C and 10Hz	64@25°C	(Pan et al., 2017c)

(Continued on next page)

Table 2. Continued

Polymer Nanocomposites	Structure	Polymer matrix	Fillers	Dielectric breakdown strength (MV/m)	Maximum discharged energy density (J/cm ³)	Charge-discharge efficiency (%)	Ref
BT@TO@AO NFs/PVDF composite	Core-double-shell structure	PVDF	BT@TO@AO NFs	450@25°C	14.8@25°C and 100Hz	65@25°C	(Pan et al., 2017b)
f-DOPA@TiO ₂ NWs/P(VDF-HFP) nanocomposite	Single layer	P(VDF-HFP)	f-DOP@TiO ₂ NWs	530@25°C	11.48@25°C and 100Hz	60@25°C	(Wang et al., 2017b)
TO@BT NWs/P(VDF-HFP) nanocomposite	Core-shell structure	P(VDF-HFP)	TO@BT NWs	440@25°C	9.53@25°C and 10Hz	64@25°C	(Wang et al., 2017c)
Sandwich-structured BT/PVDF nanocomposites	Sandwich structure	PVDF	BT NPs	410@25°C	16.2@25°C and 10Hz	70@25°C	(Wang et al., 2017a)
Gradient layer-structured BT/PVDF nanocomposites	Gradient layered structure	PVDF	BT NPs	390@25°C	16.5@25°C	55@25°C	(Wang et al., 2017b)
P(VDF-CTFE)/BT NWs nanocomposites	Single layer	P(VDF-CTFE)	BT NWs	240@25°C	10.8@25°C and 100Hz	61.4@25°C	(Xie et al., 2017)
Multilayered P(VDF-HFP)/PMMA composite	Sandwich structure	P(VDF-HFP)	PMMA	440@25°C	20.3@25°C and 10Hz	84@25°C	(Chen et al., 2018b)
BZT-BCT NFs/PVDF composite	Single layer	PVDF	BZT-BCT NFs	240@25°C	3.08@25°C and 10Hz	60@25°C	(Chi et al., 2018)
P(VDF-HFP)/Ag-OMMT composite	Single layer	P(VDF-HFP)	Ag-OMMT	400@25°C	10.51@25°C and 100Hz	45@25°C	(Wang et al., 2018a)
P-BST/PVDF nanocomposites	Single layer	PVDF	P-BST	151.9@25°C	6.36@25°C and 1kHz	–	(Wang et al., 2018b)
Sandwich-structured BT/P(VDFHFP) nanocomposite	Sandwich structure	P(VDF-HFP)	BT NPs	530@25°C	26.4@25°C and 10Hz	72@25°C	(Wang et al., 2018c)
PVDF/TOML nanocomposites	Single layer	PVDF	TOML	650@25°C	21.1@25°C and 10Hz	61@25°C	(Wen et al., 2017)
PVDF/OH-BNNS nanocomposites	Single layer	PVDF	OH-BNNS	517@25°C	13.1@25°C	–	(Wu et al., 2018b)
ST NWs/P(VDF-CTFE) nanocomposite	Single layer	P(VDF-CTFE)	ST NWs	338.1@25°C	8.8@25°C and 100Hz	45@25°C	(Zhang et al., 2018c)
Sandwiched BZT-BCT NFs-PVDF/Fe ₃ O ₄ @BNNSs-PVDF/BZT-BCT NFs-PVDF composite	Sandwich structure	PVDF	BZT-BCT NFs/Fe ₃ O ₄ @BNNSs/BZT-BCT NFs	350@25°C	8.9@25°C and 10Hz	48@25°C	(Zhang et al., 2018d)

(Continued on next page)

Table 2. Continued

Polymer Nanocomposites	Structure	Polymer matrix	Fillers	Dielectric breakdown strength (MV/m)	Maximum discharged energy density (J/cm ³)	Charge-discharge efficiency (%)	Ref
PMMA/P(VDF-HFP)/TiO ₂ composite	Single layer	P(VDF-HFP)	DOPA@TiO ₂ /PMMA	570@25°C	13@25°C and 10Hz	–	(Zhu et al., 2018)
Tri-layered DE/PMMA/P(VDF-HFP) nanocomposite	Sandwich structure	P(VDF-HFP)	DE/PMMA	300@25°C	11.8@25°C and 10Hz	89@25°C	(Chen et al., 2019)
The ternary BT/MXene/PVDF nanocomposites	Single layer	PVDF	BT/MXene	220@25°C	7@25°C and 10Hz	42@25°C	(Feng et al., 2019)
Ni(OH) ₂ /PVDF composite	Single layer	PVDF	Ni(OH) ₂	421@25°C	17.3@25°C and 1kHz	56@25°C	(Ji et al., 2019)
c-BCB/Al ₂ O ₃ NWs nanocomposite	Single layer	c-BCB	Al ₂ O ₃ NWs	450@150°C	3.31@150°C and 1kHz	90@150°C	(Li et al., 2019)
The ternary PEI/BT NPs/BNNS nanocomposites	Single layer	PEI	BT NPs/BNNS	547@150°C	2.92@150°C and 10 Hz	–	(Li et al., 2019)
NN@AO Ps/P(VDF-HFP) nanocomposite	Single layer	P(VDF-HFP)	NN@AO Ps	450@25°C	14.59@25°C and 10Hz	70.1@25°C	(Pan et al., 2019)
P(VDF-TrFE-CTFE)-g-PMMA/eMica nanocomposite	Single layer	P(VDF-TrFE-CTFE)-g-PMMA	eMica	250@25°C	9.6@25°C and 10Hz	78@25°C	(Wang et al., 2019b)
P-NBT4/PVDF composites	Single layer	PVDF	P-NBT4	300@25°C	9.45@25°C and 100Hz	52.28@25°C	(Wang et al., 2019c)
PVDF/BT nanocomposites	Single layer	PVDF	BT platelets	450@25°C	9.7@25°C and 100Hz	–	(Wen et al., 2019)
BN-BCB@DPAES nanocomposites	Single layer	DPAES	BN-BCB	400@150°C	2.7@150°C and 100Hz	90@25°C	(Xu et al., 2019)
sandwich-structured BNNS/PVDF nanocomposite	Sandwich structure	PVDF	BNNS	612@25°C	14.3@25°C and 10Hz	71@25°C	(Zhu et al., 2019)
CNO/PVDF nanocomposites	Single layer	PVDF	CNO	792@25°C	36.2@25°C and 10Hz	61@25°C	(Bao et al., 2020)
Sandwich-structured BN/PI/BN films	Sandwich structure	PI	BN	200@25°C	0.943@25°C and 10Hz	90@25°C	(Cheng et al., 2020)
PVDF/IL/MMT composite	Single layer	PVDF	IL/MMT	360@25°C	12.8@25°C and 1kHz	81.4@25°C	(Song et al., 2020)
RCH/BN nanocomposites	Single layer	RCH	BN	400@25°C	8.67@25°C and 100Hz	90@25°C	(Wang et al., 2020c)
Gradient-layered BT NWs/P(VDF-HFP) nanocomposites	Gradient layered structure	P(VDF-HFP)	BT NWs	510@25°C	17.6@25°C and 10Hz	71.2@25°C	(Wang et al., 2020a)

(Continued on next page)

Table 2. Continued

Polymer Nanocomposites	Structure	Polymer matrix	Fillers	Dielectric breakdown strength (MV/m)	Maximum discharged energy density (J/cm ³)	Charge-discharge efficiency (%)	Ref
Sandwich-structured BT/MMT/PAI nanocomposites	Sandwich structure	PAI	BT/MMT	400@25°C	3.6@25°C and 10Hz	70@25°C	(Wang et al., 2020b)
BNNs/P(VDF-CTFE) nanocomposite	Single layer	P(VDF-CTFE)	BNNs	250@25°C	7@25°C and 100Hz	56@25°C	(Zhang et al., 2020b)

PVDF: polyvinylidene fluoride; PI: polyimide; PEI: poly(ether imide); P(VDF-HFP): poly(vinylidene fluoride-co-hexafluoro propylene); P(VDF-TrFE): poly(vinylidene-fluoridetri-fluoroethylene); P(VDF-CTFE): poly(vinylidene fluoride-chlorotrifluoroethylene); P(VDF-TrFE-CTFE): poly(vinylidene-fluoride-tertrifluoroethylene-ter-chlorotrifluoroethylene); PMMA: poly(methyl methacrylate); c-BCB: crosslinked divinyltetramethylsiloxane-bis(benzocyclobutene); RCH: chitin; PATP: the polypropylene acyl tetraethylene pentaamine; DPAES: poly(aryl ether sulfone); IL: ionic liquid; BT NPs: BaTiO₃ nanoparticles; BT NWs: BaTiO₃ nanowires; Al₂O₃ NWs: Al₂O₃ nanoplates; PZT NWs: lead zirconate titanate; ST NWs: SrTiO₃ nanowires; ZrO₂ NSs: ZrO₂ nanosheets; BCZT NFs: 0.5(Ba_{0.7}Ca_{0.3})TiO₃-0.5Ba(Zr_{0.2}Ti_{0.8})O₃ nanofibers; BST NWs: Ba_{0.2}Sr_{0.8}TiO₃ nanowires; BCZT NFs: 0.5(Ba_{0.7}Ca_{0.3})TiO₃-0.5Ba(Zr_{0.2}Ti_{0.8})O₃ nanofibers; m-BT NPs: modified BaTiO₃ nanoparticles; m-TiO₂ NPs: modified TiO₂ nanoparticles; m-TiO₂ NWs: modified TiO₂ nanowires; m-BZT NFs: surface-modified Ba(Zr_{0.3}Ti_{0.7})O₃ nanofibers; f-DOPA@TiO₂ NWs: fluoro-polydopamine modified-TiO₂ nanowires; DOPA@TiO₂: polydopamine coated TiO₂; BT-DA NTs: BaTiO₃ nanotubes coated with a dense dopamine layer; BT-ST: SrTiO₃ nanowires grafted onto the surface of BaTiO₃ nanoparticles; SSBT: Bi₂O₃-doped Ba_{0.3}Sr_{0.7}TiO₃; F-BST NFs: surface fluorinated Ba_{0.6}Sr_{0.4}TiO₃ nanofibers; BZT-BCT NFs: 0.5Ba(Zr_{0.2}Ti_{0.8})O₃0.5(Ba_{0.7}Ca_{0.3})TiO₃ nanofibers; P-BST: plate-like (Ba_{0.6}Sr_{0.4})TiO₃ particles; TOMLs: titania monolayers; AR71: polyacrylate elastomers; BNNs: boron nitride nanosheets; OH-BNNs: surface hydroxylated BNNs; MMT: montmorillonite nanoplatelets; MXene: Titanium carbide MXene; BT@BN: BaTiO₃@BN nanosheets; BT@TO NPs: core-shell structured BaTiO₃@TiO₂ nanoparticles; TO@BT NFs: core-shell structured TiO₂@BaTiO₃ nanofibers; TO@BT NWs: core-shell structured TiO₂@BaTiO₃ nanowires; BT@SiO₂: core-shell structured BaTiO₃/SiO₂ nanoparticles; BT@Al₂O₃ NFs: core-shell structured BaTiO₃@Al₂O₃ nanofibers; BT@TO@AO NFs: core-double-shell structured BaTiO₃@TiO₂@Al₂O₃ nanofibers; BCZT@PATP NFs: PATP grafted into the surface of BCZT NFs; Fe₃O₄@BNNs: Fe₃O₄@boron nitride nanosheets; 2D NN@AO Ps: two-dimensional core-shell NaNbO₃@Al₂O₃ platelets; P-NBT4: The plate-like Na_{0.5}Bi_{4.5}Ti₄O₁₅ particles; RCH/BN: chitin/boron nitride nanosheets; Ni(OH)₂: platelet 2D Nickel hydroxide; eMica: ultrasonic-exfoliated mica nanosheets; TNA: 1-dimensional TiO₂ nanorod array; Ag-OMMT: silver-deposited exfoliated montmorillonite nanoplatelets; P(VDF-TrFE-CTFE)-g-PMMA: PMMA grafted into P(VDF-TrFE-CTFE); GNs-HAP-PBO: core/shell-structured hyperbranched aromatic polyamide functionalized graphene nanosheets-poly(p-phenylene benzobisoxazole).

NOMENCLATURE

U_e	the energy density
E_b	breakdown strength
ϵ_0	vacuum dielectric constant
ϵ_r	relative dielectric constant
BOPP	biaxially oriented polypropylen
0D	zero-dimensional
1D	one-dimensional
2D	two-dimensional
μ	electric dipole moment
P	electric polarization
χ	polarizability
E	the electric field
D	the electric displacement
U_b	the breakdown voltage
ρ	the density
C	the heat capacity
k	the electrical conductivity
σ	the thermal conductivity
η	charge-discharge efficiency
Y	Young's modulus
D-E loop	the electric displacement-electric field loop
T_c	the Curie temperature
T_m	the melting temperature
T_g	glass transition temperature
PVDF	poly(vinylidene fluoride)
P(VDF-TrFE)	poly(vinylidene fluoride-trifluoroethylene)
P(VDF-HFP)	poly(vinylidene fluoride-hexafluoropropylene)
P(VDF-TrFE-CFE)	poly(vinylidene-fluoride-trifluoroethylene-chlorofluoroethylene)
VDF	vinylidene fluoride
TrFE	trifluoroethylene
TFE	tetrafluoroethylene
HFP	hexafluoropropylene
CFE	chlorofluoroethylene
HEVs	hybrid electric vehicles
PMMA	Poly(methyl methacrylate)
PC	polycarbonate
PI	polyimide
PP	polypropylene
PPS	polyphenylene sulfide
PEIs	Poly(ether imides)
PEEK	poly(ether ether ketone)
PEKK	poly(ether ketone ketone)
PPEK	poly(phthalazinone ether ketone)
SO ₂ -PPO	sulfonylated poly(2,6-dimethyl-1,4-phenylene oxide)
BT	BaTiO ₃
TO	TiO ₂
SO	SiO ₂
BT-NTs	BT nanotubes
BT-NFs	BT nanofibers
BT-NPs	BT nanoparticles
BT-NWs	BT nanowires
BT-NPLs	BT nanoplates
NTO NWs	Na ₂ Ti ₃ O ₇ nanowires
TO NWs	TiO ₂ nanowires
ST NWs	SrTiO ₃ nanowires
PZT NWs	PbZrTiO ₃ nanowires
TNA	TiO ₂ nanorod array
MMT	montmorillonite
BN	hexagonal boron nitride
BNNS	hexagonal boron nitride nanosheets

. Continued

RCH	regenerated chitin
BCB	divinyltetramethyldisi-oxane-bis(benzocyclobutene)
c-BCB	crosslinked divinyltetramethyldisiloxane-bis(benzocyclobutene)
DPAES	anchoring poly(aryl ether sulfone)
CNO	$\text{Ca}_2\text{Nb}_3\text{O}_{10}$
Al_2O_3 -NPs	Al_2O_3 nanoparticles
Al_2O_3 -NWs	Al_2O_3 nanowires
Al_2O_3 -NPLs	Al_2O_3 nanoplates
E_g	bandgap
POFNB	polyoxafluoronor-bornene
TPU	thermoplastic polyurethane
CNS	carbon nanostructures
GNP	graphene nanoplatelets
Ti_3C_2	titanium carbide
IL	ionic liquid
Na+ MMT	nano-montmorillonite
rGO	reduced graphene oxide
DE	dielectric elastomers
PMF	paraelectric-moderate-ferroelectric
F4C	2,3,4,5-tetrafluorobenzoic acid
F4C2	tetrafluorophthalic acid
C2	phthalic acid
BST NFs	$\text{Ba}_{0.6}\text{Sr}_{0.4}\text{TiO}_3$ nanofibers
F-BST NF	surface-fluorinated BST NFs
BZT NFs	$\text{Ba}(\text{Zr}_{0.3}\text{Ti}_{0.7})\text{O}_3$ nanofibers
f-DOPA	fluoro-polydopamine
PATP	polypropylene acyl tetraethylene pentaamine
BCZT NFs	$0.5(\text{Ba}_{0.7}\text{Ca}_{0.3})\text{TiO}_3-0.5\text{Ba}(\text{Zr}_{0.2}\text{Ti}_{0.8})\text{O}_3$ nanofibers
BT@SO NPs	core-shell structured BT/SO nanoparticles
BT@SO NFs	core-shell structured BT/SO nanofibers
BT@TO NFs	core-shell structured BT/TO nanofibers
BT@ Al_2O_3 NFs	core-shell structured BT@ Al_2O_3 nanofibers
BT@TO@AO NFs	core-double-shell structure BT@TO@ Al_2O_3 nanofibers
CVD	chemical vapor deposition
PVD	physical vapor deposition
PECVD	plasma-enhanced chemical vapor deposition

core-shell structured fillers by introducing a shell layer with a moderating dielectric constant possess reduced energy loss and improved energy discharged density. In order to further improve the high energy density of polymer dielectrics, the single-layer nanocomposites have met great challenges, a series of topologically sandwich-structured films were prepared as a promising route to provide concurrent enhancements in the dischargeable U_e and η .

In addition, macro-interface engineering enables to interpose of high-aspect-ratio nanosheets as topological barriers to suppress electrical conduction. Coating wide-bandgap insulating materials onto the surface of polymers is believed to be an effective approach to suppress the surface charge injection and improve the high-temperature performance of polymer dielectrics. Alternatively, introducing highly insulating nanostructures into the polymer matrix has proved to be another effective strategy to improving the high-temperature capacitive properties. In our opinion, the approach of interfacial modification via 2D materials is the most promising strategy of developing BOPP substitutes in the above discussion. For example, 2D MMT are interposed at the interfaces of a sandwich-structured BT/PI film, resulting in an ultrahigh U_e of 3.6 J/cm^3 accompanied with a η of 70% at 150°C and 400 MV/m , which is at least two times higher than that of state-of-the-art high-temperature polymers.

Although great progress has been achieved in developing high-energy-density polymer dielectrics for electrical energy storage and applications, challenges remain. First, the incorporation of nanofillers is beneficial to improving the energy storage properties of the nanocomposites, but still could not meet the needs of electrical energy storage and applications. For nanofillers, 0D nanoparticles with high packing volume fraction added into composites improve ϵ_r at the expense of the breakdown strength, which in turn

limits the energy density of the capacitor. 1D nanofibers with a large aspect ratio provide the highest polarizability and breakdown strength, but the energy loss is still higher and thus leads to low charge-discharge efficiency. Compared with 0D and 1D nanofillers, 2D nanosheets have higher breakdown strength and lower dielectric loss. 2D fillers also show some problems, such as high conductivity, low polarization, or large thickness. Therefore, at present, the composition of nanocomposites needs to be further optimized for achieving excellent energy storage performance.

Secondly, the multi-interfaces of 2D multiphase systems and the topologically sandwich structure are effective in improving the energy storage properties of nanocomposites. Although synergic integrations of the multiple components and the introduction of multi-interfaces are a perfect combination of compositional and structural tailoring, the mechanisms underlying the interplay of multi-interfaces remain unclear. For example, the hierarchical polymer composites and films achieved higher E_b in comparison with the single-layered counterparts by adjusting the electric distribution. However, the internal breakdown process is difficult to observe by experimental methods so there are challenges for optimizing the structural design to further achieve the outstanding energy storage properties.

Finally, the preparation methods of nanocomposite films also hinder the advancements. Although the powerful electrospinning method tends to be used for preparing complicated sandwich-structured nanocomposites, its throughput rate is extremely low. Besides, it is difficult to simultaneously achieve large-scale and high-quality films by a layer-by-layer hot-pressing method. The methods for orienting 2D materials include shearing and electrospinning, but the achieved orientation by those methods lacks variety and is not as strict as that of 1D fillers. Therefore, the effective preparation methods for application still need to be further developed. All in all, advancing the development of polymer dielectrics requires close interdisciplinary cooperation among chemists, materials scientists, mechanical engineers, and other experts.

ACKNOWLEDGMENTS

This work was funded by the National Natural Science Foundation of China (No. 51977137) and Central Guidance on Local Science and Technology Development Found of Shanxi Province (YDZJSX2021A021).

AUTHOR CONTRIBUTIONS

Y.F.W. and Z.P.L. conceived the idea and initiated the project; R.C., R.J.M., and Y.Y.L.: Investigation; R.C.: Writing-Original Draft; R.J.M., Y.Y.L., and J.C.S.: Reviewing and editing; J.C.S., M.Q.G., and Z.P.L.: Funding acquisition; Y.F.W. and Z.P.L.: Supervision, reviewing and editing; Y.F.W. and Z.P.L. guided the entire work. All authors read and provided feedback on the manuscript.

DECLARATION OF INTERESTS

The authors declare no competing interests.

REFERENCES

- Ai, D., Li, H., Zhou, Y., Ren, L., Han, Z., Yao, B., Zhou, W., Zhao, L., Xu, J., and Wang, Q. (2020). Tuning nanofillers in situ prepared polyimide nanocomposites for high-temperature capacitive energy storage. *Adv. Energy Mater.* 10, 1903881. <https://doi.org/10.1002/aenm.201903881>.
- Almadhoun, M.N., Bhansali, U.S., and Alshareef, H.N. (2012). Nanocomposites of ferroelectric polymers with surface-hydroxylated BaTiO₃ nanoparticles for energy storage applications. *J. Mater. Chem.* 22, 11196. <https://doi.org/10.1039/c2jm30542a>.
- Andrews, C., Lin, Y., and Sodano, H.A. (2009). Effect of aspect ratio on the electroelastic properties of piezoelectric nanocomposites. *Smart Mater. Struct.* 19, 328–335. <https://doi.org/10.1117/12.815136>.
- Azizi, A., Gadinski, M.R., Li, Q., Alsaud, M.A., Wang, J., Wang, Y., Wang, B., Liu, F., Chen, L., Alem, N., and Wang, Q. (2017). High-performance polymers sandwiched with chemical vapor deposited hexagonal boron nitrides as scalable high-temperature dielectric materials. *Adv. Mater.* 29, 1701864. <https://doi.org/10.1002/adma.201701864>.
- Bao, Z., Hou, C., Shen, Z., Sun, H., Zhang, G., Luo, Z., Dai, Z., Wang, C., Chen, X., Li, L., et al. (2020). Negatively charged nanosheets significantly enhance the energy-storage capability of polymer-based nanocomposites. *Adv. Mater.* 32, 1907227. <https://doi.org/10.1002/adma.201907227>.
- Bendler, J.T., Boyles, D.A., Edmondson, C.A., Filipova, T., Fontanella, J.J., Westgate, M.A., and Wintersgill, M.C. (2013). Dielectric properties of bisphenol A polycarbonate and its tethered nitrile analogue. *Macromolecules* 46, 4024–4033. <https://doi.org/10.1021/ma4002269>.
- Bharti, V., Zhao, X.Z., Zhang, Q.M., Romotowski, T., Tito, F., and Ting, R. (1998). Ultrahigh field induced strain and polarization response in electron irradiated poly(vinylidene fluoride-trifluoroethylene) copolymer. *Mater. Res. Innovat.* 2, 57–63. <https://doi.org/10.1007/s100190050063>.
- Cai, Z., Wang, X., Luo, B., and Li, L. (2018). Hierarchical-structured dielectric permittivity and breakdown performances of polymer-ceramic nanocomposites. *Ceram.Int.* 44, 843–848. <https://doi.org/10.1016/j.ceramint.2017.10.008>.
- Binder, K. (1986). Spin glasses: experimental facts, theoretical concepts, and open questions. *Rev. Mod. Phys.* 58, 801–976. <https://doi.org/10.1103/revmodphys.58.801>.
- Cai, Z., Wang, X., Luo, B., Hong, W., Wu, L., and Li, L. (2017). Dielectric response and breakdown behavior of polymer-ceramic nanocomposites: the effect of nanoparticle distribution. *Compos. Sci. Technol.* 145, 105–113. <https://doi.org/10.1016/j.compscitech.2017.03.039>.
- Cao, Y., Irwin, P.C., and Younsi, K. (2004). The future of nanodielectrics in the electrical power

- industry. *IEEE Trans. Dielectr. Electr. Insul.* 11, 797–807. <https://doi.org/10.1109/TDEI.2004.1349785>.
- Chen, L., Batra, R., Ranganathan, R., Sotzing, G., Cao, Y., and Ramprasad, R. (2018a). Electronic structure of polymer dielectrics: the role of chemical and morphological complexity. *Chem. Mater.* 30, 7699–7706. <https://doi.org/10.1021/acs.chemmater.8b02997>.
- Chen, L., Huan, T.D., Quintero, Y.C., and Ramprasad, R. (2015a). Charge injection barriers at metal/polyethylene interfaces. *J. Mater. Sci.* 51, 506–512. <https://doi.org/10.1007/s10853-015-9369-2>.
- Chen, Q., Chu, B., Zhou, X., and Zhang, Q.M. (2007). Effect of metal-polymer interface on the breakdown electric field of poly(vinylidene fluoride-trifluoroethylene-chlorofluoroethylene) terpolymer. *Appl. Phys. Lett.* 91, 062907. <https://doi.org/10.1063/1.2768205>.
- Chen, Q., Shen, Y., Zhang, S., and Zhang, Q.M. (2015b). Polymer-based dielectrics with high energy storage density. *Annu. Rev. Mater. Res.* 45, 433–458. <https://doi.org/10.1146/annurev-matsci-070214-021017>.
- Chen, X., Liu, L., Liu, S.Z., Cui, Y.S., Chen, X.Z., Ge, H.X., and Shen, Q.D. (2013). P(VDF-TrFE-CFE) terpolymer thin-film for high performance nonvolatile memory. *Appl. Phys. Lett.* 102, 063103. <https://doi.org/10.1063/1.4791598>.
- Chen, J., Wang, Y., Yuan, Q., Xu, X., Niu, Y., Wang, Q., and Wang, H. (2018b). Multilayered ferroelectric polymer films incorporating low-dielectric-constant components for concurrent enhancement of energy density and charge-discharge efficiency. *Nano Energy* 54, 288–296. <https://doi.org/10.1016/j.nanoen.2018.10.028>.
- Cheng, S., Zhou, Y., Hu, J., He, J., and Li, Q. (2020). Polyimide films coated by magnetron sputtered boron nitride for high-temperature capacitor dielectrics. *IEEE Trans. Dielectr. Electr. Insul.* 27, 498–503. <https://doi.org/10.1109/TDEI.2020.008592>.
- Chi, Q., Liu, G., Zhang, C., Cui, Y., Wang, X., and Lei, Q. (2018). Microstructure and dielectric properties of BZT-BCT/PVDF nanocomposites. *Results Phys.* 8, 391–396. <https://doi.org/10.1016/j.rinp.2017.12.052>.
- Chi, Q., Ma, T., Zhang, Y., Cui, Y., Zhang, C., Lin, J., Wang, X., and Lei, Q. (2017). Significantly enhanced energy storage density for poly(vinylidene fluoride) composites by induced PDA-coated 0.5Ba(Zr_{0.2}Ti_{0.8})O₃-0.5(Ba_{0.7}Ca_{0.3})TiO₃ nanofibers. *J. Mater. Chem. A Mater.* 5, 16757–16766. <https://doi.org/10.1039/C7TA03897F>.
- Chi, Q., Wang, B., Zhang, T., Zhang, C., Zhang, Y., Wang, X., and Lei, Q. (2019). Designing of surface modification and sandwich structure: effective routes to improve energy storage property in polyimide-based composite films. *J. Mater. Sci. Mater. Electron.* 30, 19956–19965. <https://doi.org/10.1007/s10854-019-02362-1>.
- Chiu, F.C. (2014). A review on conduction mechanisms in dielectric films. *Adv. Mater. Sci. Eng.* 2014, 1–18. <https://doi.org/10.1155/2014/578168>.
- Choudhury, A. (2012). Preparation, characterization and dielectric properties of polyetherimide nanocomposites containing surface-functionalized BaTiO₃ nanoparticles. *Polym. Int.* 61, 696–702. <https://doi.org/10.1002/pi.4181>.
- Chu, B.J., Zhou, X., Neese, B., Zhang, Q.M., and Bauer, (2006a). Relaxor ferroelectric poly(vinylidene fluoride-trifluoroethylene-chlorofluoroethylene) terpolymer for high energy density storage capacitors. *IEEE Trans. Dielectr. Electr. Insul.* 13, 1162–1169. <https://doi.org/10.1109/TDEI.2006.247845>.
- Chu, B., Zhou, X., Ren, K., Neese, B., Lin, M., Wang, Q., Bauer, F., and Zhang, Q.M. (2006b). A dielectric polymer with high electric energy density and fast discharge speed. *Science* 313, 334–336. <https://doi.org/10.1126/science.1127798>.
- Dang, Z.M., Yan, W.T., and Xu, H.P. (2007). Novel high-dielectric-permittivity poly(vinylidene fluoride)/polypropylene blend composites: the influence of the poly(vinylidene fluoride) concentration and compatibilizer. *J. Appl. Polym. Sci.* 105, 3649–3655. <https://doi.org/10.1002/app.26447>.
- Deng, Q., Feng, Y., Li, W., Xu, X., Peng, C., and Wu, Q. (2019). Strong interface effect induced high-k property in polymer based ternary composites filled with 2D layered Ti₃C₂ MXene nanosheets. *J. Mater. Sci. Mater. Electron.* 30, 9106–9113. <https://doi.org/10.1007/s10854-019-01239-7>.
- Fan, B., Liu, F., Yang, G., Li, H., Zhang, G., Jiang, S., and Wang, Q. (2018). Dielectric materials for high-temperature capacitors. *IET Nanodielectrics* 1, 32–40. <https://doi.org/10.1049/iet-nde.2018.0002>.
- Feng, Y.F., Deng, Q., Peng, C., and Wu, Q. (2019). High dielectric and breakdown properties achieved in ternary BaTiO₃/MXene/PVDF nanocomposites with low-concentration fillers from enhanced interface polarization. *Ceram. Int.* 45, 7923–7930. <https://doi.org/10.1016/j.ceramint.2019.01.104>.
- Feng, H., Ma, W., Cui, Z.K., Liu, X., Gu, J., Lin, S., and Zhuang, Q. (2017). Core/shell-structured hyperbranched aromatic polyamide functionalized graphene nanosheets-poly(p-phenylene benzobisoxazole) nanocomposite films with improved dielectric properties and thermostability. *J. Mater. Chem. A Mater.* 5, 8705–8713. <https://doi.org/10.1039/c7ta00587c>.
- Fournier, D., and Lamarre, L. (1992). Effect of Pressure and Length on Interfacial Breakdown between Two Dielectric Surfaces. *IEEE*, 270–272. <https://doi.org/10.1109/ELINSL.1992.247004>.
- Fu, J., Hou, Y., Liu, X., Zheng, M., and Zhu, M. (2020). A construction strategy of ferroelectrics by the molten salt method and its application in the energy field. *J. Mater. Chem. C Mater.* 8, 8704–8731. <https://doi.org/10.1039/D0TC01924K>.
- Fu, J., Hou, Y., Zheng, M., Wei, Q., Zhu, M., and Yan, H. (2015). Improving dielectric properties of PVDF composites by employing surface modified strong polarized BaTiO₃ particles derived by molten salt method. *ACS Appl. Mater. Interfaces* 7, 24480–24491. <https://doi.org/10.1021/acsami.5b05344>.
- Gao, L., He, J., Hu, J., and Li, Y. (2014). Large enhancement in polarization response and energy storage properties of poly(vinylidene fluoride) by improving the interface effect in nanocomposites. *J. Phys. Chem. C* 118, 831–838. <https://doi.org/10.1021/jp409474k>.
- Gao, W., Dickinson, L., Grozinger, C., Morin, F.G., and Reven, L. (1996). Self-assembled monolayers of alkylphosphonic acids on metal oxides. *Langmuir* 12, 6429–6435. <https://doi.org/10.1021/la9607621>.
- Gross, S., Camozzo, D., Di Noto, V., Armelao, L., and Tondello, E. (2007). PMMA: a key macromolecular component for dielectric low-k hybrid inorganic-organic polymer films. *Eur. Polym. J.* 43, 673–696. <https://doi.org/10.1016/j.eurpolymj.2006.12.012>.
- Guo, F., Shen, X., Zhou, J., Liu, D., Zheng, Q., Yang, J., Jia, B., Lau, A.K.T., and Kim, J. (2020). Highly thermally conductive dielectric nanocomposites with synergistic alignments of graphene and boron nitride nanosheets. *Adv. Funct. Mater.* 30, 1910826. <https://doi.org/10.1002/adfm.201910826>.
- Hao, Y., Wang, X., Bi, K., Zhang, J., Huang, Y., Wu, L., Zhao, P., Xu, K., Lei, M., and Li, L. (2017). Significantly enhanced energy storage performance promoted by ultimate sized ferroelectric BaTiO₃ fillers in nanocomposite films. *Nano Energy* 31, 49–56. <https://doi.org/10.1016/j.nanoen.2016.11.008>.
- He, D., Wang, Y., Zhang, L., Song, S., and Deng, Y. (2018). Poly(vinylidene fluoride)-based composites modulated via multiscale two-dimensional fillers for high dielectric performances. *Compos. Sci. Technol.* 159, 162–170. <https://doi.org/10.1016/j.compscitech.2018.02.040>.
- He, F., Lau, S., Chan, H.L., and Fan, J. (2009). High dielectric permittivity and low percolation threshold in nanocomposites based on poly(vinylidene fluoride) and exfoliated graphite nanoplates. *Adv. Mater.* 21, 710–715. <https://doi.org/10.1002/adma.200801758>.
- Ho, J., and Jow, R. (2009). Characterization of High Temperature Polymer Thin Films for Power Conditioning Capacitors (Adelphi, MD: Army Research Lab Adelphi MD Sensors and Electron Devices Directorate).
- Ho, J.S., and Greenbaum, S.G. (2018). Polymer capacitor dielectrics for high temperature applications. *ACS Appl. Mater. Interfaces* 10, 29189–29218. <https://doi.org/10.1021/acsami.8b07705>.
- Hu, J., Zhang, S., and Tang, B. (2021). 2D filler-reinforced polymer nanocomposite dielectrics for high-k dielectric and energy storage applications. *Energy Storage Mater.* 34, 260–281. <https://doi.org/10.1016/j.ensm.2020.10.001>.
- Hu, P., Song, Y., Liu, H., Shen, Y., Lin, Y., and Nan, C.W. (2013). Largely enhanced energy density in flexible P(VDF-TrFE) nanocomposites by surface-modified electrospun BaSrTiO₃ fibers. *J. Mater. Chem.* 1, 1688–1693. <https://doi.org/10.1039/C2TA00948J>.
- Iijima, M., Sato, N., Wuled Lenggoro, I., and Kamiya, H. (2009). Surface modification of BaTiO₃ particles by silane coupling agents in different

solvents and their effect on dielectric properties of BaTiO₃/epoxy composites. *Colloids Surf. A Physicochem. Eng. Asp.* 352, 88–93. <https://doi.org/10.1016/j.colsurfa.2009.10.005>.

Jayasuriya, A.C., Schirokauer, A., and Scheinbeim, J.I. (2001). Crystal-structure dependence of electroactive properties in differently prepared poly(vinylidene fluoride/hexafluoropropylene) copolymer films. *J. Polym. Sci. B Polym. Phys.* 39, 2793–2799. <https://doi.org/10.1002/polb.10035>.

Jeong, D.Y., Wang, Y.K., Huang, M., Zhang, Q.M., Kavarnos, G.J., and Bauer, F. (2004). Electro-optical response of the ferroelectric relaxor poly(vinylidene fluoride-trifluoroethylene-chlorofluoroethylene) terpolymer. *J. Appl. Phys.* 96, 316–319. <https://doi.org/10.1063/1.1757032>.

Ji, W., Deng, H., Sun, C., and Fu, Q. (2019). Nickel hydroxide as novel filler for high energy density dielectric polymer composites. *Compos. Sci. Technol.* 172, 117–124. <https://doi.org/10.1016/j.compscitech.2019.01.010>.

Chen, J., Wang, Y., Dong, J., Niu, Y., Chen, W., and Wang, H. (2020). Enhanced dielectric performance in flexible MWCNT/poly(vinylidene fluoride-co-hexafluoropropylene)-based nanocomposites by designing a tri-layered structure. *J. Mater. Chem. C Mater.* 8, 5950–5957. <https://doi.org/10.1039/D0TC00148A>.

Chen, J., Wang, Y., Xu, X., Yuan, Q., Niu, Y., Wang, Q., and Wang, H. (2019). Ultrahigh discharge efficiency and energy density achieved at low electric fields in sandwich-structured polymer films containing dielectric elastomers. *J. Mater. Chem. A Mater.* 7, 3729–3736. <https://doi.org/10.1039/C8TA11790J>.

Kang, S.J., Park, Y.J., Bae, I., Kim, K.J., Kim, H.C., Bauer, S., Thomas, E.L., and Park, C. (2009). Printable ferroelectric PVDF/PMMA blend films with ultralow roughness for low voltage non-volatile polymer memory. *Adv. Funct. Mater.* 19, 2812–2818. <https://doi.org/10.1002/adfm.200900589>.

Ke, K., McMaster, M., Christopherson, W., Singer, K.D., and Manas-Zloczower, I. (2019). Effects of branched carbon nanotubes and graphene nanoplatelets on dielectric properties of thermoplastic polyurethane at different temperatures. *Compos. B Eng.* 166, 673–680. <https://doi.org/10.1016/j.compositesb.2019.03.005>.

Kim, P., Doss, N.M., Tillotson, J.P., Hotchkiss, P.J., Pan, M.J., Marder, S.R., Li, J., Calame, J.P., and Perry, J.W. (2009). High energy density nanocomposites based on surface-modified BaTiO₃ and a ferroelectric polymer. *ACS Nano* 3, 2581–2592. <https://doi.org/10.1021/nn9006412>.

Kim, Y.H., Kim, H.J., Osada, M., Li, B.W., Ebina, Y., and Sasaki, T. (2014). 2D perovskite nanosheets with thermally-stable high-kappa response: a new platform for high-temperature capacitors. *ACS Appl. Mater. Interfaces* 6, 19510–19514. <https://doi.org/10.1021/am506629g>.

Klein, R.J., Xia, F., Zhang, Q.M., and Bauer, F. (2005). Influence of composition on relaxor ferroelectric and electromechanical properties of poly(vinylidene fluoride-trifluoroethylene-chlorofluoroethylene). *J. Appl. Phys.* 97, 094105. <https://doi.org/10.1063/1.1882769>.

Li, H., Ai, D., Ren, L., Yao, B., Han, Z., Shen, Z., Wang, J., Chen, L.Q., and Wang, Q. (2019). Scalable polymer nanocomposites with record high-temperature capacitive performance enabled by rationally designed nanostructured inorganic fillers. *Adv. Mater.* 31, 1900875. <https://doi.org/10.1002/adma.201900875>.

Li, H., Gadinski, M.R., Huang, Y., Ren, L., Zhou, Y., Ai, D., Han, Z., Yao, B., and Wang, Q. (2020a). Crosslinked fluoropolymers exhibiting superior high-temperature energy density and charge-discharge efficiency. *Energy Environ. Sci.* 13, 1279–1286. <https://doi.org/10.1039/C9EE03603B>.

Li, H., Ren, L., Ai, D., Han, Z., Liu, Y., Yao, B., and Wang, Q. (2020b). Ternary polymer nanocomposites with concurrently enhanced dielectric constant and breakdown strength for high-temperature electrostatic capacitors. *Inf. Manage.* 2, 389–400. <https://doi.org/10.1002/inf2.12043>.

Li, H., Zhou, Y., Liu, Y., Li, L., Liu, Y., and Wang, Q. (2021). Dielectric polymers for high-temperature capacitive energy storage. *Chem. Soc. Rev.* 50, 6369–6400. <https://doi.org/10.1039/D0CS00765J>.

Li, J., Seok, S.I., Chu, B., Dogan, F., Zhang, Q., and Wang, Q. (2009). Nanocomposites of ferroelectric polymers with TiO₂ nanoparticles exhibiting significantly enhanced electrical energy density. *Adv. Mater.* 21, 217–221. <https://doi.org/10.1002/adma.200801106>.

Li, J.Y., Zhang, L., and Ducharme, S. (2007). Electric energy density of dielectric nanocomposites. *Appl. Phys. Lett.* 90, 132901. <https://doi.org/10.1063/1.2716847>.

Li, Q., Chen, L., Gadinski, M.R., Zhang, S., Zhang, G., Li, H., Iagodkine, E., Haque, A., Chen, L.Q., Jackson, T., and Wang, Q. (2015a). Flexible high-temperature dielectric materials from polymer nanocomposites. *Nature* 523, 576–579. <https://doi.org/10.1038/nature14647>.

Li, Q., Han, K., Gadinski, M.R., Zhang, G., and Wang, Q. (2014). High energy and power density capacitors from solution-processed ternary ferroelectric polymer nanocomposites. *Adv. Mater.* 26, 6244–6249. <https://doi.org/10.1002/adma.201402106>.

Li, Q., Zhang, G., Liu, F., Han, K., Gadinski, M.R., Xiong, C., and Wang, Q. (2015b). Solution-processed ferroelectric terpolymer nanocomposites with high breakdown strength and energy density utilizing boron nitride nanosheets. *Energy Environ. Sci.* 8, 922–931. <https://doi.org/10.1039/C4EE02962C>.

Li, Q., Yao, F.Z., Liu, Y., Zhang, G., Wang, H., and Wang, Q. (2018). High-temperature dielectric materials for electrical energy storage. *Annu. Rev. Mater. Res.* 48, 219–243. <https://doi.org/10.1146/annurev-matsci-070317-124435>.

Li, W., Yang, J., Wu, Z., Wang, J., Li, B., Feng, S., Deng, Y., Zhang, F., and Zhao, D. (2012). A versatile kinetics-controlled coating method to construct uniform porous TiO₂ shells for multifunctional core-shell structures. *J. Am. Chem. Soc.* 134, 11864–11867. <https://doi.org/10.1021/ja3037146>.

Li, W.J., Meng, Q.J., Zheng, Y.S., Zhang, Z.C., Xia, W.M., and Xu, Z. (2010). Electric energy storage properties of poly(vinylidene fluoride). *Appl. Phys. Lett.* 96, 192905. <https://doi.org/10.1090/S0002-9939-2011-10775-5>.

Lin, X., Hu, P., Jia, Z., and Gao, S. (2016). Enhanced electric displacement induces large energy density in polymer nanocomposites containing core-shell structured BaTiO₃@TiO₂ nanofibers. *J. Mater. Chem. A Mater.* 4, 2314–2320. <https://doi.org/10.1039/C5TA09547F>.

Liu, F., Li, Q., Cui, J., Li, Z., Yang, G., Liu, Y., Dong, L., Xiong, C., Wang, H., and Wang, Q. (2017a). High-energy-density dielectric polymer nanocomposites with trilayered architecture. *Adv. Funct. Mater.* 27, 1606292. <https://doi.org/10.1002/adfm.201770125>.

Liu, F., Li, Q., Li, Z., Liu, Y., Dong, L., Xiong, C., and Wang, Q. (2017b). Poly(methyl methacrylate)/boron nitride nanocomposites with enhanced energy density as high temperature dielectrics. *Compos. Sci. Technol.* 142, 139–144. <https://doi.org/10.1016/j.compscitech.2017.02.006>.

Wang, F., Xia, R., Li, X., Qin, J., Shao, H., Jian, G., Liu, R., Wang, F., and Liu, H. (2020). Improving the electrical and mechanical performances of embedded capacitance materials by introducing tungsten disulfide nanoflakes into the dielectric layer. *J. Mater. Sci. Mater. Electron.* 31, 7889–7897. <https://doi.org/10.1007/s10854-020-03327-5>.

Liu, S., Wang, J., Shen, B., and Zhai, J. (2017c). Enhanced discharged energy density and efficiency of poly(vinylidene fluoride) nanocomposites through a small loading of core-shell structured BaTiO₃@Al₂O₃ nanofibers. *Ceram. Int.* 43, 585–589. <https://doi.org/10.1016/j.ceramint.2016.09.198>.

Liu, S., Xiao, S., Xiu, S., Shen, B., Zhai, J., and An, Z. (2015a). Poly(vinylidene fluoride) nanocomposite capacitors with a significantly enhanced dielectric constant and energy density by filling with surface-fluorinated Ba_{0.6}Sr_{0.4}TiO₃ nanofibers. *RSC Adv.* 5, 40692–40699. <https://doi.org/10.1039/C5RA05095B>.

Liu, S., Xue, S., Shen, B., and Zhai, J. (2015b). Reduced energy loss in poly(vinylidene fluoride) nanocomposites by filling with a small loading of core-shell structured BaTiO₃@TiO₂ nanofibers. *Appl. Phys. Lett.* 107, 032907. <https://doi.org/10.1063/1.4927330>.

Liu, S., Xue, S., Xiu, S., Shen, B., and Zhai, J. (2016). Surface-modified Ba(Zr_{0.3}Ti_{0.7})O₃ nanofibers by polyvinylpyrrolidone filler for poly(vinylidene fluoride) composites with enhanced dielectric constant and energy storage density. *Sci. Rep.* 6, 26198. <https://doi.org/10.1038/srep26198>.

Luo, B., Wang, X., Wang, H., Cai, Z., and Li, L. (2017a). P(VDF-HFP)/PMMA flexible composite films with enhanced energy storage density and efficiency. *Compos. Sci. Technol.* 151, 94–103. <https://doi.org/10.1016/j.compscitech.2017.08.013>.

Luo, S., Shen, Y., Yu, S., Wan, Y., Liao, W.H., Sun, R., and Wong, C.P. (2017b). Construction of a 3D-BaTiO₃ network leading to significantly enhanced dielectric permittivity and energy storage density of polymer composites. *Energy Environ. Sci.* 10, 137–144. <https://doi.org/10.1039/C6EE03190K>.

- Luo, S., Yu, J., Yu, S., Sun, R., Cao, L., Liao, W.H., and Wong, C.P. (2018). Significantly enhanced electrostatic energy storage performance of flexible polymer composites by introducing highly insulating-ferroelectric microhybrids as fillers. *Adv. Energy Mater.* 9, 1803204. <https://doi.org/10.1002/aenm.201803204>.
- Luo, S., Yu, S., Sun, R., and Wong, C.P. (2014). Nano Ag-deposited BaTiO₃ hybrid particles as fillers for polymeric dielectric composites: toward high dielectric constant and suppressed loss. *ACS Appl. Mater. Interfaces* 6, 176–182. <https://doi.org/10.1021/am404556c>.
- Ma, W.F., Zhang, Y., Li, L.L., You, L.J., Zhang, P., Zhang, Y.T., Li, J.M., Yu, M., Guo, J., Lu, H.J., and Wang, C.C. (2012). Tailor-made magnetic Fe₃O₄@mTiO₂ microspheres with a tunable mesoporous anatase shell for highly selective and effective enrichment of phosphopeptides. *ACS Nano* 6, 3179–3188. <https://doi.org/10.1021/nn3009646>.
- Martins, P., Lopes, A.C., and Lanceros-Mendez, S. (2014). Electroactive phases of poly(vinylidene fluoride): determination, processing and applications. *Prog. Polym. Sci.* 39, 683–706. <https://doi.org/10.1016/j.progpolymsci.2013.07.006>.
- Mendes, S.F., Costa, C.M., Caparros, C., Sencadas, V., and Lanceros-Mendez, S. (2011). Effect of filler size and concentration on the structure and properties of poly(vinylidene fluoride)/BaTiO₃ nanocomposites. *J. Mater. Sci.* 47, 1378–1388. <https://doi.org/10.1007/s10853-011-5916-7>.
- Meng, N., Ren, X., Santagiuliana, G., Ventura, L., Zhang, H., Wu, J., Yan, H., Reece, M.J., and Bilotti, E. (2019). Ultrahigh β -phase content poly(vinylidene fluoride) with relaxor-like ferroelectricity for high energy density capacitors. *Nat. Commun.* 10, 4535. <https://doi.org/10.1038/s41467-019-12391-3>.
- Merche, D., Vandecasteele, N., and Reniers, F. (2012). Atmospheric plasmas for thin film deposition: a critical review. *Thin Solid Films* 520, 4219–4236. <https://doi.org/10.1016/j.tsf.2012.01.026>.
- Mittal, A., Jain, V., and Mittal, J. (2001). Temperature dependence of dielectric constant on pure polymethyl methacrylate. *Asian J. Chem.* 13, 1216–1218.
- Ngai, K.L. (2003). The effects of changes of intermolecular coupling on glass transition dynamics in polymer thin films and glass-formers confined in nanometer pores. *Eur. Phys. J. E Soft Matter* 12, 93–100. <https://doi.org/10.1140/epje/i2003-10029-3>.
- Niu, Y., Bai, Y., Yu, K., Wang, Y., Xiang, F., and Wang, H. (2015a). Effect of the modifier structure on the performance of barium titanate/poly(vinylidene fluoride) nanocomposites for energy storage applications. *ACS Appl. Mater. Interfaces* 7, 24168–24176. <https://doi.org/10.1021/acsami.5b07486>.
- Niu, Y., Xiang, F., Wang, Y., Chen, J., and Wang, H. (2018). Effect of the coverage level of carboxylic acids as a modifier for barium titanate nanoparticles on the performance of poly(vinylidene fluoride)-based nanocomposites for energy storage applications. *Phys. Chem. Chem. Phys.* 20, 6598–6605. <https://doi.org/10.1039/c7cp08312b>.
- Niu, Y., Yu, K., Bai, Y., Xiang, F., and Wang, H. (2015b). Fluorocarboxylic acid-modified barium titanate/poly(vinylidene fluoride) composite with significantly enhanced breakdown strength and high energy density. *RSC Adv.* 5, 64596–64603. <https://doi.org/10.1039/C5RA09023G>.
- Osada, M., Ebina, Y., Funakubo, H., Yokoyama, S., Kiguchi, T., Takada, K., and Sasaki, T. (2006). High-k dielectric nanofilms fabricated from titania nanosheets. *Adv. Mater.* 18, 1023–1027. <https://doi.org/10.1002/adma.200501224>.
- Osada, M., Takanashi, G., Li, B.W., Akatsuka, K., Ebina, Y., Ono, K., Funakubo, H., Takada, K., and Sasaki, T. (2011). Controlled polarizability of one-nanometer-thick oxide nanosheets for tailored, high-k nanodielectrics. *Adv. Funct. Mater.* 21, 3482–3487. <https://doi.org/10.1002/adfm.201100580>.
- Pan, J., Li, K., Chuayprakong, S., Hsu, T., and Wang, Q. (2010). High-temperature poly(phthalazinone ether ketone) thin films for dielectric energy storage. *ACS Appl. Mater. Interfaces* 2, 1286–1289. <https://doi.org/10.1021/am100146u>.
- Pan, J., Li, K., Li, J., Hsu, T., and Wang, Q. (2009). Dielectric characteristics of poly(ether ketone) for high temperature capacitive energy storage. *Appl. Phys. Lett.* 95, 022902. <https://doi.org/10.1063/1.3176219>.
- Pan, Z., Ding, Q., Yao, L., Huang, S., Xing, S., Liu, J., Chen, J., and Zhai, J. (2019). Simultaneous enhanced discharge energy density and efficiency in nanocomposite film capacitors utilizing two-dimensional NaNbO₃@Al₂O₃ platelets. *Nanoscale* 11, 10546–10554. <https://doi.org/10.1039/C9NR00874H>.
- Pan, Z., Yao, L., Zhai, J., Shen, B., and Wang, H. (2017a). Significantly improved dielectric properties and energy density of polymer nanocomposites via small loading of BaTiO₃ nanotubes. *Compos. Sci. Technol.* 147, 30–38. <https://doi.org/10.1016/j.compscitech.2017.05.004>.
- Pan, Z., Yao, L., Zhai, J., Shen, B., Liu, S., Wang, H., and Liu, J. (2016). Excellent energy density of polymer nanocomposites containing BaTiO₃@Al₂O₃ nanofibers induced by moderate interfacial area. *J. Mater. Chem. A Mater.* 4, 13259–13264. <https://doi.org/10.1039/C6TA05233A>.
- Pan, Z., Yao, L., Zhai, J., Wang, H., and Shen, B. (2017b). Ultrafast discharge and enhanced energy density of polymer nanocomposites loaded with 0.5(Ba_{0.7}Ca_{0.3})TiO₃-0.5ba(Zr_{0.2}Ti_{0.8})O₃ one-dimensional nanofibers. *ACS Appl. Mater. Interfaces* 9, 14337–14346. <https://doi.org/10.1021/acsami.7b01381>.
- Pan, Z., Yao, L., Zhai, J., Yang, K., Shen, B., and Wang, H. (2017c). Ultrafast discharge and high-energy-density of polymer nanocomposites achieved via optimizing the structure design of barium titanates. *ACS Sustainable Chem. Eng.* 5, 4707–4717. <https://doi.org/10.1021/acssuschemeng.7b00080>.
- Pan, Z., Zhai, J., and Shen, B. (2017d). Multilayer hierarchical interfaces with high energy density in polymer nanocomposites composed of BaTiO₃@TiO₂@Al₂O₃ nanofibers. *J. Mater. Chem. A Mater.* 5, 15217–15226. <https://doi.org/10.1039/C7TA03846A>.
- Paniagua, S.A., Hotchkiss, P.J., Jones, S.C., Marder, S.R., Mudalige, A., Marrikar, F.S., Pemberton, J.E., and Armstrong, N.R. (2008). Phosphonic acid modification of indium-tin oxide electrodes: combined XPS/UPS/contact angle studies. *J. Phys. Chem. C* 112, 7809–7817. <https://doi.org/10.1021/jp710893k>.
- Paniagua, S.A., Kim, Y., Henry, K., Kumar, R., Pery, J.W., and Marder, S.R. (2014). Surface-initiated polymerization from barium titanate nanoparticles for hybrid dielectric capacitors. *ACS Appl. Mater. Interfaces* 6, 3477–3482. <https://doi.org/10.1021/am4056276>.
- Pellerite, M.J., Dunbar, T.D., Boardman, L.D., and Wood, E.J. (2003). Effects of fluorination on self-assembled monolayer formation from alkanephosphonic acids on aluminum kinetics and structure. *J. Phys. Chem. B* 107, 11726–11736. <https://doi.org/10.1021/jp0354200>.
- Pelrine, R., Kornbluh, R., Pei, Q.B., and Joseph, J. (2000). High-speed electrically actuated elastomers with strain greater than 100. *Science* 287, 836–839. <https://doi.org/10.1126/science.287.5454.836>.
- Prateek, Thakur, V.K., and Gupta, R.K. (2016). Recent progress on ferroelectric polymer-based nanocomposites for high energy density capacitors: synthesis, dielectric properties, and future aspects. *Chem. Rev.* 116, 4260–4317. <https://doi.org/10.1021/acs.chemrev.5b00495>.
- Qiao, Y., Islam, M.S., Han, K., Leonhardt, E., Zhang, J., Wang, Q., Ploehn, H.J., and Tang, C. (2013). Polymers containing highly polarizable conjugated side chains as high-performance all-organic nanodielectric materials. *Adv. Funct. Mater.* 23, 5638–5646. <https://doi.org/10.1002/adfm.201300736>.
- Picci, G., and Rabuffi, M. (2002). Status quo and future prospects for metallized polypropylene energy storage capacitors. *IEEE Trans. Plasma Sci.* 30, 1939–1942. <https://doi.org/10.1109/PPPS.2001.961090>.
- Rahimabady, M., Mirshekarloo, M.S., Yao, K., and Lu, L. (2013). Dielectric behaviors and high energy storage density of nanocomposites with core-shell BaTiO₃@TiO₂ in poly(vinylidene fluoride-hexafluoropropylene). *Phys. Chem. Chem. Phys.* 15, 16242–16248. <https://doi.org/10.1039/C3CP52267A>.
- Rawlins, K.A., Lees, A.J., Fuerniss, S.J., and Papatthomas, K.I. (1996). Luminescence of W(CO)₄(4-Me-phen) in photosensitive thin films: a molecular probe of acrylate polymerization. *Chem. Mater.* 8, 1540–1544. <https://doi.org/10.1021/cm960145y>.
- Rong, M.Z., Zhang, M.Q., and Ruan, W.H. (2013). Surface modification of nanoscale fillers for improving properties of polymer nanocomposites: a review. *Mater. Sci. Technol.* 22, 787–796. <https://doi.org/10.1179/174328406X101247>.
- Schulmeyer, T., Paniagua, S.A., Veneman, P.A., Jones, S.C., Hotchkiss, P.J., Mudalige, A., Pemberton, J.E., Marder, S.R., and Armstrong, N.R. (2007). Modification of BaTiO₃ thin

- films: adjustment of the effective surface work function. *J. Mater. Chem.* **17**, 4563–4570. <https://doi.org/10.1039/B706949A>.
- Schuman, T.P., Siddabattuni, S., Cox, O., and Dogan, F. (2012). Improved dielectric breakdown strength of covalently-bonded interface polymer-particle nanocomposites. *Compos. Interfac.* **17**, 719–731. <https://doi.org/10.1163/092764410X495315>.
- Shen, Y., Du, J., Zhang, X., Huang, X., Song, Y., Wu, H., Lin, Y., Li, M., and Nan, C.W. (2016). Enhanced breakdown strength and suppressed leakage current of polyvinylidene fluoride nanocomposites by two-dimensional ZrO₂ nanosheets. *Mat. Express* **6**, 277–282. <https://doi.org/10.1166/mex.2016.1309>.
- Shen, Y., Hu, Y., Chen, W., Wang, J., Guan, Y., Du, J., Zhang, X., Ma, J., Li, M., Lin, Y., et al. (2015). Modulation of topological structure induces ultrahigh energy density of graphene/Ba_{0.6}Sr_{0.4}TiO₃ nanofiber/polymer nanocomposites. *Nano Energy* **18**, 176–186. <https://doi.org/10.1016/j.nanoen.2015.10.003>.
- Siddabattuni, S., Schuman, T.P., and Dogan, F. (2011). Improved polymer nanocomposite dielectric breakdown performance through barium titanate to epoxy interface control. *Mater. Sci. Eng., B* **176**, 1422–1429. <https://doi.org/10.1016/j.mseb.2011.07.025>.
- Tang, H., Sodano, H.A., and Henry, A. (2013). High energy density nanocomposite capacitors using non-ferroelectric nanowires. *Appl. Phys. Lett.* **102**, 063901. <https://doi.org/10.1063/1.4792513>.
- Song, L., Ci, L., Lu, H., Sorokin, P.B., Jin, C., Ni, J., Kvashnin, A.G., Kvashnin, D.G., Lou, J., Yakobson, B.I., and Ajayan, P.M. (2010). Large scale growth and characterization of atomic hexagonal boron nitride layers. *Nano Lett.* **10**, 3209–3215. <https://doi.org/10.1021/nl1022139>.
- Song, S., Xia, S., Liu, Y., Lv, X., and Sun, S. (2020). Effect of Na⁺ MMT-ionic liquid synergy on electroactive, mechanical, dielectric and energy storage properties of transparent PVDF-based nanocomposites. *Chem. Eng. J.* **384**, 123365. <https://doi.org/10.1016/j.cej.2019.123365>.
- Song, Y., Shen, Y., Liu, H., Lin, Y., Li, M., and Nan, C.W. (2012). Improving the dielectric constants and breakdown strength of polymer composites: effects of the shape of the BaTiO₃ nano-inclusions, surface modification and polymer matrix. *J. Mater. Chem.* **22**, 16491. <https://doi.org/10.1039/C2JM32579A>.
- Spori, D.M., Venkataraman, N.V., Tosatti, S.G.P., Durmaz, F., Spencer, N.D., and Zürcher, S. (2007). Influence of alkyl chain length on phosphate self-assembled monolayers. *Langmuir* **23**, 8053–8060. <https://doi.org/10.1021/la700474v>.
- Sun, L., Shi, Z., He, B., Wang, H., Liu, S., Huang, M., Shi, J., Dastan, D., and Wang, H. (2021a). Asymmetric trilayer all-polymer dielectric composites with simultaneous high efficiency and high energy density: a novel design targeting advanced energy storage capacitors. *Adv. Funct. Mater.* **31**, 2100280. <https://doi.org/10.1002/adfm.202100280>.
- Sun, L., Shi, Z., Wang, H., Zhang, K., Dastan, D., Sun, K., and Fan, R. (2020). Ultrahigh discharge efficiency and improved energy density in rationally designed bilayer polyetherimide-BaTiO₃/P(VDF-HFP) composites. *J. Mater. Chem. A Mater.* **8**, 5750–5757. <https://doi.org/10.1039/d0ta00903b>.
- Sun, S., Shi, Z., Sun, L., Liang, L., Dastan, D., He, B., Wang, H., Huang, M., and Fan, R. (2021b). Achieving concurrent high energy density and efficiency in all-polymer layered paraelectric/ferroelectric composites via introducing a moderate layer. *ACS Appl. Mater. Interfaces* **13**, 27522–27532. <https://doi.org/10.1021/acsmi.1c08063>.
- Sun, Y., Boggs, S.A., and Ramprasad, R. (2012). The intrinsic electrical breakdown strength of insulators from first principles. *Appl. Phys. Lett.* **101**, 132906. <https://doi.org/10.1063/1.4755841>.
- Tan, D., Zhang, L., Chen, Q., and Irwin, P. (2014). High-temperature capacitor polymer films. *J. Electron. Mater.* **43**, 4569–4575. <https://doi.org/10.1007/s11664-014-3440-7>.
- Tang, H., and Sodano, H.A. (2013). Ultrahigh energy density nanocomposite capacitors with fast discharge using Ba_{0.2}Sr_{0.8}TiO₃ nanowires. *Nano Lett.* **13**, 1373–1379. <https://doi.org/10.1021/nl3037273>.
- Tang, H., Lin, Y., and Sodano, H.A. (2012). Enhanced energy storage in nanocomposite capacitors through aligned PZT nanowires by uniaxial strain assembly. *Adv. Energy Mater.* **2**, 393–476. <https://doi.org/10.1002/aenm.201290019>.
- Tang, H., Zhou, Z., and Sodano, H.A. (2014). Relationship between BaTiO₃ nanowire aspect ratio and the dielectric permittivity of nanocomposites. *ACS Appl. Mater. Interfaces* **6**, 5450–5455. <https://doi.org/10.1021/am405038r>.
- Kogelschatz, U. (2003). Dielectric-barrier discharges: their history, discharge physics, and industrial applications. *Plasma Chem. Plasma Process.* **23**, 1–46. <https://doi.org/10.1023/A:1022470901385>.
- Wang, G., Huang, X., and Jiang, P. (2015a). Tailoring dielectric properties and energy density of ferroelectric polymer nanocomposites by high-k nanowires. *ACS Appl. Mater. Interfaces* **7**, 18017–18027. <https://doi.org/10.1021/acsmi.5b06480>.
- Wang, G., Huang, X., and Jiang, P. (2017a). Bio-inspired polydopamine coating as a facile approach to constructing polymer nanocomposites for energy storage. *J. Mater. Chem. C Mater.* **5**, 3112–3120. <https://doi.org/10.1039/C7TC00387K>.
- Wang, G., Huang, X., and Jiang, P. (2017b). Mussel-inspired fluoro-polydopamine functionalization of titanium dioxide nanowires for polymer nanocomposites with significantly enhanced energy storage capability. *Sci. Rep.* **7**, 43071. <https://doi.org/10.1038/srep43071>.
- Wang, G., Huang, Y., Wang, Y., Jiang, P., and Huang, X. (2017c). Substantial enhancement of energy storage capability in polymer nanocomposites by encapsulation of BaTiO₃ NWs with variable shell thickness. *Phys. Chem. Chem. Phys.* **19**, 21058–21068. <https://doi.org/10.1039/C7CP04096B>.
- Wang, H., Xie, H., Wang, S., Gao, Z., Li, C., Hu, G.H., and Xiong, C. (2018a). Enhanced dielectric property and energy storage density of PVDF-HFP based dielectric composites by incorporation of silver nanoparticles-decorated exfoliated montmorillonite nanoplatelets. *Compos. Appl. Sci. Manuf.* **108**, 62–68. <https://doi.org/10.1016/j.compositesa.2018.02.020>.
- Wang, J., Xie, Y., Liu, J., Zhang, Z., and Zhang, Y. (2019a). Towards high efficient nanodielectrics from linear ferroelectric (PVDF-TrFE-CTFE)-g-PMMA matrix and exfoliated mica nanosheets. *Appl. Surf. Sci.* **469**, 437–445. <https://doi.org/10.1016/j.apsusc.2018.11.073>.
- Wang, J., Chen, H., Li, X., Zhang, C., Yu, W., Zhou, L., Yang, Q., Shi, Z., and Xiong, C. (2020a). Flexible dielectric film with high energy density based on chitin/boron nitride nanosheets. *Chem. Eng. J.* **383**, 123147. <https://doi.org/10.1016/j.cej.2019.123147>.
- Wang, L., Gao, F., Xu, J., Zhang, K., Kong, J., Reece, M., and Yan, H. (2018b). Enhanced dielectric tunability and energy storage properties of plate-like Ba_{0.6}Sr_{0.4}TiO₃/poly(vinylidene fluoride) composites through texture arrangement. *Compos. Sci. Technol.* **158**, 112–120. <https://doi.org/10.1016/j.compscitech.2018.02.015>.
- Wang, M., Li, W.L., Feng, Y., Hou, Y.F., Zhang, T.D., Fei, W.D., and Yin, J.H. (2015b). Effect of BaTiO₃ nanowires on dielectric properties and energy storage density of polyimide composite films. *Ceram. Int.* **41**, 13582–13588. <https://doi.org/10.1016/j.ceramint.2015.07.153>.
- Wang, Q., and Zhu, L. (2011). Polymer nanocomposites for electrical energy storage. *J. Polym. Sci. B Polym. Phys.* **49**, 1421–1429. <https://doi.org/10.1002/polb.22337>.
- Wang, Y., Wang, G., Wang, L., Xu, X., Xia, J., Huang, X., Wu, Y., and Zhang, C. (2010). Recent development of high energy density polymers for dielectric capacitors. *IEEE Trans. Dielectr. Electr. Insul.* **50**, 1036–1043. <https://doi.org/10.1109/TDEI.2010.5539672>.
- Wang, Y., Cui, J., Wang, L., Yuan, Q., Niu, Y., Chen, J., Wang, Q., and Wang, H. (2017d). Compositional tailoring effect on electric field distribution for significantly enhanced breakdown strength and restrained conductive loss in sandwich-structured ceramic/polymer nanocomposites. *J. Mater. Chem.* **5**, 4710–4718. <https://doi.org/10.1039/c6ta10709e>.
- Wang, Y., Cui, J., Yuan, Q., Niu, Y., Bai, Y., and Wang, H. (2015c). Significantly enhanced breakdown strength and energy density in sandwich-structured barium titanate/poly(vinylidene fluoride) nanocomposites. *Adv. Mater.* **27**, 6658–6663. <https://doi.org/10.1002/adma.201503186>.
- Wang, Y., Chen, J., Li, Y., Niu, Y., Wang, Q., and Wang, H. (2019b). Multilayered hierarchical polymer composites for high energy density capacitors. *J. Mater. Chem. A Mater.* **7**, 2965–2980. <https://doi.org/10.1039/C8TA11392K>.
- Wang, Y., Li, Y., Wang, L., Yuan, Q., Chen, J., Niu, Y., Xu, X., Wang, Q., and Wang, H. (2020b). Gradient-layered polymer nanocomposites with significantly improved insulation performance for dielectric energy storage. *Energy Storage Mater.*

- 24, 626–634. <https://doi.org/10.1016/j.ensm.2019.06.013>.
- Wang, Y., Li, Z., Wu, C., and Cao, Y. (2020c). High-temperature dielectric polymer nanocomposites with interposed montmorillonite nanosheets. *Chem. Eng. J.* 401, 126093. <https://doi.org/10.1016/j.cej.2020.126093>.
- Wang, Y., Nasreen, S., Kamal, D., Li, Z., Wu, C., Huo, J., Chen, L., Ramprasad, R., and Cao, Y. (2021). Tuning surface states of metal/polymer contacts toward highly insulating polymer-based dielectrics. *ACS Appl. Mater. Interfaces* 13, 46142–46150. <https://doi.org/10.1021/acsami.1c12854>.
- Wang, Y., Wang, L., Yuan, Q., Chen, J., Niu, Y., Xu, X., Cheng, Y., Yao, B., Wang, Q., and Wang, H. (2018c). Ultrahigh energy density and greatly enhanced discharged efficiency of sandwich-structured polymer nanocomposites with optimized spatial organization. *Nano Energy* 44, 364–370. <https://doi.org/10.1016/j.nanoen.2017.12.018>.
- Wang, Y., Wang, L., Yuan, Q., Niu, Y., Chen, J., Wang, Q., and Wang, H. (2017e). Ultrahigh electric displacement and energy density in gradient layer-structured BaTiO₃/PVDF nanocomposites with an interfacial barrier effect. *J. Mater. Chem. A Mater.* 5, 10849–10855. <https://doi.org/10.1039/C7TA01522D>.
- Wang, Z., Wang, X., Sun, Z., Li, Y., Li, J., and Shi, Y. (2019c). Enhanced energy storage property of plate-like Na_{0.5}Bi_{4.5}Ti₄O₁₅/poly(vinylidene fluoride) composites through texture arrangement. *Ceram. Int.* 45, 18356–18362. <https://doi.org/10.1016/j.ceramint.2019.06.050>.
- Wei, J., Zhang, Z., Tseng, J.K., Treufeld, I., Liu, X., Litt, M.H., and Zhu, L. (2015). Achieving high dielectric constant and low loss property in a dipolar glass polymer containing strongly dipolar and small-sized sulfone groups. *ACS Appl. Mater. Interfaces* 7, 5248–5257. <https://doi.org/10.1021/am508488w>.
- Wen, F., Lou, H., Ye, J., Bai, W., Wang, L., Li, L., Wu, W., Xu, Z., Wang, G., Zhang, Z., and Zhang, L. (2019). Preparation and energy storage performance of transparent dielectric films with two-dimensional platelets. *Compos. Sci. Technol.* 182, 107759. <https://doi.org/10.1016/j.compscitech.2019.107759>.
- Wen, R., Guo, J., Zhao, C., and Liu, Y. (2017). Nanocomposite capacitors with significantly enhanced energy density and breakdown strength utilizing a small loading of monolayer titania. *Adv. Mater. Interfaces* 5, 1701088. <https://doi.org/10.1002/admi.201701088>.
- Wu, C., Deshmukh, A.A., Li, Z., Chen, L., Alamri, A., Wang, Y., Ramprasad, R., Sotzing, G.A., and Cao, Y. (2020). Flexible temperature-invariant polymer dielectrics with large bandgap. *Adv. Mater.* 32, e2000499. <https://doi.org/10.1002/adma.202000499>.
- Wu, L., Wu, K., Liu, D., Huang, R., Huo, J., Chen, F., and Fu, Q. (2018a). Largely enhanced energy storage density of poly(vinylidene fluoride) nanocomposites based on surface hydroxylation of boron nitride nanosheets. *J. Mater. Chem. A Mater.* 6, 7573–7584. <https://doi.org/10.1039/C8TA01294F>.
- Wu, Y., Wang, Z., Shen, X., Liu, X., Han, N.M., Zheng, Q., Mai, Y.W., and Kim, J.K. (2018b). Graphene/boron nitride-polyurethane microlaminates for exceptional dielectric properties and high energy densities. *ACS Appl. Mater. Interfaces* 10, 26641–26652. <https://doi.org/10.1021/acsami.8b08031>.
- Xie, B., Zhang, H., Zhang, Q., Zang, J., Yang, C., Wang, Q., Li, M.Y., and Jiang, S. (2017). Enhanced energy density of polymer nanocomposites at a low electric field through aligned BaTiO₃ nanowires. *J. Mater. Chem. A Mater.* 5, 6070–6078. <https://doi.org/10.1039/C7TA00513J>.
- Xie, B., Zhang, Q., Zhang, H., Zhang, G., Qiu, S., and Jiang, S. (2016). Largely enhanced ferroelectric and energy storage performances of P(VDF-CTFE) nanocomposites at a lower electric field using BaTiO₃ nanowires by stirring hydrothermal method. *Ceram. Int.* 42, 19012–19018. <https://doi.org/10.1016/j.ceramint.2016.09.057>.
- Xie, L., Huang, X., Huang, Y., Yang, K., and Jiang, P. (2013). Core@double-shell structured BaTiO₃-polymer nanocomposites with high dielectric constant and low dielectric loss for energy storage application. *J. Phys. Chem. C* 117, 22525–22537. <https://doi.org/10.1021/jp407340n>.
- Xu, H. (2001). Dielectric properties and ferroelectric behavior of poly(vinylidene fluoride-trifluoroethylene) 50/50 copolymer ultrathin films. *J. Appl. Polym. Sci.* 80, 2259–2266. <https://doi.org/10.1002/app.1330.abs>.
- Xu, W., Liu, J., Chen, T., Jiang, X., Qian, X., Zhang, Y., Jiang, Z., and Zhang, Y. (2019). Bioinspired polymer nanocomposites exhibit giant energy density and high efficiency at high temperature. *Small* 15, 1901582. <https://doi.org/10.1002/smll.201901582>.
- Yang, L., Li, X., Allahyarov, E., Taylor, P.L., Zhang, Q.M., and Zhu, L. (2013). Novel polymer ferroelectric behavior via crystal isomorphism and the nanoconfinement effect. *Polymer* 54, 1709–1728. <https://doi.org/10.1016/j.polymer.2013.01.035>.
- Yao, L., Pan, Z., Liu, S., Zhai, J., and Chen, H.H.D. (2016). Significantly enhanced energy density in nanocomposite capacitors combining the TiO₂ nanorod array with poly(vinylidene fluoride). *ACS Appl. Mater. Interfaces* 8, 26343–26351. <https://doi.org/10.1021/acsami.6b09265>.
- Ye, J., Rothhaar, U., and Oechsner, H. (1998). Conditions for the formation of cubic boron nitride films by r.f. Magnetron sputtering. *Surf. Coating. Technol.* 105, 159–164. [https://doi.org/10.1016/S0257-8972\(98\)00479-4](https://doi.org/10.1016/S0257-8972(98)00479-4).
- Yu, D., Xu, N.X., Hu, L., Zhang, Q.L., and Yang, H. (2015). Nanocomposites with BaTiO₃-SrTiO₃ hybrid fillers exhibiting enhanced dielectric behaviours and energy-storage densities. *J. Mater. Chem. C Mater.* 3, 4016–4022. <https://doi.org/10.1039/c4tc02972k>.
- Yu, K., Bai, Y., Zhou, Y., Niu, Y., and Wang, H. (2014). Poly(vinylidene fluoride) polymer based nanocomposites with enhanced energy density by filling with polyacrylate elastomers and BaTiO₃ nanoparticles. *Appl. Phys. Lett.* 104, 082904. <https://doi.org/10.1063/1.4866585>.
- Yu, K., Niu, Y., Bai, Y., Zhou, Y., and Wang, H. (2013a). Poly(vinylidene fluoride) polymer based nanocomposites with significantly reduced energy loss by filling with core-shell structured BaTiO₃@SiO₂ nanoparticles. *Appl. Phys. Lett.* 102, 102903. <https://doi.org/10.1063/1.4795017>.
- Yu, K., Niu, Y., Xiang, F., Zhou, Y., Bai, Y., and Wang, H. (2013b). Enhanced electric breakdown strength and high energy density of barium titanate filled polymer nanocomposites. *J. Appl. Phys.* 114, 174107. <https://doi.org/10.1063/1.4829671>.
- Yu, K., Niu, Y., Zhou, Y., Bai, Y., and Wang, H. (2013c). Nanocomposites of surface-modified BaTiO₃ nanoparticles filled ferroelectric polymer with enhanced energy density. *J. Am. Ceram. Soc.* 96, 2519–2524. <https://doi.org/10.1111/jace.12338>.
- Yuan, M., Li, B., Zhang, S., Rajagopalan, R., and Lanagan, M.T. (2020). High-field dielectric properties of oriented poly(vinylidene fluoride-co-hexafluoropropylene): structure-dielectric property relationship and implications for energy storage applications. *ACS Appl. Polym. Mater.* 2, 1356–1368. <https://doi.org/10.1021/acspap.9b01224>.
- Zhang, B., Liu, J., Ren, M., Wu, C., Moran, T.J., Zeng, S., Chavez, S.E., Hou, Z., Li, Z., Lachance, A.M., et al. (2021). Reviving the "Schottky" barrier for flexible polymer dielectrics with a superior 2D nanoassembly coating. *Adv. Mater.* 33, 2101374. <https://doi.org/10.1002/adma.202101374>.
- Zhang, H., Marwat, M.A., Xie, B., Ashtar, M., Liu, K., Zhu, Y., Zhang, L., Fan, P., Samart, C., and Ye, Z.G. (2020). Polymer matrix nanocomposites with 1D ceramic nanofillers for energy storage capacitor applications. *ACS Appl. Mater. Interfaces* 12, 1–37. <https://doi.org/10.1021/acsami.9b15005>.
- Zhang, H., Zhu, Y., Li, Z., Fan, P., Ma, W., and Xie, B. (2018a). High discharged energy density of polymer nanocomposites containing paraelectric SrTiO₃ nanowires for flexible energy storage device. *J. Alloys Compd.* 744, 116–123. <https://doi.org/10.1016/j.jallcom.2018.02.052>.
- Zhang, Q.M., Bharti, V.V., and Zhao, X. (1998). Giant electrostriction and relaxor ferroelectric behavior in electron-irradiated poly(vinylidene fluoride-trifluoroethylene) copolymer. *Science* 280, 2101–2104. <https://doi.org/10.1126/science.280.5372.2101>.
- Zhang, S., Zou, C., Kushner, D.I., Zhou, X., Orchard, R.J., Zhang, N., Zhang, Q.M., and Zhang, Q.M. (2012). Semicrystalline polymers with high dielectric constant, melting temperature, and charge-discharge efficiency. *IEEE Trans. Dielectr. Electr. Insul.* 19, 1158–1166. <https://doi.org/10.1109/TDEI.2012.6259984>.
- Zhang, T., Chen, X., Thakur, Y., Lu, B., Zhang, Q., Runt, J., and Zhang, Q.M. (2020a). A highly scalable dielectric metamaterial with superior capacitor performance over a broad temperature. *Sci. Adv.* 6, eaax6622. <https://doi.org/10.1126/sciadv.aax6622>.
- Zhang, X., Chen, W., Wang, J., Shen, Y., Gu, L., Lin, Y., and Nan, C.W. (2014). Hierarchical interfaces induce high dielectric permittivity in nanocomposites containing TiO₂@BaTiO₃ nanofibers. *Nanoscale* 6, 6701–6709. <https://doi.org/10.1039/c4nr00703d>.

Zhang, X., Jiang, J., Shen, Z., Dan, Z., Li, M., Lin, Y., Nan, C., Chen, L., and Shen, Y. (2018b). Polymer nanocomposites with ultrahigh energy density and high discharge efficiency by modulating their nanostructures in three dimensions. *Adv. Mater.* 30, 1707269. <https://doi.org/10.1002/aenm.201970047>.

Zhang, X., Shen, Y., Xu, B., Zhang, Q., Gu, L., Jiang, J., Ma, J., Lin, Y., and Nan, C.W. (2016). Giant energy density and improved discharge efficiency of solution-processed polymer nanocomposites for dielectric energy storage. *Adv. Mater.* 28, 2055–2061. <https://doi.org/10.1002/adma.201503881>.

Zhang, X., Shen, Y., Zhang, Q., Gu, L., Hu, Y., Du, J., Lin, Y., and Nan, C.W. (2015). Ultrahigh energy density of polymer nanocomposites containing BaTiO₃@TiO₂ nanofibers by atomic-scale interface engineering. *Adv. Mater.* 27, 819–824. <https://doi.org/10.1002/adma.201404101>.

Zhang, X., Chen, H., Ye, H., Liu, A., and Xu, L. (2020b). Enhanced interfacial polarization in poly(vinylidene fluoride-chlorotrifluoroethylene) nanocomposite with parallel boron nitride nanosheets. *Nanotechnology* 31, 165703. <https://doi.org/10.1088/1361-6528/ab69b4>.

Zhang, Y., Zhang, T., Liu, L., Chi, Q., Zhang, C., Chen, Q., Cui, Y., Wang, X., and Lei, Q. (2018c). Sandwich-structured PVDF-based composite

incorporated with hybrid Fe₃O₄@BN nanosheets for excellent dielectric properties and energy storage performance. *J. Phys. Chem. C* 122, 1500–1512. <https://doi.org/10.1021/acs.jpcc.7b10838>.

Zhang, Z., Wang, D.H., Litt, M.H., Tan, L., and Zhu, L. (2018d). High-temperature and high-energy-density dipolar glass polymers based on sulfonated poly(2, 6-dimethyl-1, 4-phenylene oxide). *Angew. Chem. Int. Ed. Engl.* 130, 1544–1547. <https://doi.org/10.1002/ange.2017110474>.

Zhou, T., Zha, J.W., Cui, R.Y., Fan, B.H., Yuan, J.K., and Dang, Z.M. (2011). Improving dielectric properties of BaTiO₃/ferroelectric polymer composites by employing surface hydroxylated BaTiO₃ nanoparticles. *ACS Appl. Mater. Interfaces* 3, 2184–2188. <https://doi.org/10.1021/am200492q>.

Zhou, W.Y., and Yu, D.M. (2011). Effect of coupling agents on the dielectric properties of aluminum particles reinforced epoxy resin composites. *J. Compos. Mater.* 45, 1981–1989. <https://doi.org/10.1177/0021998310394694>.

Zhou, X., Zhao, X., Suo, Z., Zou, C., Runt, J., Liu, S., Zhang, S., and Zhang, Q.M. (2009). Electrical breakdown and ultrahigh electrical energy density in poly(vinylidene fluoride-hexafluoropropylene) copolymer. *Appl. Phys. Lett.* 94, 162901. <https://doi.org/10.1063/1.3123001>.

Let. 94, 162901. <https://doi.org/10.1063/1.3123001>.

Zhou, Y., Li, Q., Dang, B., Yang, Y., Shao, T., Li, H., Hu, J., Zeng, R., He, J., and Wang, Q. (2018). A scalable, high-throughput, and environmentally benign approach to polymer dielectrics exhibiting significantly improved capacitive performance at high temperatures. *Adv. Mater.* 30, 1805672. <https://doi.org/10.1002/adma.201805672>.

Zhu, P., Weng, L., Zhang, X., Wang, X., Guan, L., and Liu, L. (2020). Graphene@poly (dopamine)-Ag core-shell nanoplatelets as fillers to enhance the dielectric performance of polymer composites. *J. Mater. Sci.* 55, 7665–7679. <https://doi.org/10.1007/s10853-020-04557-y>.

Zhu, Y., Yao, H., Jiang, P., Wu, J., Zhu, X., and Huang, X. (2018). Two-dimensional high-k nanosheets for dielectric polymer nanocomposites with ultrahigh discharged energy density. *J. Phys. Chem. C* 122, 18282–18293. <https://doi.org/10.1021/acs.jpcc.8b04918>.

Zhu, Y., Zhu, Y., Huang, X., Chen, J., Li, Q., He, J., and Jiang, P. (2019). High energy density polymer dielectrics interlayered by assembled boron nitride nanosheets. *Adv. Energy Mater.* 9, 1901826. <https://doi.org/10.1002/aenm.201901826>.